

Numerical Simulation of Microwave Sintering of Zinc Oxide

by
Patrick Fischer

Thesis submitted to the faculty of the Virginia Polytechnic Institute and State University in partial fulfillment of the requirements for the degree of Master of Science
in
Mechanical Engineering

APPROVED:

Dr. J.R. Thomas, Chairman

Dr. E.P. Scott

Dr. T.E. Diller

May, 1997
Blacksburg, Virginia

keywords: zinc oxide, microwave, heat transfer, permittivity, thermal wave

NUMERICAL SIMULATION OF MICROWAVE SINTERING OF ZINC OXIDE

by

Patrick Fischer

J.R Thomas

Mechanical Engineering Department

(ABSTRACT)

Experiments at the University of Maryland Plasma Physics Laboratory have discovered an unusual temperature response in the form of a “thermal wave” which begins at the center and propagates towards the surface of a zinc oxide sample, when heated in a microwave cavity without the presence of oxygen. This effect is believed to be caused by the irregular temperature dependence of the dielectric properties of zinc oxide, particularly dielectric loss. Two thermocouple probes were used to measure the temperature response in a small cylindrical sample of zinc oxide packed in powder insulation, and heated in a microwave oven. In order to determine if the unusual response is caused by the dielectric properties, this work uses a finite-difference mathematical model to simulate the experiments, both for the case of zinc oxide heated in ordinary air, as well as for the case of zinc oxide heated in nitrogen. A revised version of the model is used to determine if the thermocouple probe has any effect on the temperature of the sample. The spatial and temporal temperature distribution results from the model indicate that the thermocouple probe has a negligible effect on the results and that the “thermal wave” can be attributed to the irregular temperature dependence of the dielectric loss of the material.

Acknowledgments

I would like to thank my advisor, Dr. J.R. Thomas, for his guidance through my graduate studies including this thesis. His knowledge, patience, and enthusiasm for research proved to be very valuable in assisting me in this endeavor. I would also like to thank Dr. E.P. Scott and Dr. T.E. Diller for serving on my committee.

In addition, I would like to thank the Department of Mechanical Engineering of Virginia Polytechnic Institute and State University for an excellent graduate education, as well as for providing me with the opportunity to earn the necessary funding through a teaching assistant position.

Finally, I would like to thank my family for their limitless encouragement and support.

Table of Contents

	<u>Page</u>
ACKNOWLEDGMENTS	iii
LIST OF FIGURES	v
NOMENCLATURE	vi
1 INTRODUCTION	1
1.1 Executive Summary	1
1.2 Background	2
1.3 Motivations and Objectives	5
2. LITERATURE REVIEW	6
3. EXPERIMENT	7
3.1 Set up and Procedure	7
3.2 Experimental Results	9
3.3 Thermal wave	11
4. MATHEMATICAL MODEL.....	13
4.1 General model	13
4.2 Heat Generation	16
4.2.1 Dielectric Loss or permittivity	16
4.2.2 Electric field strength	20
4.2.3 Electric field attenuation	20
4.3 Properties	22
4.4 Thermocouple Model	23
4.5 Solution Technique	27
4.6 Finite difference Method	27
4.6.1 Explicit	28
4.6.2 Implicit	28
4.6.3 Alternating Direction Implicit (ADI)	29
4.6.4 Comparison of the ADI and implicit methods	29
4.7 Computer program	30
4.8 Lumped Capacitance Constant Property Model	30
5. RESULTS FROM THE MODEL CALCULATIONS	33
5.1 Simulation results assuming uniform constant properties	33
5.2 Simulation results of the uniform field strength model	35
5.3 Simulation results with electric field attenuation	38
5.4 Effect of the thermocouple probe on the results	46
6. CONCLUSIONS AND RECOMMENDATIONS FOR FURTHER WORK	49
REFERENCES	50
APPENDIX A - PROPERTY DATA	52
APPENDIX B - DERIVATION OF FINITE DIFFERENCE EQUATIONS	53
APPENDIX C - PROGRAMS	70
Vita	94

List of Figures

<u>Figure</u>		<u>Page</u>
3-1	Experiment	8
3-2	Experimental Temperature Response for ZnO in air atmosphere	9
3-3	Experimental Temperature Response for ZnO in nitrogen atmosphere	10
3-4	Experimental Temperature Response During “Thermal Wave”	12
4-1	General Model	15
4-2	Dielectric loss (ϵ'') of ZnO vs. temperature and heating rate	17
4-3	Dielectric loss of ZnO vs. Temperature in air atmosphere.....	18
4-4	Dielectric loss of ZnO vs. Temperature in nitrogen atmosphere	18
4-5	Dielectric loss of ZnO in nitrogen and air vs. Temperature	19
4-6	Schematic of the Thermocouple Probe.....	24
4-7	Model of the thermocouple probe not in contact with sample.....	25
4-8	Model of the thermocouple probe in contact with sample.....	26
4-9	Constant heat generation lumped capacitance model fully insulated.....	31
4-10	Constant heat generation lumped capacitance model imperfectly insulated...	31
5-1	Fully insulated lumped capacitance vs. Simulation	34
5-2	Partially insulated lumped capacitance vs. Simulation	35
5-3	ZnO in air atmosphere with uniform field simulation.....	37
5-4	ZnO in nitrogen atmosphere with uniform field simulation.....	37
5-5	ZnO in air atmosphere simulation with attenuated field simulation.....	38
5-6	ZnO in air atmosphere with attenuated vs. uniform field simulation.....	39
5-7	ZnO in air atmosphere, simulation vs. experiment.....	40
5-8	ZnO in nitrogen atmosphere with attenuated field, simulation.....	41
5-9	ZnO in nitrogen atmosphere with attenuated vs. uniform field simulation ...	41
5-10	ZnO in nitrogen atmosphere simulation vs. experiment.....	42
5-11	ZnO in nitrogen atmosphere Temperature vs. r for z=0 at various times.....	44
5-12	ZnO in nitrogen atmosphere Temperature vs. r for z=0 at various times.....	45
5-13	Probe modeled as not in contact with sample vs. general simulation	47
5-14	Probe modeled as in contact with sample vs. general simulation	48

Nomenclature

T = Temperature [$^{\circ}\text{C}$]
t = Time [sec]
r = Radial axis [m]
R = Radius of structure [m]
z = Axial axis [m]
H = Distance from center to top of structure [m]
p = Integer time step counter
m = Integer node counter along r axis, ranges from 0 to M
n = Integer node counter along z axis, ranges from 0 to N
 Δt = Time Step [sec]
 Δr = Length of Discretized Control Volume in the Radial Direction [m]
 Δz = Height of Discretized Control Volume in the Axial Direction [m]
k = Thermal Conductivity [$\text{W}/(\text{m}^{\circ}\text{C})$]
A = Area across boundary of discretized control volume [m^2]
 ρ = Density [kg/m^3]
 c_p = Specific Heat Capacity [$\text{J}/\text{kg}^{\circ}\text{C}$]
h = Convection Coefficient [$\text{W}/(\text{m}^2^{\circ}\text{C})$]
 h_c = Contact Conductance [$\text{W}/(\text{m}^2^{\circ}\text{C})$]
 \dot{q} = Volumetric Power Generation [W/m^3]
 ϵ_0 = Free Space Electric Permittivity [F/m]
 ϵ' = Real Electric Permittivity
 ϵ'' = Imaginary Electric Permittivity, or Dielectric Loss
 μ_0 = Free Space Magnetic Permeability [H/m]
 μ' = Real Magnetic Permeability
 μ'' = Imaginary Magnetic Permeability
E = Local Electric Field Strength [V/m]
 $\langle E^2 \rangle$ = Time Average of the Square of Local Electric Field [$(\text{V}/\text{m})^2$]
 α = Attenuation Constant [m^{-1}]
 d_s = Skin Depth [m]
s = Distance of electric field attenuation [m]
 T_{∞} = Ambient Temperature [$^{\circ}\text{C}$]
 ω = Angular Frequency [radians/sec]

A subscript on T represents the node number, and a superscript represents the number of time steps up to that time. For example, $T_{m,n}^p$ means the temperature at radial node m, axial node n, and time p.

For k and A , a subscript represents the axis, and a superscript of $+$ or $-$ means the direction. For example, k_m^- means the thermal conductivity between a node and its preceding node in the m (radial) direction.

Chapter 1: Introduction

1.1 Executive Summary

The experiment to be modeled in this work was performed at the University of Maryland Plasma Physics Laboratory by Gershon, et al. [1] A small ceramic cylinder is placed in a casket of insulating powder, inside an alumina enclosure, and sintered in a microwave oven. The cylinder was made of zinc oxide and the powder is also zinc oxide at a lower density. The sample has a diameter of 0.031 m, and a thickness of 0.017 m, and a density of 3000 kg/m^3 . The enclosure is approximately 0.1 m in diameter, with a height of 0.20 m. Microwave power was initially set at 40 watts and kept there for the first 50 minutes, and then increased to 80 watts for the duration of the experiment. The heating was done in two different atmospheres, nitrogen and air. In the nitrogen atmosphere, measurements of the center and surface temperature suggest that a sharp "thermal wave" occurs. In air, the temperature reaches steady state without this effect.

The present work is an attempt to understand this phenomenon through mathematical modeling. An axisymmetric finite-difference model was developed to simulate the complete temperature response of the system. The general heat equation was discretized, as well as the boundary conditions.

A model is developed for the thermocouple probe, in order to determine whether the thermocouple has any effect on the temperature of the sample. This work does not attempt to determine if the thermocouple is measuring the temperature of the sample, and assumes the temperature reading is the true temperature.

Internal heat generation due to absorption of microwave energy is dependent on temperature and position, as well as the material properties. It is calculated at each node based on known equations.

The Alternating Direction Implicit solution method is chosen for its efficiency. It leads to three or less unknowns per equation, in the form of a tridiagonal matrix. The Thomas Algorithm for tridiagonal matrices gives very quick results, compared to the lengthy sparse matrix routine needed for the pentadiagonal matrix that the implicit method yields.

The probe is found to have a negligible effect on the temperature of the sample. The "thermal wave" that occurs in an oxygen free environment is shown to be caused by the unusual temperature dependence of the dielectric constant of zinc oxide when oxygen is not present.

1.2 Background

Microwave technology has the potential to be a useful tool for the sintering of ceramics. The potential advantages include more uniform temperatures in the sample, improved product uniformity, higher energy efficiency, less total time and space. Also, smaller grain sizes are achieved at any given density, leading to better and more uniform properties. The disadvantages include the high cost of microwave systems, limited applicability, wide variation in dielectric properties with temperature, inefficiency of electric power, and difficulty in repeatability of measurement.

Microwaves are electromagnetic waves with frequencies between 300 MHz and 300 GHz. Ceramics are insulators, thus electrons do not flow in response to an electric field. However, an electric field can cause a reorientation of dipoles, which can lead to heating. The rapidly changing electric fields associated with microwaves lead to rapidly changing orientations of the dipoles in the material. There is a natural frequency that causes maximum reorientation, thus maximum heating of the material. This is often referred to as "coupling". This is usually a very broad maximum, so that the frequency dependence is not strong.

Each material has intrinsic properties relative to the absorption of microwave energy. The most important property is the dielectric constant, or permittivity, ϵ . The permittivity is a measure of a material's ability to absorb and to store electrical potential energy. Permittivity is a complex number, represented by the equation $\epsilon = \epsilon' + i\epsilon''$, where ϵ' is the real permittivity, a measure of the penetration of microwaves into the material, and ϵ'' is the imaginary permittivity or dielectric loss, a measure of the material's ability to store the energy. Dielectric loss is often highly temperature dependent, therefore can lead to thermal runaway and uneven heating in materials with low thermal conductivity.

Local heat generated by the microwaves is described by the equation [1]

$$\dot{q} = \epsilon_0 \epsilon'' \omega \langle E^2 \rangle,$$

where ϵ_0 is the dielectric loss of free space, ω is the angular frequency, and E is the local rms electric field. ϵ_0 is a universal constant equal to 8.845×10^{-12} F/m[2]; and ω is controlled by the experimenter, 15.39 GHz for this experiment [1]. E varies in both time and space, and must be calculated. Therefore, the microwave effect on the system can be modeled as temperature dependent internal heat generation, according to the equation

$$\dot{q} = q_0 \epsilon''(T) \langle E^2(T, r, z) \rangle,$$

where $q_0 = 0.136$ W/m³ in the experiment modeled in this work.

In a conventional furnace, heat is transferred from the air to the surface of the sample by convection, then toward the sample core by conduction. Thus, the surface temperature is

always higher than the core temperature. In a microwave oven, molecules of the sample are excited directly by the electromagnetic field. As energy is absorbed by the sample, its temperature increases. The surface temperature becomes higher than the surroundings, and loses heat by convection. Therefore the surface temperature is lower than the core temperature. Because heat is being generated in the sample and conducted out of the sample, a stable temperature gradient can be achieved.

If the goal is uniform heating, then a combined approach may be a solution. Since conventional ovens lead to higher surface temperatures and microwaves lead to higher core temperatures, the right combination of the two could theoretically lead to equal core and surface temperatures. This would likely be a very difficult combination to arrive at experimentally, because the combinations would change over time. Also, the temperature would still probably not be constant throughout the entire sample, so the best case scenario would be to minimize the temperature gradient to achieve the most even heating.

Unlike conventional ovens, microwaves have "penetrating radiation, controllable electric field distributions, rapid heating, selective heating of materials through differential absorption, and self-limiting reactions." [2]

There are some potential problems with the use of microwaves. Materials with high electrical conductivity generally are difficult to process because of poor penetration of the microwave energy. Insulators with low dielectric loss are hard to heat because of poor absorption of microwave energy. Some materials have highly temperature dependent dielectric properties, often causing uneven heating and thermal runaway.

In recent years, extensive research has been done in the area of microwave processing of ceramics. Part of the reason for the increase in study in this area is the expectation of different, and perhaps better, properties than those achieved in traditional convection ovens. The fact that microwaves heat materials by internal absorption that resembles heat generation makes uniform heating, and thus uniform final properties, seem achievable. Experimental evidence shows that uniform heating is not achieved, and very large temperature gradients can result. This is caused by the loss of heat due to convection at the surface. The non-uniformity is then compounded by the temperature dependence of the absorption of microwave energy, which increases with temperature in some materials. There is evidence that microwave sintering of ceramics can have superior qualities when compared to conventional sintering. These include "enhanced ceramic sintering, grain growth, and diffusion rates, as well as faster apparent kinetics in polymers and synthetic chemistry." [2]

Zinc oxide is studied partly because it is useful in electronic applications. Experiments have found that zinc oxide has highly inhomogeneous microwave heating in an oxygen-free environment [3]. The result is a slow, steady increase in temperature at first, then a "thermal wave", a sharp increase in temperature that starts at the center, then propagates

toward the surface. This "thermal wave" is believed to be caused by two peaks in the imaginary permittivity in the 200-500 °C temperature range when ZnO is heated without oxygen. These peaks are believed to be caused by "the interaction between absorbed oxygen, conduction electrons, and neutral and ionized electron donor sites near the surface of the zinc oxide powder particles." [3] Because microwaves generally cause materials to have a temperature gradient, there will be different levels of absorption of power within the sample. Measurements of the dielectric properties of ZnO have been done for both air and nitrogen atmospheres at various temperatures, and linear interpolation is used to approximate the values at other temperatures in the present model.

In the experiment to be modeled in this work, a small ZnO cylinder is placed in a low density powder insulation, with an alumina enclosure around it. The entire structure is placed in a microwave applicator, and heated until sintering or steady state.

This problem can be modeled as axisymmetric. The alumina enclosure is small relative to the entire structure, so it can be modeled as part of the effective convection coefficient at the outer boundary. The temperature difference on the outside of the insulation is small relative to the sample, so the convection boundary has a very small effect on the results. In fact, using a constant temperature at the boundary has little effect on the temperature of the sample.

The internal heat generation produced by the microwaves is governed by the equation,

$$\dot{q} = \omega \epsilon_0 \epsilon'' \langle E^2 \rangle,$$

where ω is the angular frequency of the microwave, ϵ_0 is the dielectric permittivity of free space, ϵ'' is the dielectric loss, and E is the local electric field strength.

Dielectric loss, or imaginary permittivity, is a measure of a material's ability to store microwave energy. The unusual behavior of the temperature dependence of ϵ'' of ZnO in an oxygen free atmosphere is believed to be the cause of the "thermal wave" effect. Dielectric loss is highly temperature dependent for ZnO heated without oxygen.

The electric field is dependent on position and temperature, because of the temperature dependence of ϵ' and ϵ'' . The first approximation ignores this effect, and assumes a constant electric field. Then the model is improved by taking into account the variable electric field (time average) according to the equation [2]

$$E = E_0 e^{-\alpha s},$$

where E_0 is the maximum electric field, s is the distance from the surface, and α is the attenuation constant. The attenuation constant is dependent on both ϵ' and ϵ'' , and therefore dependent on temperature as well. Because the attenuation constant tends to increase with ϵ'' , electric field tends to decrease with ϵ'' . Therefore the effect of the attenuation is to slow down the rate of temperature increase.

Real permittivity is not constant for ZnO, but it ranges from about 3.84 to 4.02 [4] for the temperatures in this experiment, while imaginary permittivity ranges from 0.1 to 23.0 [1]. Therefore, imaginary permittivity is the primary controlling factor in electric field attenuation. Skin depth, the inverse of the attenuation constant, ranges from 0.764 m for low imaginary permittivities, to about 0.0057 m at high permittivities, when the thermal wave occurs. For ZnO heated in air, skin depth is never lower than 0.31 m. Since the sample is 0.0155 m in radius and 0.0085 m from the core to the top, the attenuation factor is very small at low permittivities, but highly significant at high permittivities.

In a two dimensional problem, the distance of electric field attenuation, s , can be taken from two surfaces. The approach taken in this work is to use the shorter distance.

The thermocouple probe used in the experiments can be modeled as if it were not at all in contact with the sample, with no heat flow across the boundary. The probe can also be modeled as if it were in contact with the sample, with a contact conductance.

A simple lumped capacitance model can be used to find a solution to the analogous constant property, constant heat generation problem. This can be used to test the accuracy of the computer simulation.

1.3 Motivations and Objectives

There are several reasons this system needs to be modeled mathematically. One reason is that it may be necessary to predict the temperature profile of a similar experiment, and that will be far easier to do once this model is complete. Also, the model helps to find a physical and mathematical explanation of the results, most significantly the "thermal wave". Another reason for modeling is to determine the effect of the thermocouple probe on the temperature profile. This is done by first modeling the system without the probe, and then with the probe. The results are then compared to each other, to see if the thermocouple significantly changes the temperature profile. The results are also compared to the experimental data.

Earlier one dimensional models [5] did not produce good agreement with the experiment. The authors were unsure whether this was a limitation of the one dimensional model, or the effect of the thermocouple penetration. This present work was undertaken partially as an attempt to answer these questions.

The objectives of this work are to determine if the thermocouple probe has any effect on the temperature of the sample, to verify that the anomalous temperature dependence of the imaginary permittivity is the cause of the thermal wave, and to develop a code with the ability to predict the temperature response of zinc oxide and other ceramics during microwave heating at points in the sample which are not measured.

Chapter 2: Literature Review

Microwave processing of ceramic materials has been the subject of numerous experiments in the last several years. The desire to attain uniform properties in the final ceramic, due to what was expected to be uniform heating within the sample, was one of the motivations. Experiments have shown that uniform heating is not achieved, because of surface losses. Research by Johnson at Northwestern University [6] has shown that thermal insulation can reduce temperature gradients, by reducing surface losses. Brandon [13] has experimentally shown that spheres heated by microwaves have a different core and surface temperature, although the difference is smaller than a conventional oven produces. Research done by Gershon, et al., at the University of Maryland [1] has discovered that small ZnO cylinders can develop temperature gradients of over 100 °C during microwave sintering. Their research also discovered a sharp "thermal wave", a rapid rise in the temperature beginning at the core, then propagating toward the surface. This present work attempts to model that effect mathematically. Work by Clark, et al., [8] has shown that there is no phase change or reduction of specific heat of ZnO over this temperature range. Therefore the effect cannot be explained by changes in phase or specific heat. Hutcheon, et al., [3] have measured the dielectric properties as a function of temperature, and found that the imaginary electric permittivity has two peaks in the 200°C to 500°C temperature range, the same temperature range in which the "thermal wave" occurs. Martin, et al. [9], have attributed the "thermal wave" effect to these peaks, and attributed the peaks in imaginary permittivity to chemical reactions between the sample and the atmosphere, such as the ionization of oxygen vacancies.

Finite-difference models have been developed to find the temperature profile for objects heated in a microwave applicator. Iskander, et al., [10-11] have done extensive work in this area. Barmatz and Johnson [12] have developed a model for steady state temperatures for spheres that are heated by microwaves. Olmstead and Brodwin [13] have proposed a model that suggests the thermocouple may have an effect on the temperature of the sample. Thomas [5,14] has modeled the two-dimensional cylindrical case of microwave sintered alumina with variable dielectric constant. The variable electromagnetic field has been modeled by Chaussecourte [2]. This present work attempts to take into account the effects the temperature dependent permittivity, the attenuated electric field, and the thermocouple probe.

Chapter 3: Experiment

3.1 Setup and Procedure

The experiment modeled in this work was performed by Martin, et al., [9] at the University of Maryland Plasma Physics Laboratory. Small ceramic cylinders, encased in a casket of low-density powder insulation, were sintered in a multimode microwave oven. The cylinders have diameter 0.031 m, and height 0.017 m. The surrounding insulation and enclosure has a 0.100 m diameter and a height of 0.20 m, as shown in Figure 3-1. [9]

The experiment uses a sample of zinc oxide (ZnO). The sample is encased in powder zinc oxide insulation of one third the density of the sample. The enclosure is porous alumina of 3% theoretical density.

Two cases are tried. The first uses an ordinary air atmosphere, and the second uses a nitrogen atmosphere.

Zinc oxide has temperature dependent dielectric loss, but approximately constant thermal conductivity and specific heat. Density is approximated as constant in both materials for this problem.

The temperature during the experiment was measured at the core and surface of the sample, by two Type K thermocouples.

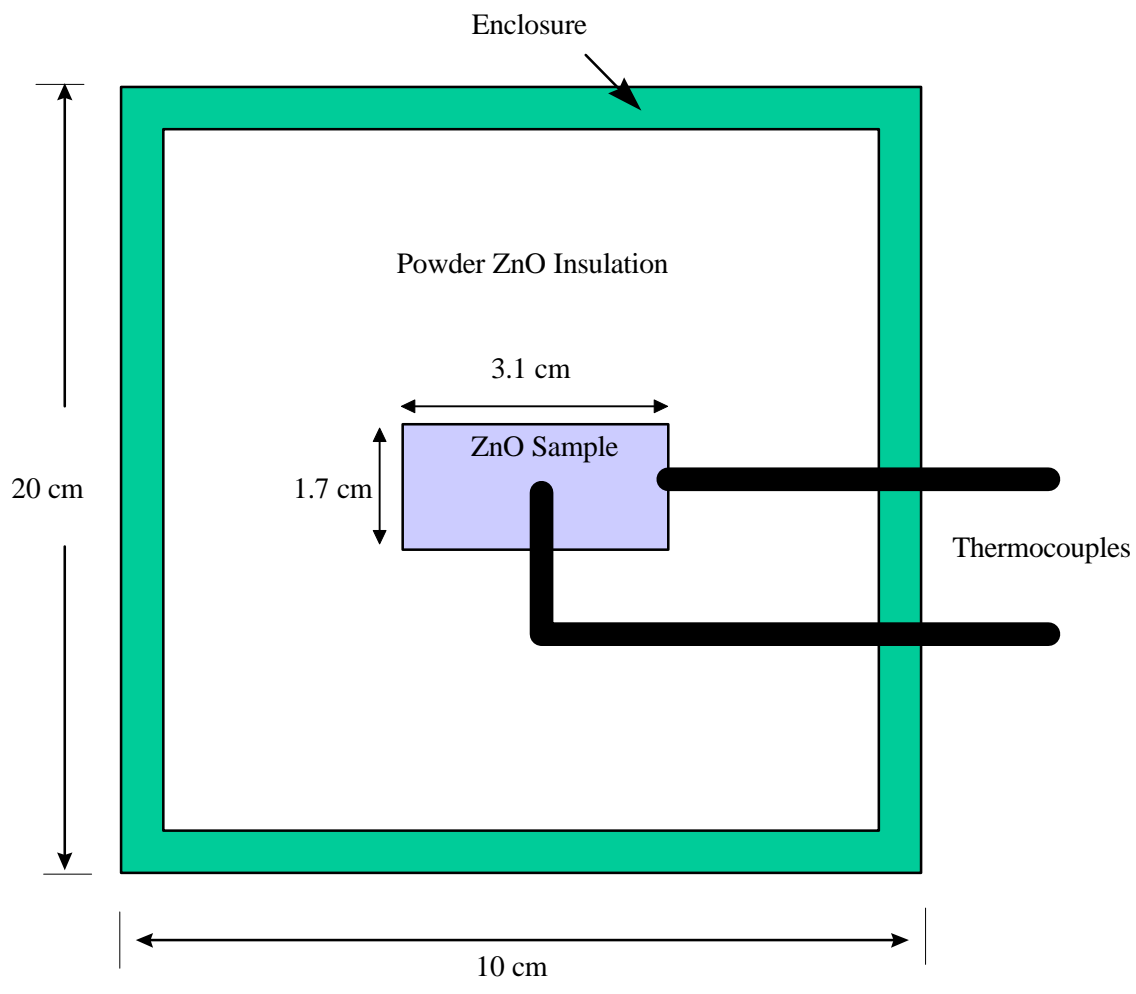


Figure 3-1: Experimental set up.

3.2 Experimental results

The results of the experiment are explained in detail in the literature [9].

When the experiment is carried out in an air atmosphere, as shown in Figure 3-2, the temperature at the core of the sample is always higher than the temperature at the surface. Both the core and surface temperature increase at a slower rate as time passes, and eventually reach a steady state temperature.

Figure 3-3 displays the results for the experiment in a nitrogen atmosphere. The temperature for the core of the zinc oxide increases slowly at first, then rapidly increases after it reaches about 230 °C, until it levels off at some higher temperature. A second rapid increase in temperature occurs at about 400 °C, until it levels off again at about 577 °C. The surface experiences this rapid increase, but slightly later, and levels off at lower final temperature. Thus it appears that a thermal wave runs through the cylinder, starting at the core, and propagates towards the surface.

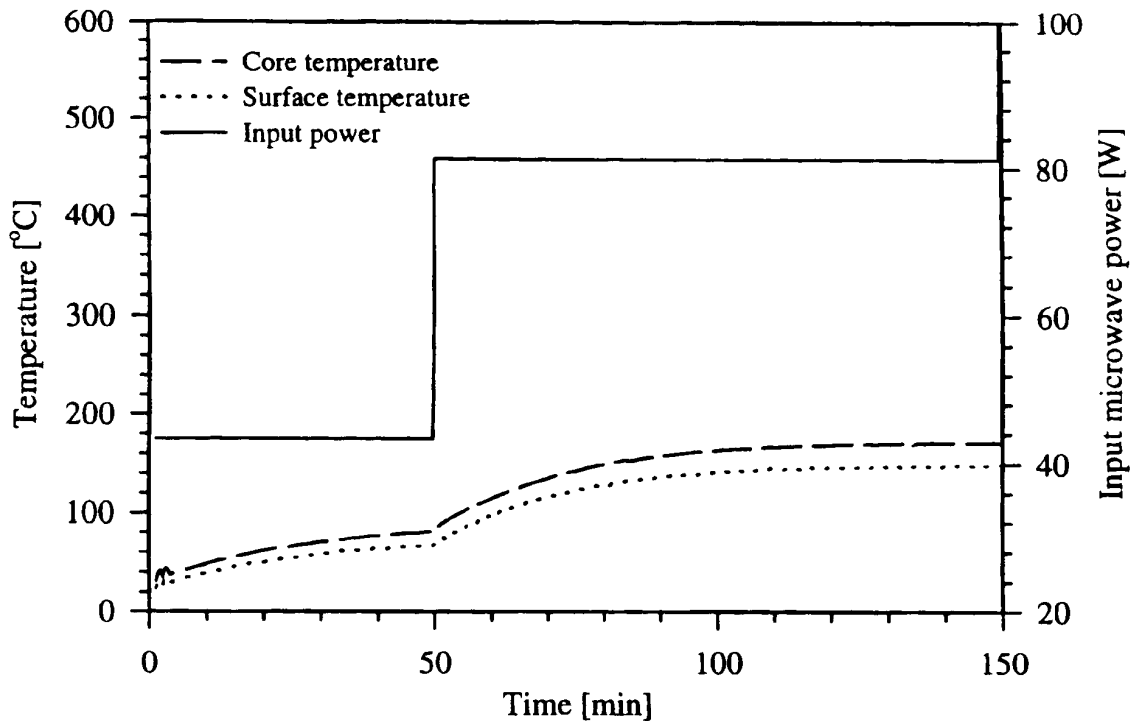


Figure 3-2: Measured core and surface temperature response of the ZnO sample during microwave heating in an air atmosphere. [9]

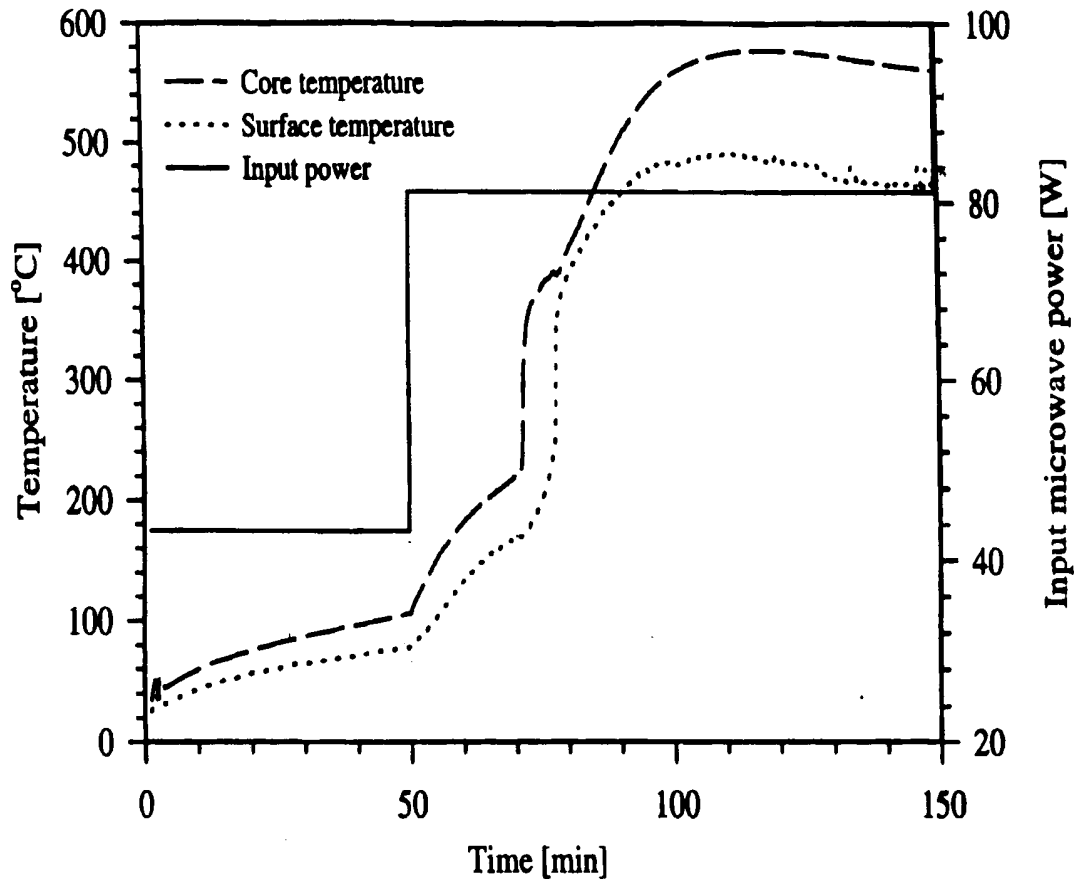


Figure 3-3: Measured core and surface temperature response of the ZnO sample during microwave heating in a nitrogen atmosphere. [9]

3.3 Thermal wave

Perhaps the most striking feature of this experiment is the "thermal wave" [3]. Figure 3-4 is a graph of the temperature response of the zinc oxide during the "thermal wave". It is the same as Figure 3-3, except it only shows from 60-85 minutes so it is easier to see the "thermal wave". The temperature in the sample increases slowly at first, then at temperatures of approximately 230 °C a rapid temperature increase is observed, approximately 200 °C /min. It begins at the center, then propagates radially toward the surface. This is referred to as a "thermal wave". It is believed to be caused by the two high peaks in dielectric constant at approximately 230 °C, and 450 °C. The temperature is highest in the center of the sample, thus the center reaches the critical temperature first, therefore the "thermal wave" begins at the center. Then the heat is conducted radially, causing the "thermal wave" to propagate toward the surface. The "thermal wave" in this experiment travels to the surface at a rate of approximately 3.33×10^{-5} m/sec.

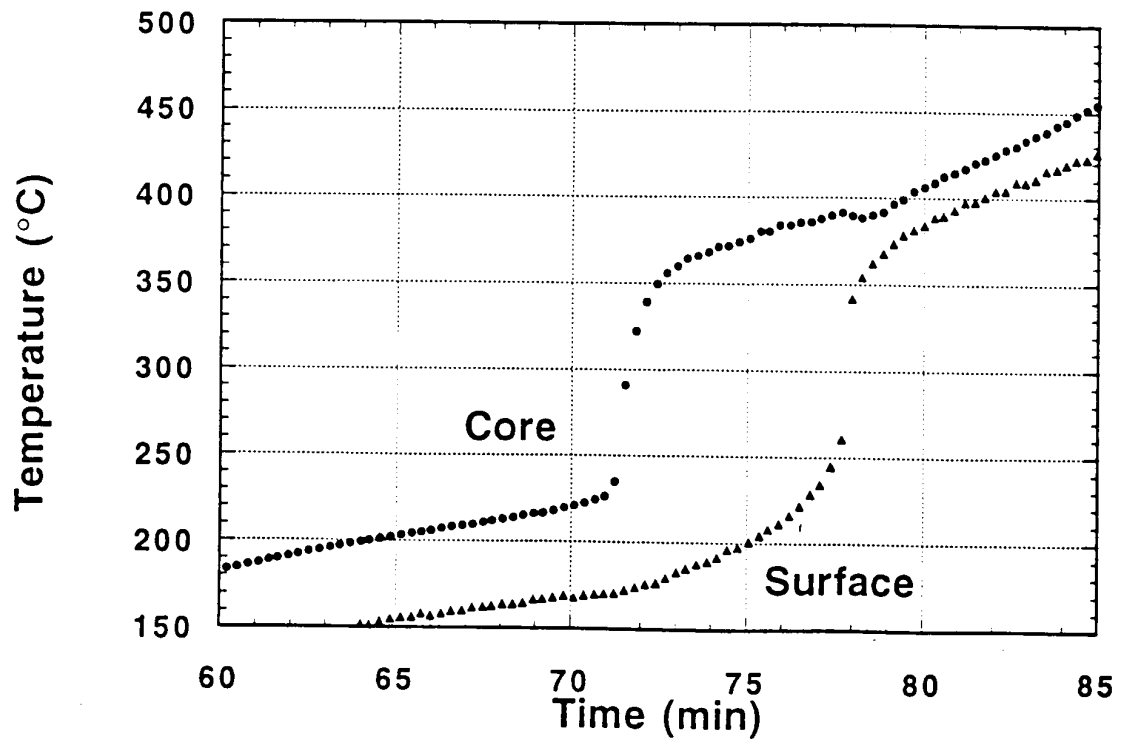


Figure 3-4: Measured temperature response during the “thermal wave” that occurs when microwave heating ZnO in nitrogen atmosphere.[13]

Chapter 4: Mathematical Model

4.1 General Model

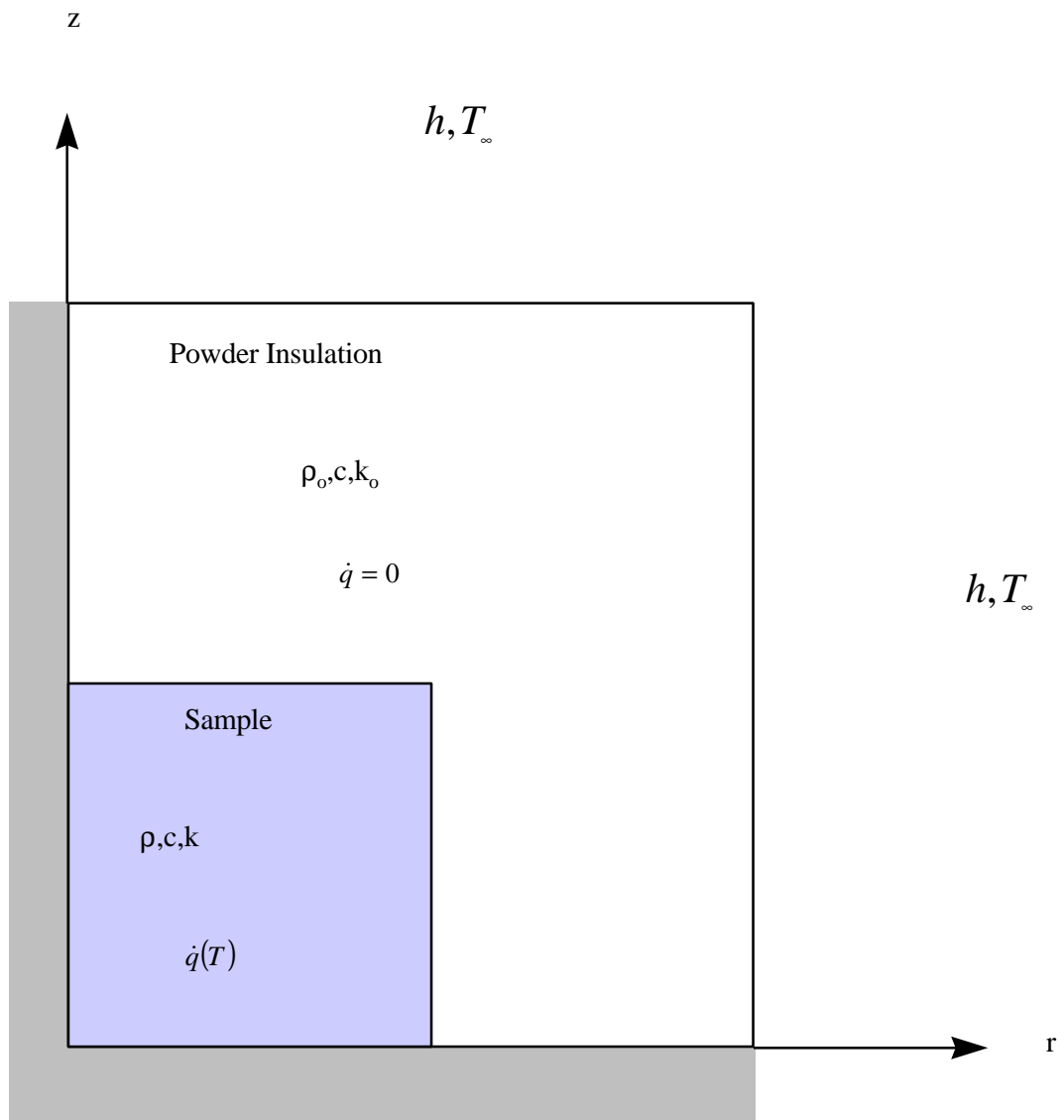
In this experiment, small cylindrical zinc oxide samples are encased in low density powder zinc oxide insulation, surrounded by an alumina enclosure, as shown in Figure 5-1. Then the system is placed in a microwave cavity, and microwave energy is applied until a steady state temperature is reached. The r and z axes begin at the center of the sample, with the r axis going outward in the radial direction and the z axis going up in the axial direction. By taking advantage of symmetry, the system can be modeled as insulated at r and $z = 0$. Figure 4-1 shows the general model of the system. The model assumes the sample has variable heat generation, caused by the absorption of microwave energy as described in section 1.2 of this work. Heat generation in the insulation is neglected, because its low density leads to negligible absorption of microwave energy. The insulation is assumed to have constant density, one third the density of the sample. The thermal conductance of the insulation is unknown, but it can be approximated from the other known data. Specific heat capacity is the same for the powder insulation and the sample. The alumina enclosure is small relative to the rest of the system, and relatively far away from the sample, so the thermal resistance through the enclosure is combined with the convection coefficient into an effective convection coefficient at the surface. In practice, the temperature change of the enclosure is small relative to the temperature change of the sample, so the enclosure can be modeled as a constant surface temperature without significantly effecting the calculated sample temperature.

The first step is to use the basic heat equation. For a given unit of volume, heat generated plus net heat flowing into the volume equals the change in stored energy. Then the cylinder is divided into several very small control volumes, and an energy balance is applied to each.

At this point the decision must be made as to what time to evaluate the spatial derivatives. The traditional approaches are the explicit method, which evaluates the derivative at the beginning of the time step (p), and the implicit method, which evaluates the derivative at the end of the time step ($p+1$). The explicit method has only one unknown per equation, but can require an extremely small maximum time step for stability. In this case, the implicit method has five unknowns per equation, and is solved by a sparse matrix solver. The implicit method takes much more computer time per time step than the explicit method, but has no limiting time step. Another approach is the alternating direction implicit(ADI) [2] method, which has three unknowns per time equation, in the form of a tridiagonal matrix. This can be solved very quickly with the Thomas Algorithm, and the solution is still stable at time steps far higher than the explicit scheme. This work used the ADI for most runs, but occasionally used the implicit method as a check for accuracy. Since the properties, especially heat generation, are temperature dependent, a guess must

be taken for the temperature. At each node, the properties are evaluated by subprograms. The initial guess is the temperature at the beginning of the time step, and then an iterative approach is used until the error is below some specified tolerance.

In this work, the effect of the thermocouple probe on the sample is taken into account is through an adjustment in the program, to set the value for heat flow across the boundary between the probe and the sample to the appropriate value. For the case of the non-contact probe, we set $k=0$ at the nodes where the probe borders the sample. For the case of the contact probe, we set the heat flow to $h_c(T_\infty - T)$.



Insulated Boundary (symmetry)

Figure 4-1: General model

4.2 Heat Generation

The effect of the absorption of microwave energy is modeled as internal heat generation. Previous work [1] has found the internal heat generation, \dot{q} , to be governed by the equation $\dot{q} = \epsilon_0 \epsilon'' \omega \langle E^2 \rangle$, where ϵ_0 is the dielectric permittivity of free space, ϵ'' is the imaginary permittivity, ω is the angular frequency of the microwaves, and $\langle E^2 \rangle$ is the time squared average of the local electric field. For many materials, ϵ'' varies greatly with temperature, and there is tabulated data available. The values of ϵ_0 and ω are assumed constant. The electric field varies in both time and space, and with temperature as a result of changes in ϵ'' of the load. This attenuation effect was ignored for the first model developed in this work, and now approximated from the general equation of the attenuation constant.

4.2.1 Dielectric Loss or Permittivity

Electric permittivity of a dielectric material is a complex number of the form $\epsilon = \epsilon' + i\epsilon''$. The real part, ϵ' , a measure of the ability of microwaves to penetrate the material, is modestly temperature dependent for zinc oxide. The imaginary part, ϵ'' , also known as dielectric loss, is a measure of the material's ability to store microwave energy, and is highly temperature dependent in many materials. The imaginary permittivity of zinc oxide is also dependent on the heating rate. Figure 4-2 [1] is a plot of the imaginary permittivity of zinc oxide versus temperature in a conventional oven, in an air atmosphere and a nitrogen atmosphere at two different heating rates. The heating rate in a microwave oven is unknown, so the data for the higher heating rate is used in this work. The heating rate during the “thermal wave” is high, so this approximation is a more accurate representation of the imaginary permittivity during the “thermal wave”. The heating rate is slow during the period before and after the “thermal wave”, so this approximation should result in an over estimation of the temperature rise leading up to the “thermal wave”.

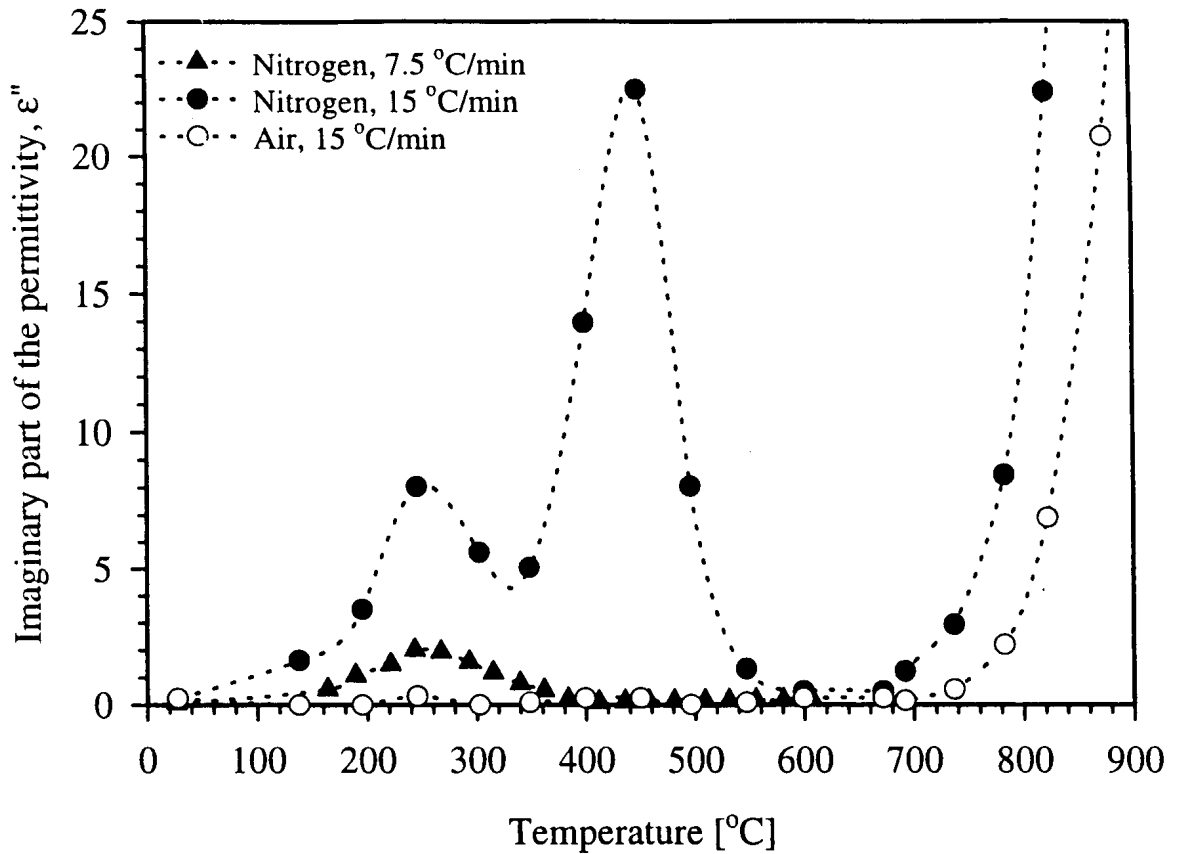


Figure 4-2: Imaginary permittivity, or dielectric loss(ϵ'') of ZnO vs. temperature during heating in a conventional oven at 7.5 and 15 °C/min in nitrogen, and 15 °C/min.[1]

Figures 4-3 and 4-4 are the curve fits to the data from Figure 4-2. Figure 4-3 shows ϵ'' at various temperatures in an air atmosphere, and the temperature dependence is evident. The peak of 0.255 is at 200 °C. Figure 4-4 is ϵ'' in a nitrogen atmosphere at the higher heating rate. The nitrogen atmosphere case also has a highly temperature dependent imaginary permittivity. There are two peaks, at 230 °C and 450 °C, of 8.0 and 23.0. Figure 4-5 plots the permittivity versus temperature data for both nitrogen and air, and the difference in the magnitudes is significant.

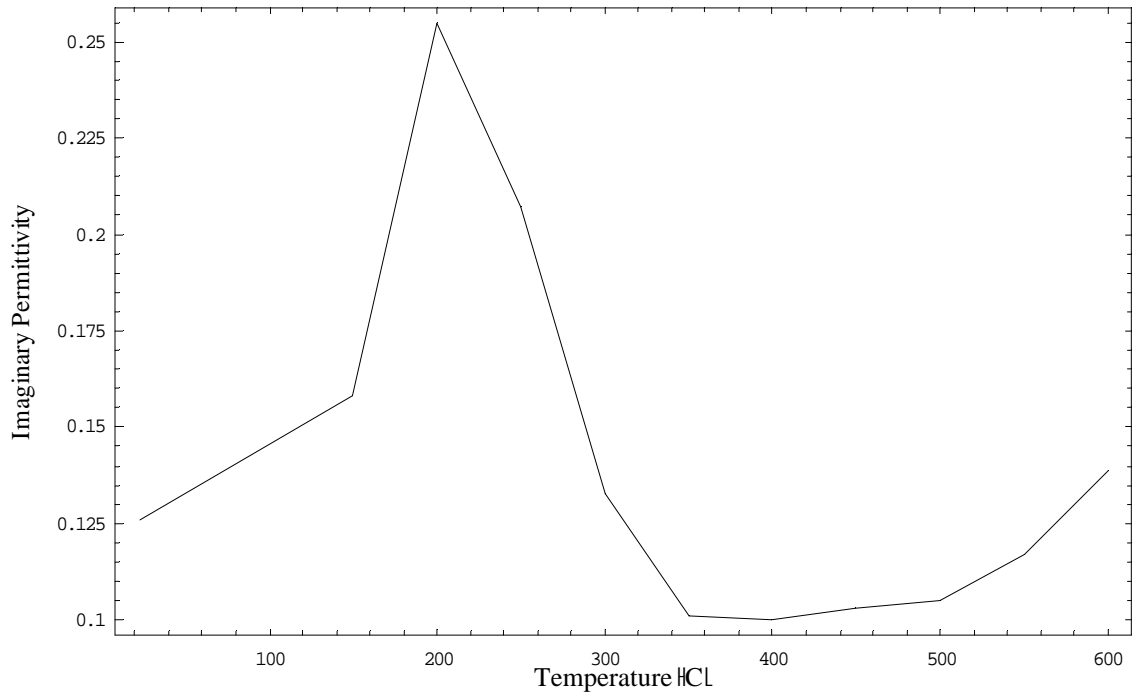


Figure 4-3: Imaginary permittivity, or dielectric loss(ϵ''), of ZnO in an air atmosphere vs. temperature.[1]

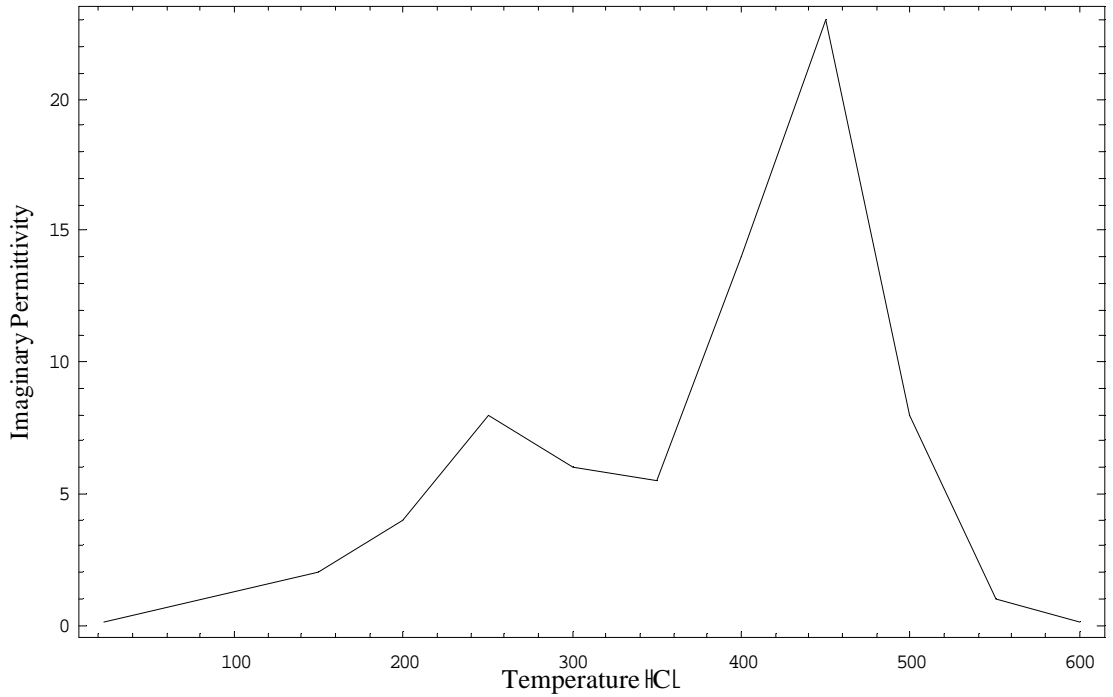


Figure 4-4: Imaginary permittivity, or dielectric loss(ϵ''), of ZnO in a nitrogen atmosphere vs. temperature.[1]

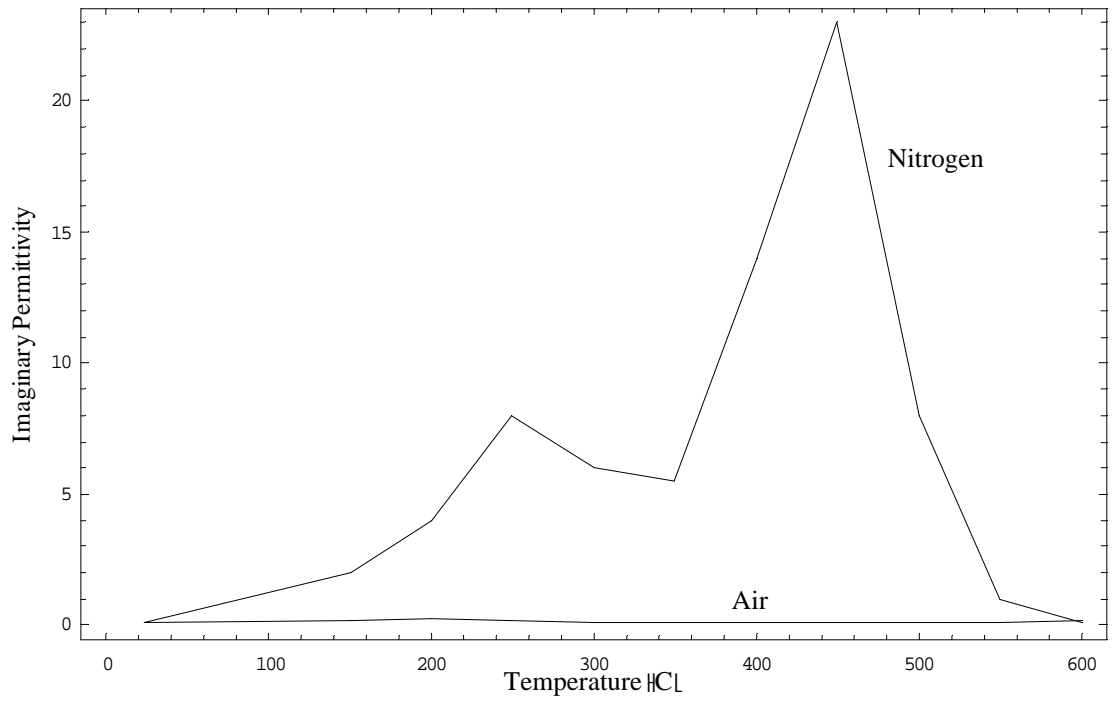


Figure 4-5: Imaginary permittivity, or dielectric loss(ϵ''), of ZnO in a nitrogen atmosphere and in an air atmosphere, vs. temperature.[1]

4.2.2 Electric Field Strength

The electric field at the core of the sample during the thermal wave can be estimated from the equation $\dot{q} = \epsilon_o \epsilon'' \omega \langle E^2 \rangle$. The value of heat generation during the thermal wave is approximately $1 \times 10^9 \text{ W/m}^3$ [1]. The maximum value of dielectric loss is 23 [1]. Permittivity of free space is a universal constant, and angular frequency is constant for this experiment. Therefore $E = 1.79 \times 10^4 \text{ V/m}$. The first run of this model assumes a constant electric field, and the second is improved by taking into account the effects of electric field attenuation.

4.2.3 Electric Field Attenuation

For a dielectric material like ZnO, the electric field varies spatially within the material according to the equation $E = E_o e^{-\alpha s}$, where α is the attenuation constant, and s is the distance from the surface. E_o is the electric field at the surface, and is a constant. It will be approximated later in this section. The attenuation constant for this experiment is given by the equation[13]

$$b - ja = \sqrt{\omega^2 \mu_o \epsilon_o (m' - jm'')(e' - je'')}$$

Ceramic materials are non-magnetic, so the magnetic permeability is equal to the magnetic permeability of free space. Therefore, $\mu' = 1$, and $\mu'' = 0$. The real part of the left side of the attenuation equation, β , is unrelated to this work. The imaginary part, the attenuation constant, can be approximated by a binomial expansion.

$$b - ja = \sqrt{\omega^2 \mu_o \epsilon_o e'} \sqrt{1 - j \frac{e''}{e'}} \quad (4.1)$$

Taking the binomial expansion,

$$\begin{aligned} \left(1 - j \frac{e''}{e'}\right)^{\frac{1}{2}} &= 1 - j \frac{1}{2} \left(\frac{e''}{e'}\right) + \frac{1}{8} \left(\frac{e''}{e'}\right)^2 + j \frac{1}{16} \left(\frac{e''}{e'}\right)^3 - \frac{5}{128} \left(\frac{e''}{e'}\right)^4 - j \frac{7}{256} \left(\frac{e''}{e'}\right)^5 \\ &\quad - \frac{21}{1024} \left(\frac{e''}{e'}\right)^6 + j \frac{231}{12288} \left(\frac{e''}{e'}\right)^7 + \dots \end{aligned}$$

Since only the imaginary part α is required for this problem, only the imaginary terms are necessary. Hence,

$$a = \sqrt{\omega^2 \mu_o \epsilon_o e'} \left[\frac{1}{2} \left(\frac{e''}{e'}\right) - \frac{1}{16} \left(\frac{e''}{e'}\right)^3 + \frac{7}{256} \left(\frac{e''}{e'}\right)^5 - \frac{231}{12288} \left(\frac{e''}{e'}\right)^7 + \dots \right] \quad (4.2)$$

When $\epsilon'' < \epsilon'$, the binomial expansion converges. For the case where $\epsilon'' \ll \epsilon'$, the equation simplifies to

$$\alpha = \frac{1}{2} \omega \sqrt{\frac{\mu_o \epsilon_o}{\epsilon'}} \epsilon''$$

For the case where $\epsilon'' < \epsilon'$, in order for the binomial expansion to converge, Eq. (4.1) needs to be rewritten as

$$\beta - j\alpha = \sqrt{\omega^2 \mu_o \epsilon_o (-j\epsilon'')} \sqrt{1 + j \frac{\epsilon'}{\epsilon''}} \quad (4.3)$$

Expanding the last term yields

$$\begin{aligned} \left(1 + j \frac{\epsilon'}{\epsilon''}\right)^{\frac{1}{2}} &= 1 + j \frac{1}{2} \left(\frac{\epsilon'}{\epsilon''}\right) + \frac{1}{8} \left(\frac{\epsilon'}{\epsilon''}\right)^2 - j \frac{1}{16} \left(\frac{\epsilon'}{\epsilon''}\right)^3 - \frac{5}{128} \left(\frac{\epsilon'}{\epsilon''}\right)^4 + j \frac{7}{256} \left(\frac{\epsilon'}{\epsilon''}\right)^5 \\ &+ \frac{21}{1024} \left(\frac{\epsilon'}{\epsilon''}\right)^6 - j \frac{231}{12288} \left(\frac{\epsilon'}{\epsilon''}\right)^7 + \dots \end{aligned} \quad (4.4)$$

The square root of $-j$ can be rewritten as

$$\sqrt{-j} = \frac{1}{\sqrt{2}}(1 - j). \quad (4.5)$$

After multiplying Eq. (4.4) by Eq. (4.5), substituting into Eq. (4.3), and keeping only the imaginary terms, the result is

$$a = \omega \sqrt{\frac{\mu_o \epsilon_o \epsilon''}{2}} \left[1 - \frac{1}{2} \left(\frac{\epsilon'}{\epsilon''}\right) + \frac{1}{8} \left(\frac{\epsilon'}{\epsilon''}\right)^2 + \frac{1}{16} \left(\frac{\epsilon'}{\epsilon''}\right)^3 - \frac{5}{128} \left(\frac{\epsilon'}{\epsilon''}\right)^4 - \frac{7}{256} \left(\frac{\epsilon'}{\epsilon''}\right)^5 + \frac{21}{1024} \left(\frac{\epsilon'}{\epsilon''}\right)^6 + \frac{231}{12288} \left(\frac{\epsilon'}{\epsilon''}\right)^7 + \dots \right] \quad (4.6)$$

This converges when $\epsilon'' > \epsilon'$. For the case where $\epsilon'' \gg \epsilon'$, the equation simplifies to

$$\alpha = \omega \sqrt{\frac{\mu_o \epsilon_o \epsilon''}{2}}.$$

The variables ϵ' and ϵ'' are the real and imaginary parts, respectively, of the permittivity. Both are temperature dependent, but ϵ' varies much less with temperature than ϵ'' does. Using the known values for free space permittivity, $\epsilon_o = 8.854 \times 10^{-12}$ F/m [2], free space magnetic permeability, $\mu_o = 1.256 \times 10^{-6}$ H/m [13], and angular frequency $\omega = 1.54 \times 10^{10}$ rad/sec [1], the equation for attenuation constant for $\epsilon'' \ll \epsilon'$ becomes

$$a = 25.66 m^{-1} \frac{\epsilon''}{(\epsilon')^{\frac{1}{2}}}.$$

The equation for $\epsilon'' \gg \epsilon'$ becomes

$$a = 36.30 m^{-1} (\epsilon'')^{\frac{1}{2}}.$$

The inverse of the attenuation constant is the skin depth, which is the distance a field travels before its strength is reduced to $1/e$ times its strength at the surface. Then for $\epsilon'' \ll \epsilon'$,

$$d_s = a^{-1} = 0.039 \frac{\sqrt{\epsilon'}}{\epsilon''} m,$$

and for $\epsilon'' \gg \epsilon'$,

$$d_s = a^{-1} = \frac{0.0275}{\sqrt{\epsilon''}} m.$$

From the above equations, it is evident that the skin depth decreases as ϵ'' increases. For the case of ZnO in nitrogen, and the temperature range of this experiment, ϵ' ranges from 3.84 to 4.02, while ϵ'' ranges from 0.1 to 23.0. Therefore, the dominant factor in the variation of field attenuation with respect to temperature is ϵ'' . The effect of this field attenuation is to slow down the "thermal wave", because the attenuation factor is strongest at the center and when ϵ'' is highest. For this simulation, the equation for $\epsilon'' < \epsilon'$, Eq (7.2), is used with terms up to the seventh power of (ϵ''/ϵ') for $\epsilon'' < 0.5 \epsilon'$, and the binomial equation for $\epsilon'' > \epsilon'$, Eq (7.6) is used with terms up to the seventh power of (ϵ'/ϵ'') for $\epsilon'' > 2.0 \epsilon'$. At these values, the next term is only 0.005% of the sum. For values of ϵ'' between $0.5 \epsilon'$ and $2.0 \epsilon'$, an interpolation is taken between the two equations.

The distance s is the distance from the surface in the direction normal to the electric field. Since this is a two dimensional model, there are two distances, one in the radial direction, and one in the axial direction. In this model of the field attenuation, the shorter of the two distances is used.

To estimate the electric field at the surface, the equations $\dot{q} = \epsilon_o \epsilon'' \omega \langle E^2 \rangle$ and $E = E_o e^{-\alpha s}$ are combined into one equation $\dot{q} = \epsilon_o \epsilon'' \omega E_o^2 e^{-2\alpha s}$. At the time of the fastest rate of temperature increase, \dot{q} has been estimated in the literature to be about $1.0 \times 10^9 \text{ W/m}^3$ [1]. At this time, ϵ'' is at its peak value of 23, and α is also at its peak of 177.8 m^{-1} . The maximum value of s is 0.007 m. Therefore, $E_o = 62035.0 \frac{\text{V}}{\text{m}}$.

4.3 Properties

The density of the sample is approximately 3000 kg/m^3 [1], and the insulation, 1000 kg/m^3 [1]. Specific heat is $500 \text{ J/(kg } ^\circ\text{C)}$ [1] in both the sample and the insulation. Neither is constant, but they are modeled as constant for this work. The sample does densify during the heating process, but in this temperature range the densification is not that large. According to the literature [13], densification begins at $600 \text{ } ^\circ\text{C}$. Since this experiment never reaches $600 \text{ } ^\circ\text{C}$, the effect of densification was neglected. The thermal conductivity k , is known [1] to be approximately $10 \text{ W/(m } ^\circ\text{C)}$ in the sample. The thermal conductivity of the powder insulation is unknown, but can be approximated from the knowledge of the conductivity of the sample, the conductivity of air, and the relative density of the powder to the sample, as follows. The standard approach for estimating the conductivity of a mixture is to use volume-fraction weighting:

$$k_{mix} = k_s v_f + k_{air} (1 - v_f),$$

where,

$$v_f = \frac{\rho_{mix} - \rho_a}{\rho_s - \rho_a} \approx \frac{1}{3}.$$

Thus,

$$k_{mix} = \frac{1}{3}k_s + \frac{2}{3}k_{air}.$$

Since

$$k_{air} = 0.03 \text{ W/(m } ^\circ\text{C)} \text{ at } 350 \text{ K,}$$

we have

$$k_{mix} = 3.3533 \text{ W/(m } ^\circ\text{C)}.$$

4.4 Thermocouple Model

The thermocouple probe used in this experiment is a shielded Type K thermocouple. Figure 4-6 is a schematic diagram of the probe. The probe has a curved surface, but it is modeled as a cylinder for simplicity. The dimensions of the probe are assumed to be 10% of those of the sample, for a diameter of 0.0031 m, and a height of 0.0017 m. [9]

Two possibilities are considered to model the effect of the probe on the sample. First, the probe is considered not to be in contact with the sample, so there is no heat flow between the sample and the probe as shown in Figure 4-7. Second, the probe is considered to be in contact with the sample, as in Figure 4-8.

If the probe is not in contact with the sample, there is no heat conduction between the sample and the probe. Therefore the interface between the sample and the probe is modeled as an insulated boundary.

To model the probe as not in contact with the sample, the boundary condition used for the interface between the probe and the sample is the same as the one used for the radial and axial axes.

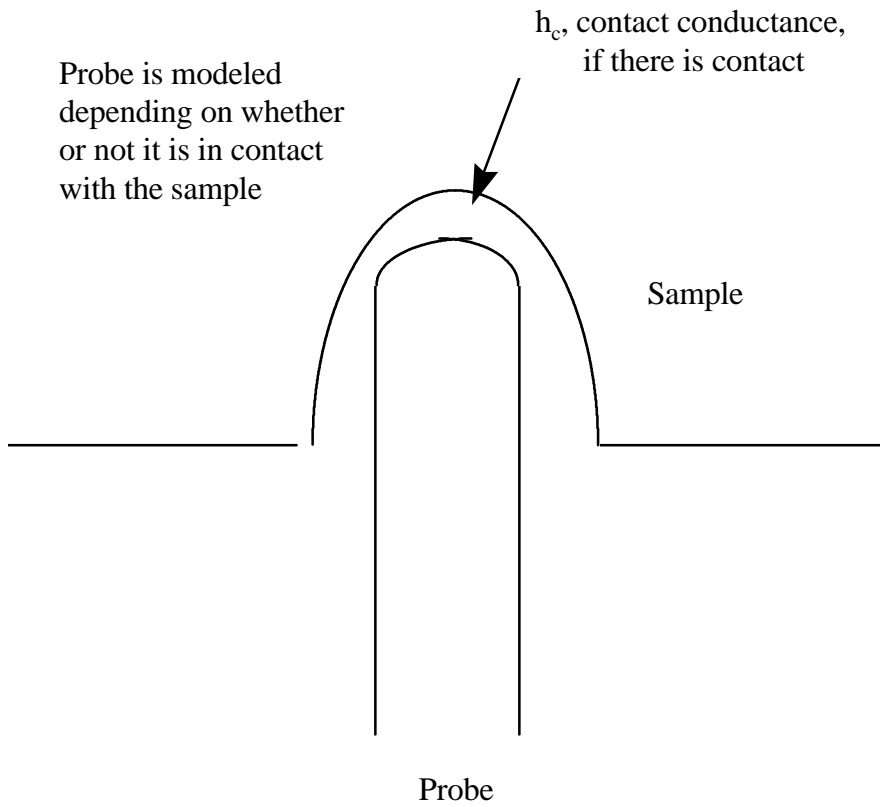


Figure 4-6: Schematic of the thermocouple probe.

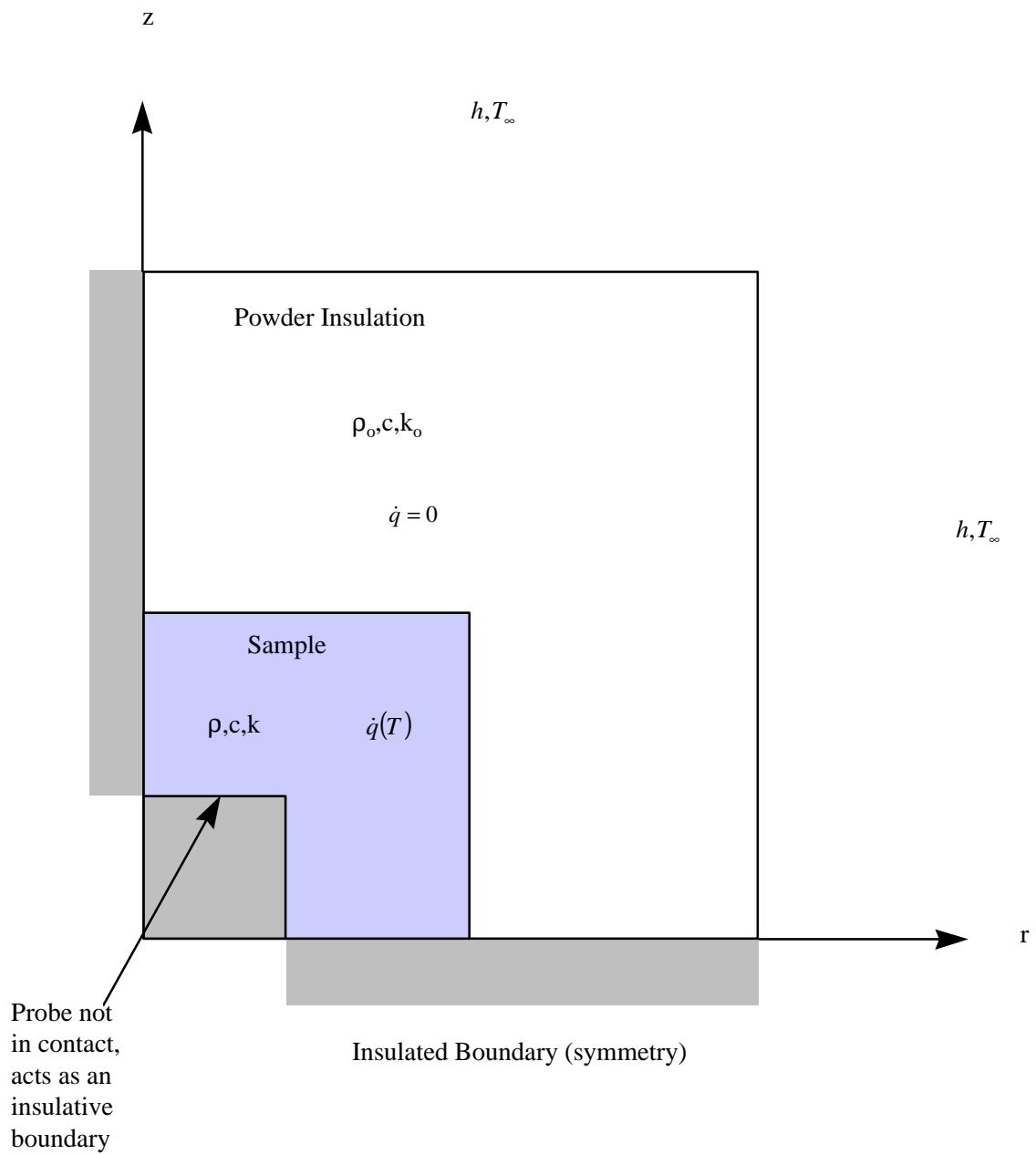


Figure 4-7: Model of the thermocouple probe not in contact with the sample.

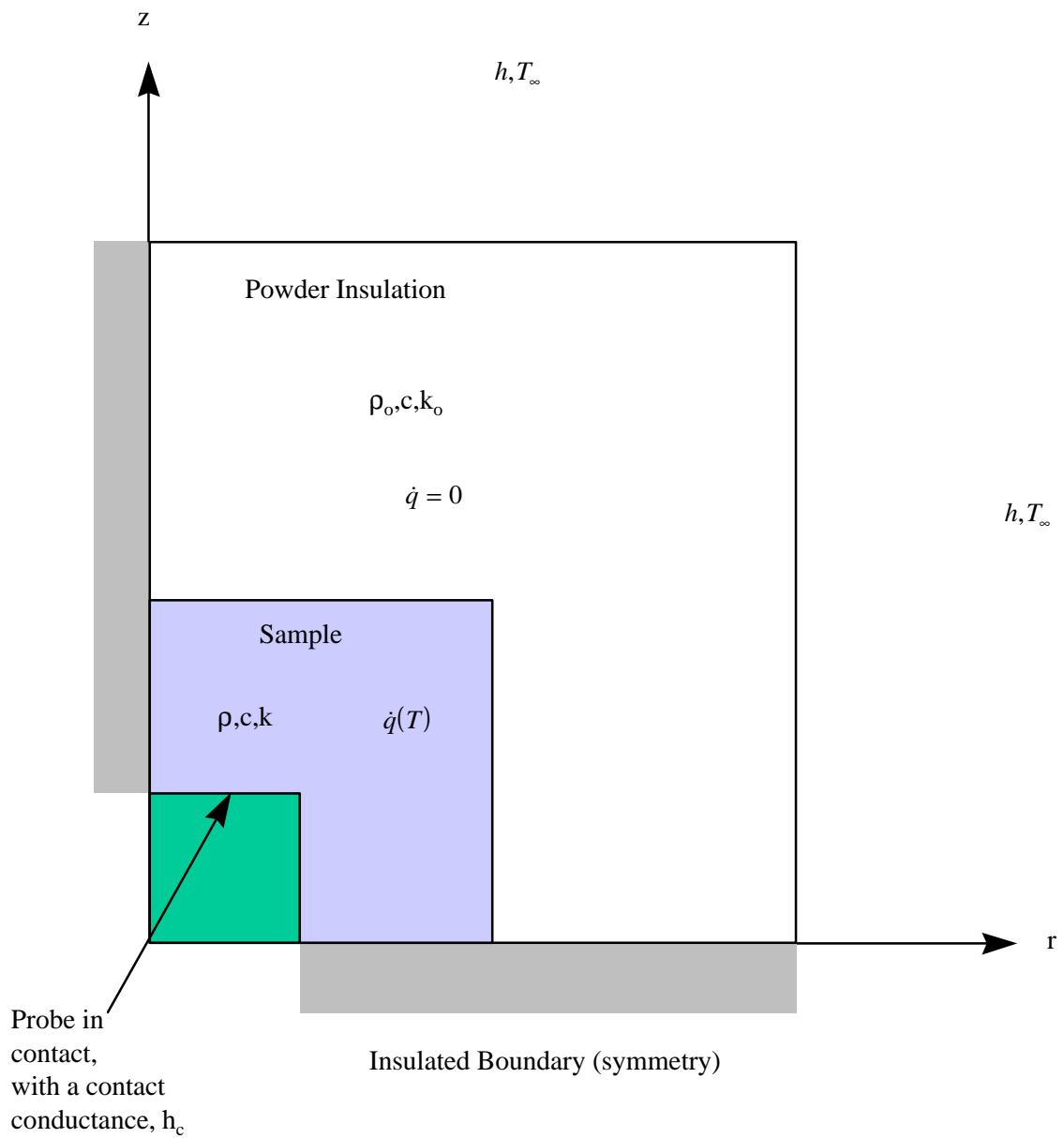


Figure 4-8: Model of thermocouple probe in contact with the sample.

If the probe is assumed to be in contact with the sample, then there must be some conduction between the sample and the probe. The quantity of heat flow is proportional to the difference in temperature between the sample and the probe. The temperature of the probe increases during the experiment, but to be conservative the probe is treated as a constant temperature region.

To model the probe as in contact with the sample, the boundary condition used for the interface between the probe and the sample is the same form as the boundary condition used for the interface between the insulation and the enclosure. Choosing the value of the contact conductance is the major difficulty. A range of values was surveyed to see what effect the various coefficients have on the overall temperature.

4.5 Solution Technique

In the experiment modeled [9], the ZnO sample is a cylinder of diameter 0.031 m, and height of 0.017 m. It is packed in a layer of ZnO powder insulation, surrounded by an alumina enclosure. The entire system is surrounded by a 0.1 m by 0.2 m enclosure. (Figure 3-1).

The sample is modeled as a two dimensional cylinder with temperature dependent internal heat generation, as well as temperature-dependent thermal properties. It is symmetric with respect to the radial and axial directions, and there is no heat conduction in the angular direction. The powder insulation is treated simply as an extension of the cylinder, with a lower density, and a dielectric loss constant of zero. The interface between the powder and the enclosure wall is treated as a convection boundary into constant temperature surroundings. The r and z axes can both be treated as insulated boundaries, because of symmetry. (Figure 4-1). The temperature distribution is governed by the thermal conduction equation,

$$c_p \rho \frac{\partial T}{\partial t} - \nabla \cdot (k \nabla T) = \dot{q} \quad (4.8)$$

where c_p is specific heat capacity, ρ is density, k is thermal conductivity, and \dot{q} is volumetric heat generation.

4.6 Finite-difference method

Because heat generation by microwave absorption is temperature dependent, *Eq. (4.8)* cannot be solved analytically. Therefore, a numerical technique is necessary. The finite-difference method is used for this work. This approach divides the problem into many nodes, each within a very small control volume, and uses an energy balance on each to get a system of equations and unknowns. A discrete time interval is used, thus the system of

equations is algebraic. The system of equations is then solved with some form of Gaussian elimination, or a similar scheme for solving systems of large equations. For a problem with temperature-dependent properties, an iterative approach is used at each time step. First, a guess is taken for the temperature at each node, and used to evaluate the properties. For convenience, the first guess is taken to be the temperature at the previous time step. Then new temperatures are calculated from these properties, and used to evaluate the properties for the next iteration. This process is repeated until the temperature at two iterations are the same, within a specified tolerance.

The cylinder in this experiment can be divided into several small discrete intervals. An energy balance is performed at each node, according to the basic equation,

$$\text{Change in Energy stored} = \text{Heat in} - \text{Heat out} + \text{Heat generated.} \quad (4.9)$$

For a general node, we get

$$\begin{aligned} \dot{q}V + k_m^- A_m^- \left(\frac{T_{m-1,n} - T_{m,n}}{\Delta r} \right) + k_m^+ A_m^+ \left(\frac{T_{m+1,n} - T_{m,n}}{\Delta r} \right) + k_n^- A_n^- \left(\frac{T_{m,n-1} - T_{m,n}}{\Delta z} \right) + k_n^+ A_n^+ \left(\frac{T_{m,n+1} - T_{m,n}}{\Delta z} \right) \\ = \rho c_p V \frac{\partial T}{\partial t} \end{aligned}$$

When the boundaries are considered, this leads to nine different types of equations, a general equation for an interior node, and eight boundary equations. The difference between the insulation and the sample is only in the properties, not the equations. The complete derivations for the finite-difference equations, done by the explicit, implicit, and ADI methods are given in Appendix B.

Next, the equations must be discretized in time. There are two traditional ways of doing this, the explicit method and the implicit method. Another option is the Alternating Direction Implicit(ADI) [2] method, which is a combination of the two. All three methods use the equation $\partial T/\partial t = [T(t+\Delta t) - T(t)]/\Delta t$ to substitute for the energy storage term. However, the other terms also depend on temperature, and it must be decided at what time the spatial temperature derivative is evaluated. Each method has its particular way of dealing with this issue.

4.6.1 Explicit

The explicit method takes all the spatial temperature derivatives at time t, the beginning of the time step. This is the simplest method, but often leads to instability in calculations, unless the time step is very small. For this reason, this method is not used.

4.6.2 Implicit

The implicit method takes all the spatial derivatives at time $t + \Delta t$. Most of the equations then have five unknowns, leading to a sparse coefficient matrix with five non-zero diagonals, and the rest of the matrix all zero. A sparse matrix solver, such as y12m [4], can be used to solve this system fairly efficiently.

The implicit method creates at most five unknowns for each equation, and at fewest three unknowns, for a pentadiagonal coefficient matrix. The non-zero elements are stored in a one dimensional array, with two parallel arrays to store the row number and the column number. Then the subroutine y12maf solves the system of equations.

4.6.3 Alternating direction implicit (ADI) method

The alternating direction implicit(ADI) method breaks the problem up into two alternating time steps. The first step takes the spatial derivatives implicitly in one direction, and explicitly in the other. For the second, the pattern is reversed. In this case, for the first time step the radial direction spatial derivatives are taken implicitly, and the axial direction spatial derivatives are taken explicitly. For the second time step, the axial direction spatial derivatives are taken implicitly, while the radial direction spatial derivatives are taken explicitly.

All of the equations in the system resulting from ADI have three or fewer unknowns, leading to a "tridiagonal matrix", i.e., all elements are zero except for those on the main diagonal and the two diagonals adjacent to the main diagonal. This allows the use of the Thomas Algorithm, and much less computing time.

4.6.4 Comparison of the ADI and implicit methods

The Alternating Direction Implicit method is clearly faster than the implicit method at any given time step. This is because the ADI method results in a tridiagonal coefficient matrix, which can be solved by the Thomas algorithm. The implicit method results in a pentadiagonal matrix, and is solved by a sparse matrix solver. The results of the ADI method and the implicit method are identical. The disadvantage of the ADI method is that it has a limiting time step for stability, while the implicit method does not. In this problem, the ADI method is stable for time steps of at least one second. The ADI method is the better choice because it is just as accurate, and several times faster than the implicit method. The following table shows the computer time for an IBM P70 RISC workstation to simulate 120 seconds of real time in this experiment.

Time Step (sec)	Computer time, ADI (sec)	Comp. time, Implicit (sec)
0.01	365	10323
0.025	251	4552
0.1	85	1245
0.5	26	311.3
1.0	15	138
1.2	11	113
2.0	7	70

4.7 Computer program

Once the equations were derived, two FORTRAN programs were written to solve the system numerically. The ADI method produces two sets of equations. The program goes through each node, and calculates the coefficients at each node. In the first section, the program starts at the center and goes through the nodes in the radial direction at each height. It does this with a radial loop nested inside an axial loop. The second part nests an axial loop inside a radial loop. Once the coefficients are calculated, the Thomas Algorithm is used to solve the system of equations. The implicit program has one set of equations, and uses the sparse matrix solver y12maf [4] to solve the system of equations.

The program divides the sample and insulation into 2601 nodes, using a 51 x 51 grid(0:50,0:50). This leads to 2601 equations with 2601 unknowns. Since the sample has temperature-dependent properties, a guess must be taken at each temperature. Initially, the guess is the temperature at the beginning of the time step. After the equations are solved, the coefficients are calculated again using the updated temperatures to evaluate the properties. This process is repeated until the calculated temperatures are sufficiently close to the temperatures calculated in the previous iteration.

The thermocouple probe is assumed to occupy m_0 by n_0 nodes of the sample, therefore nodes that are from 0 through m_0 in the r direction and from 0 through n_0 in the z direction are replaced by the probe. This is handled by changing the program so that no heat flows from node m_0 to node $m_0 + 1$ for the non-contact probe, and $h_c(T - T_\infty)$ flows across for the contact probe. The nodes represented by the probe are not used; they are just left in as place-holders so the program can keep the same form. The actual FORTRAN code is shown in Appendix C.

4.8 Lumped Capacitance Constant Property Model

In order to test the accuracy of the numerical solution, it is useful to have an analytic solution. For the analogous problem with constant properties and heat generation, a simple lumped capacitance model can be used to find an analytic solution. Two cases are

presented in this section. The first is the simple case of a perfectly insulated sample, i.e., the thermal conductivity is equal to zero. The second case treats the insulation as a thermal resistor, with a constant surface temperature T_∞ .

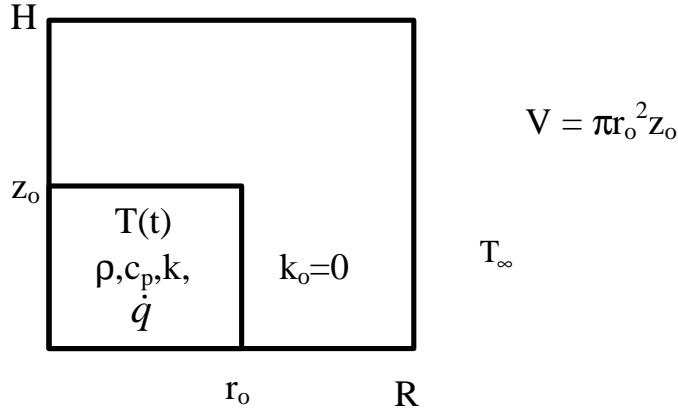


Figure 4-9: Constant heat generation lumped capacitance model, fully insulated.

The model for a constant property, constant heat generation problem can be solved by a simple energy balance. Since no heat flows into or out of the sample, the heat energy balance is given by

$$\dot{q}V = \rho c_p V \frac{dT}{dt},$$

with the initial temperature equal to that of the surroundings, T_∞ . The solution to this equation is

$$T = T_\infty + \frac{\dot{q}}{\rho c_p} t. \quad (4.7)$$

The finite-difference simulation is then run with constant properties and heat generation, and the conductivity of the insulation is set to zero.

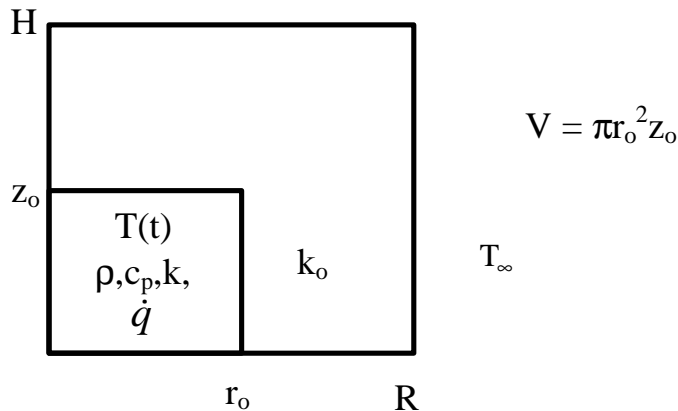
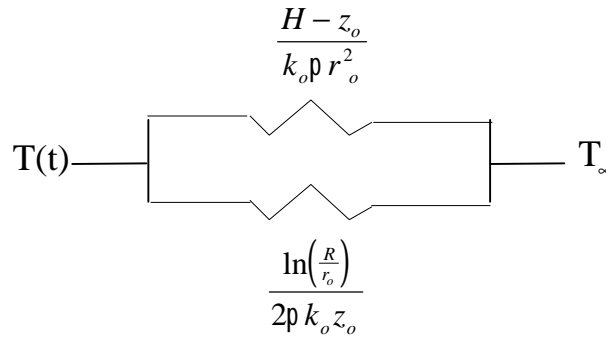


Figure 4-10: Constant heat generation lumped capacitance model, imperfectly insulated.

The model for the case where the insulation is imperfect, and has a thermal conductance, k_o , is shown in Figure 4-10. This can be approximated by treating the insulation as a thermal resistor.

The thermal resistance, R_s , is found from the equation



$$R_s^{-1} = \left(\frac{\ln\left(\frac{R}{r_o}\right)}{2\rho k_o z_o} \right)^{-1} + \left(\frac{H - z_o}{k_o \rho r_o^2} \right)^{-1}$$

Then a simple energy balance yields

$$\dot{q}V - \frac{(T(t) - T_\infty)}{R_s} = \rho c_p V \frac{dT}{dt}$$

The solution to the differential equation is

$$T(t) = T_\infty + \dot{q}VR_s \left[1 - e^{(-t/(\rho c_p VR_s))} \right] \quad (4.7)$$

This equation is used to test the finite-difference simulation. The simulation is run with all properties, including heat generation, constant.

Chapter 5: Results from the Model Calculations

5.1 Simulation results assuming uniform constant properties

In order to determine the accuracy of the computer model, an analytical solution is useful. The lumped capacitance solutions for the analogous constant property, constant heat generation problem were derived in section 4.8. Thus the simulation can be compared to the analytical solution for accuracy. In the first case, a perfectly insulated sample is assumed. The lumped capacitance model predicts that the temperature rises according to

$$T(t) = T_{\infty} + \frac{\dot{q}}{\rho c_p} t. \quad (4.7)$$

Figure 5-1 is a plot of this equation along with the temperature response predicted by the finite-difference simulation, when properties and heat generation are constant. The simulation predicts the same temperature response for every node in the sample, as expected, so any node can be used to be compared to Eq (4.7). The core temperature response calculated by the simulation is shown in Figure 5-1, along with the graph of Eq. (4.7) for a volumetric heat generation of $5.0 \times 10^6 \text{ W/m}^3$. The predicted temperatures are virtually identical, as expected. This helps to verify the accuracy of the model, as well as the program.

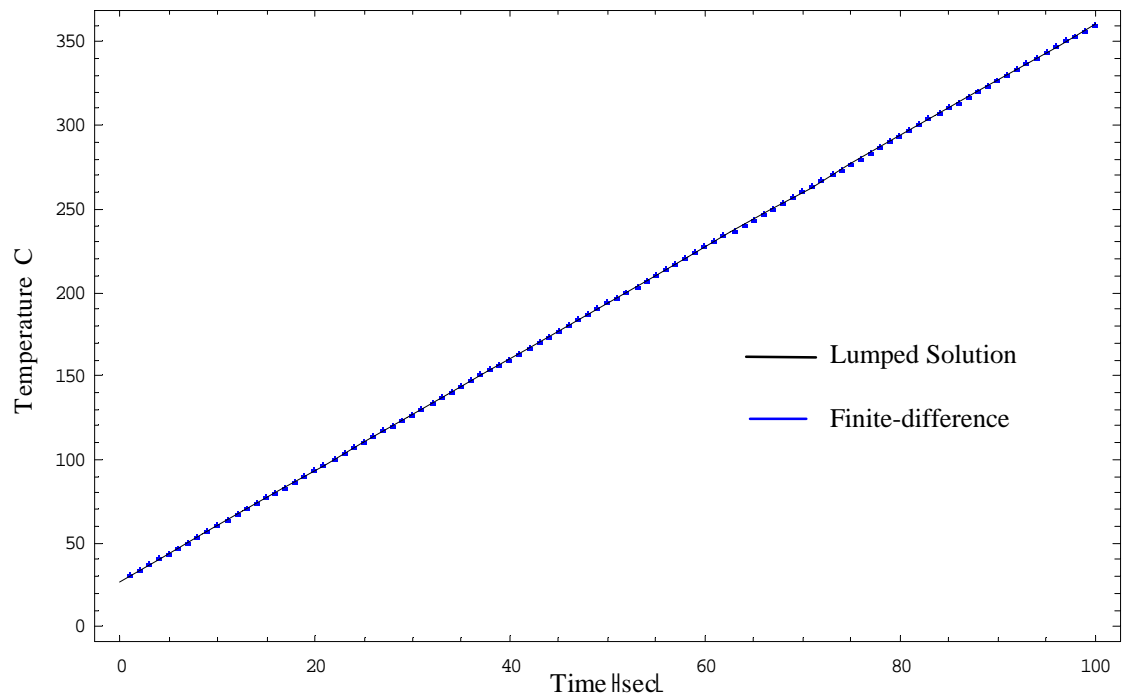


Figure 5-1: Constant heat generation, fully insulated temperature response, lumped capacitance solution vs. finite-difference computed solution.

The second lumped capacitance model derived in section 4.8 shows the more realistic case where the sample is imperfectly insulated. The lumped capacitance solution finds an average temperature for the sample, instead of the local temperature that is found by the computational solution. The lumped capacitance solution predicts a temperature response of

$$T(t) = T_{\infty} + \dot{q}VR_s \left[1 - e^{-t/(\tau c_p VR_s)} \right]. \quad (4.8)$$

Figure 5-2 is a plot of the sample core and surface temperatures calculated by the finite-difference simulation, along with the average sample temperature predicted by the lumped capacitance model, Eq. (4.8).

The lumped capacitance model predicts a temperature response that falls between the core and surface temperature predicted by the finite-difference simulation, and follows the same time pattern. It is closer to the core temperature, which is also expected. The average temperature should be closer to the core temperature than the surface temperature, because of surface heat losses.

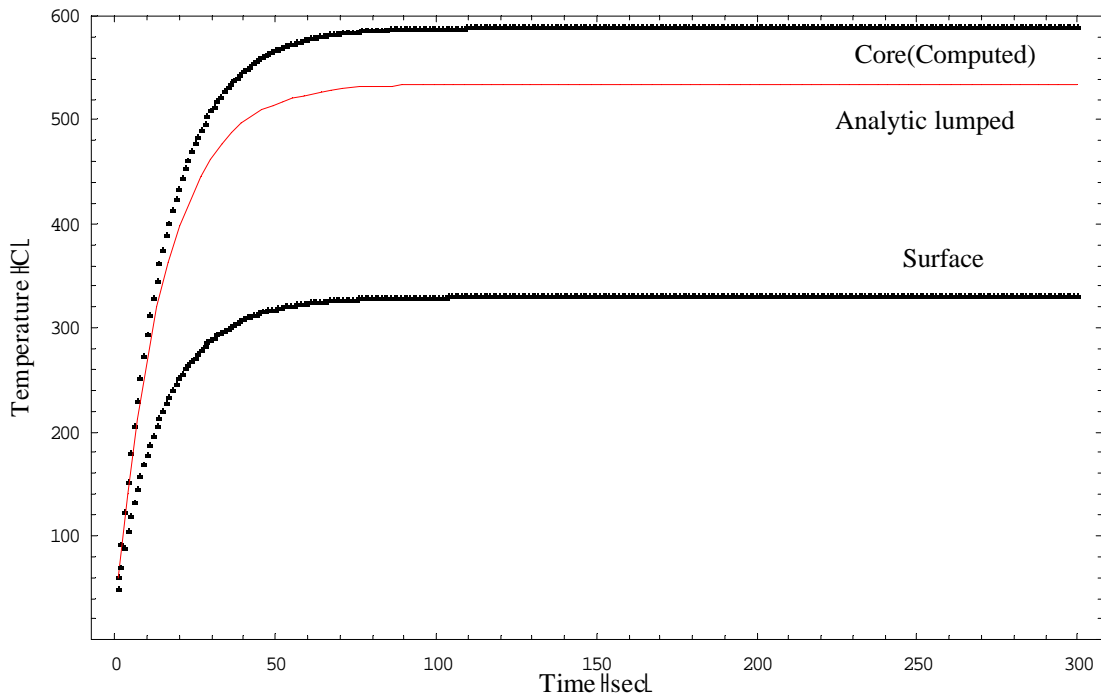


Figure 5-2: Constant heat generation, partially insulated, lumped capacitance vs. computed temperature response.

5.2 Simulation results from the uniform field strength model

Figure 5-3 shows that when the ZnO sample is heated in air, the simulation yields a steady-state core temperature of approximately 160 °C, approximately the same as the experimental result. The simulation predicts a faster time response than was observed in the experiment.

The steady-state temperature at the core of the ZnO sample heated in a nitrogen atmosphere in the experiment is approximately 560 °C (Figure 3-3), and for the simulation done with the uniform electric field assumption, it is 550 °C (Figure 5-4). The most striking feature of the experiment is the thermal wave, which occurred at temperatures of approximately 230 °C in both the experiment and the simulation. However, the simulation predicts a much faster temperature response than the experiment produced.

The only difference between the model in air and the model in nitrogen is the data for imaginary permittivity. This shows that the imaginary permittivity is the driving factor behind the thermal wave. However, it does not explain the two anomalous peaks in imaginary permittivity in ZnO in the absence of oxygen. This unusual behavior is believed to be caused by chemical reactions in the ZnO [9], which can be included in heat generation and kinetic loss.

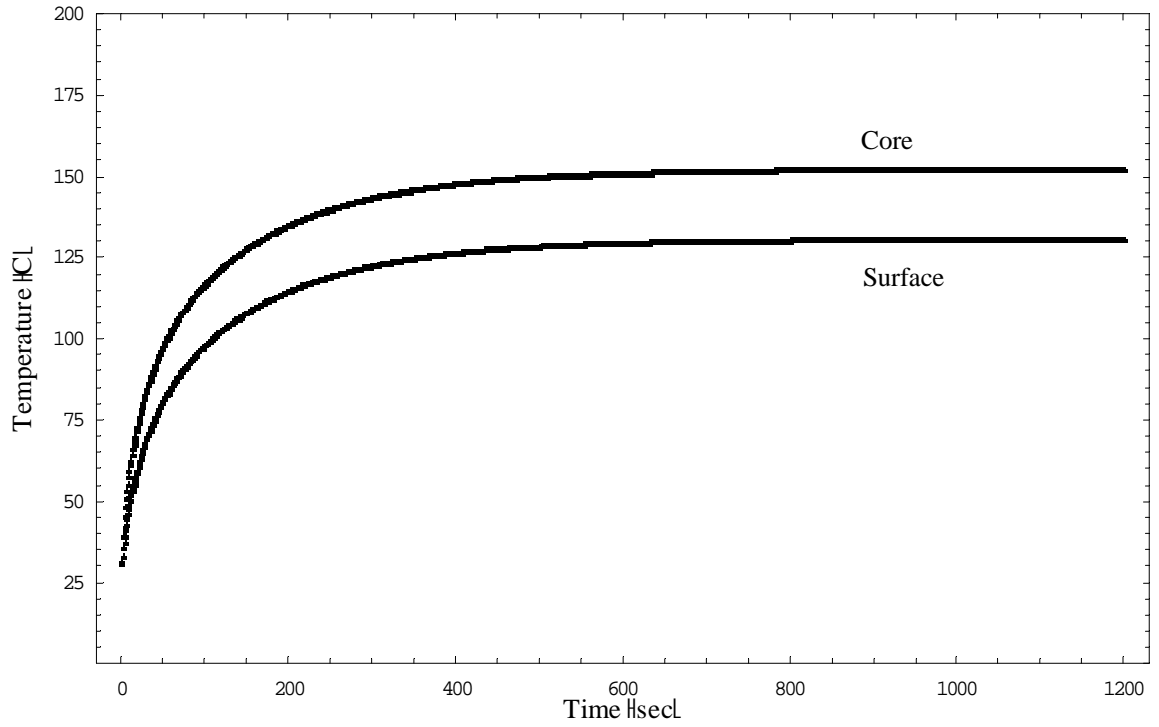


Figure 5-3: Computed core and surface temperature response of ZnO heated in air atmosphere with uniform constant field strength.

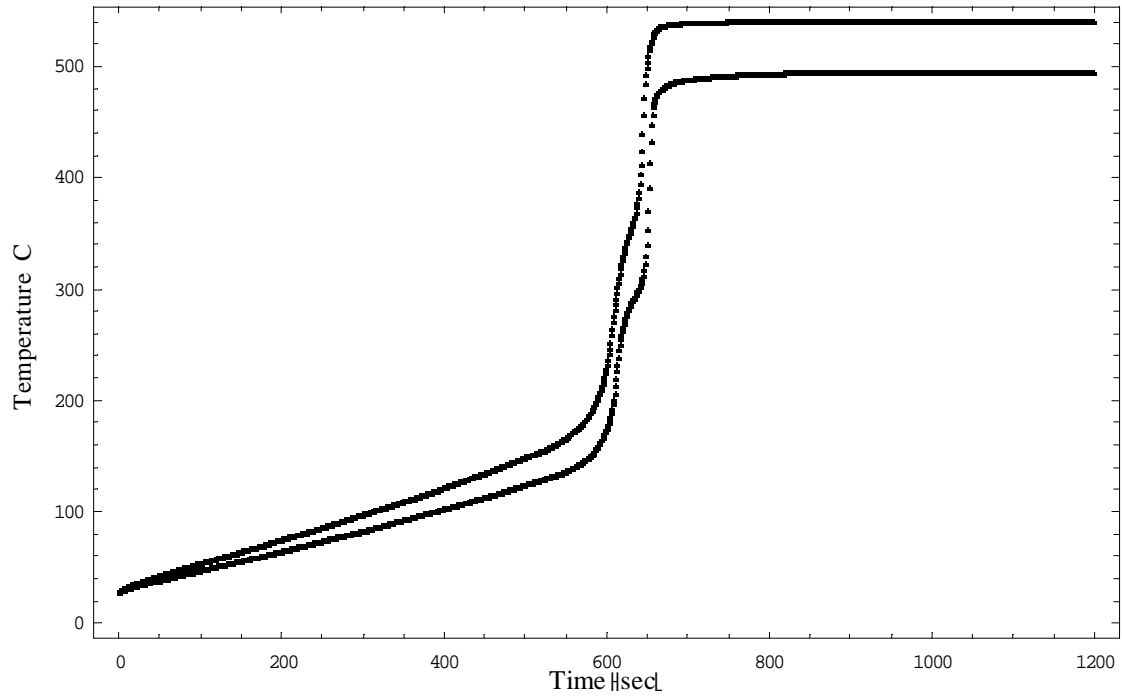


Figure 5-4: Computed core and surface temperature response of ZnO microwave heated in nitrogen atmosphere with uniform constant field strength.

5.3 Simulation results of model with electric field attenuation

Figure 5-5 shows the simulated temperature response of the core and surface of the ZnO sample in an air atmosphere, when attenuation is considered. Figure 5-6 compares this response to the simulated constant field response. There is some difference, but it is very small ($<0.1\%$), so neglecting attenuation would be a reasonable assumption for a ZnO sample of this size in an air atmosphere. This could have been predicted by the calculation that the skin depth is much larger than the sample.

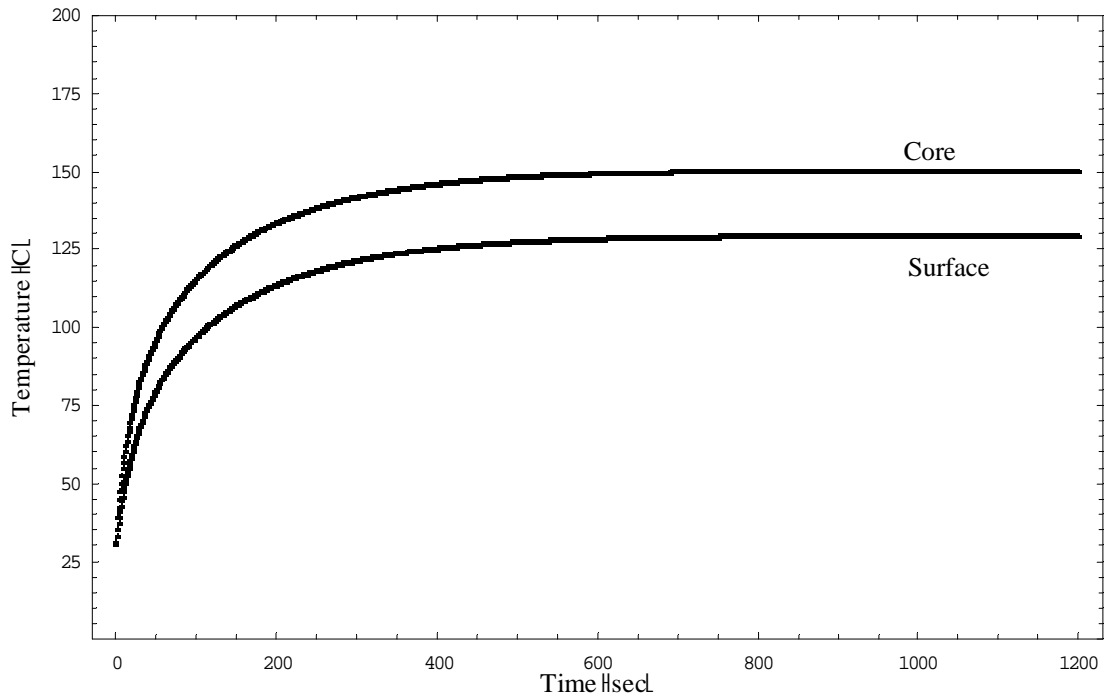


Figure 5-5: Computed core and surface temperature response of ZnO heated in air atmosphere with field strength attenuated exponentially from the surface.

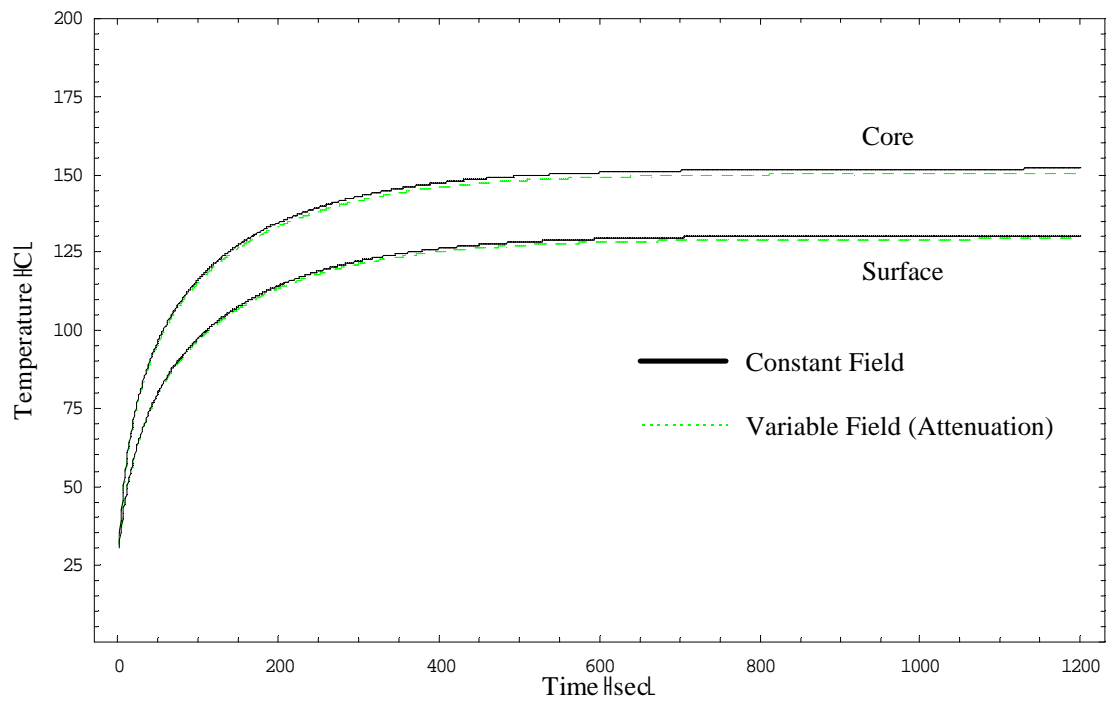


Figure 5-6: Computed core and surface temperature response of ZnO heated in air, with constant field strength (solid black), and attenuated field strength (dashed green).

The experimental results for ZnO heated in air[9] are shown in Figure 3-2, which is reproduced in Figure 5-7 along with the simulation results. Both the experiment and the simulation result in exponential temperature responses. The simulation predicts a faster time response, but approximately the same steady state temperature.

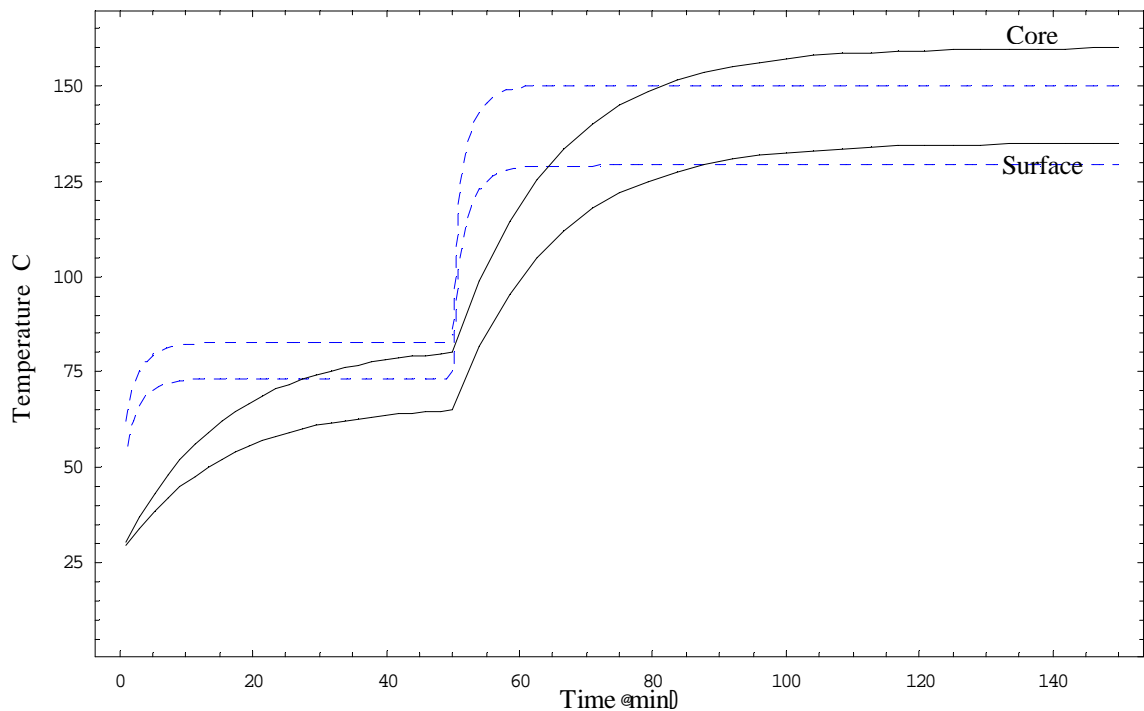


Figure 5-7: Calculated (blue-dashed) and experimental (black-solid) temperature response of ZnO during microwave heating in air, with a stepped input power of 40 W for the first 50 minutes and 80 W thereafter.

For ZnO in a nitrogen atmosphere, the skin depth is less than the radius and the height of the sample, therefore field attenuation should play a large role in the temperature response. The simulation verifies this. Figure 5-8 is the temperature response predicted by the simulation with attenuation included. Figure 5-8 and Figure 5-4 look similar, but are on different time scales. Figure 5-9 shows Figures 5-4 and 5-8 on the same time scale to show the effect of electric field attenuation. When the effect of electric field attenuation is included, the simulation result resembles the data more closely. The final steady state temperature is approximately 530 °C, and the time is on the same order of magnitude as the experiment. The measured experimental temperature response of zinc oxide during microwave heating in a nitrogen atmosphere, is plotted in Figure 5-10 along with the results of the finite-difference simulation.

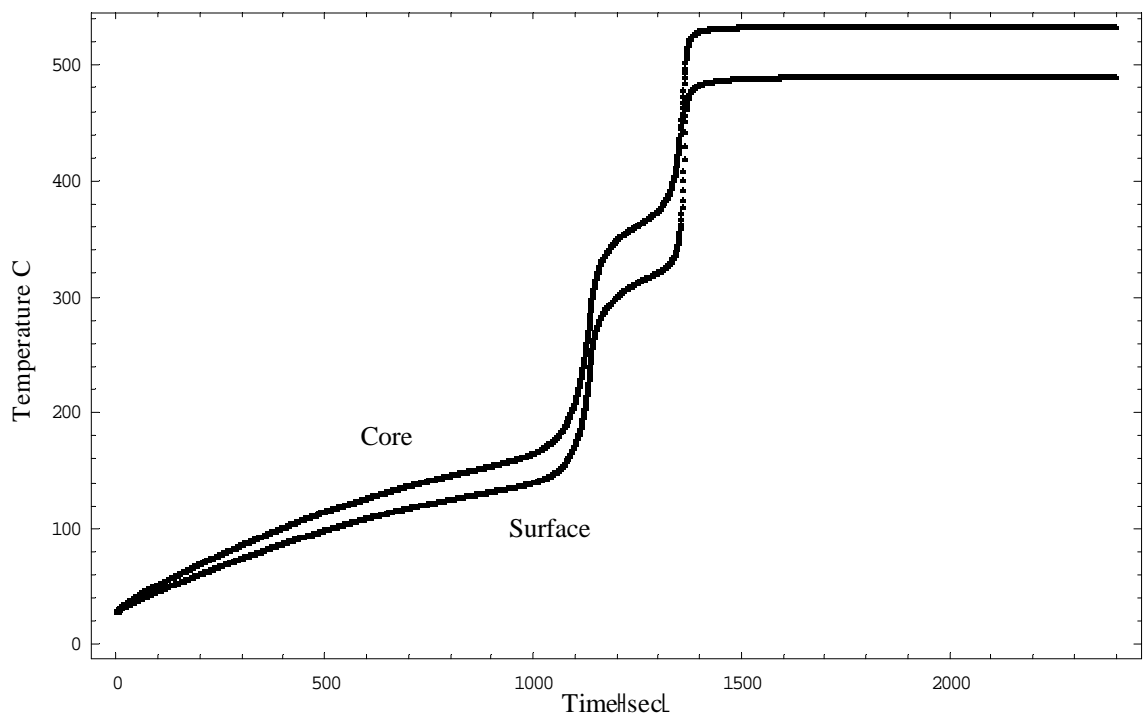


Figure 5-8: Computed core and surface temperature response of ZnO microwave heated in nitrogen atmosphere with attenuated field strength.

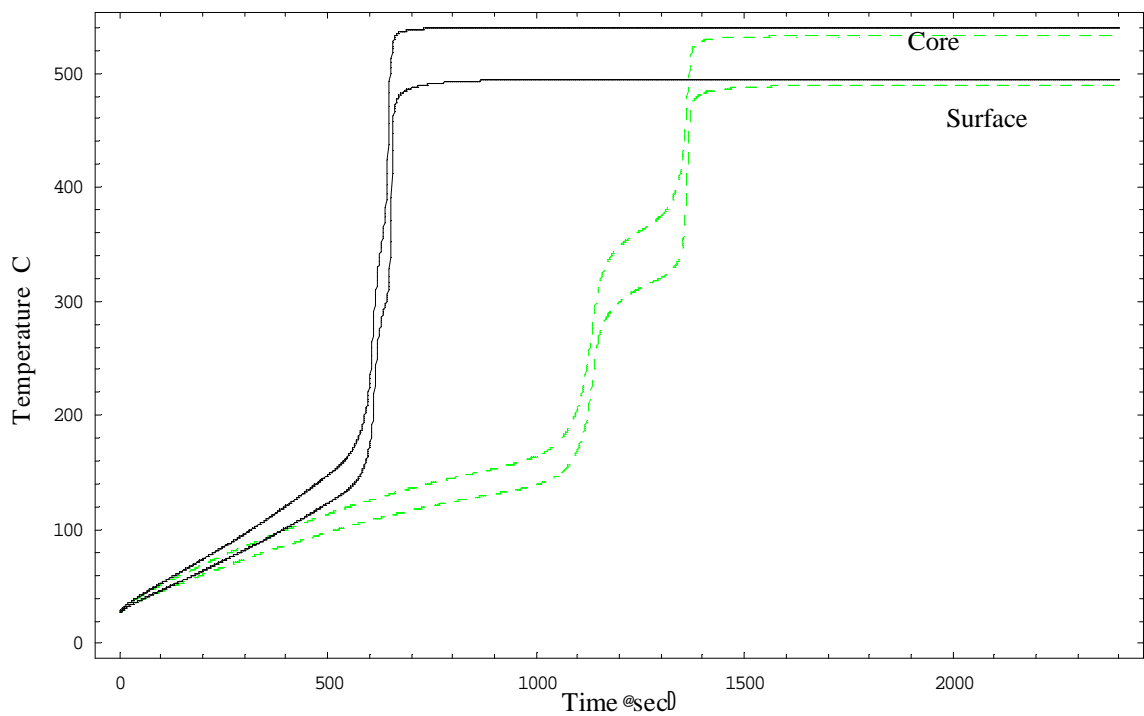


Figure 5-9: Computed core and surface temperature response of ZnO heated in air, with constant field strength (solid black), and attenuated field strength (dashed green).

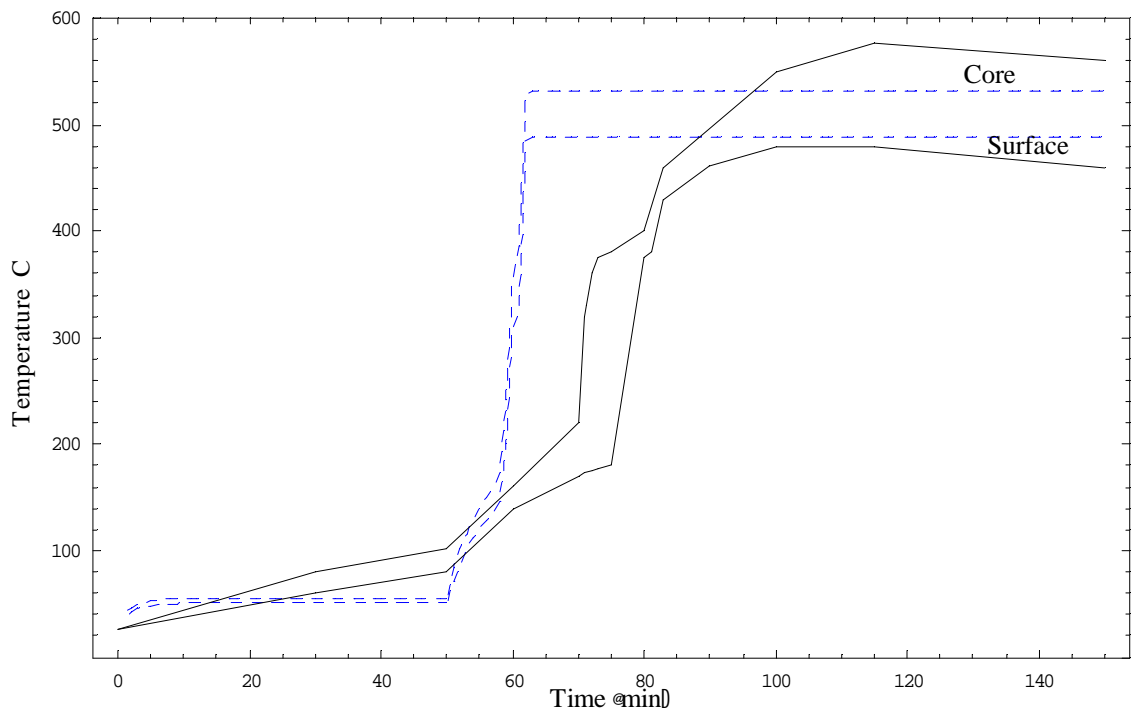


Figure 5-10: Calculated (blue-dashed) and experimental (black-solid) temperature response of ZnO during microwave heating in nitrogen, with a stepped input power of 40 W for the first 50 minutes and 80 W thereafter.

Figure 5-10 compares the simulation to the experimental data for the nitrogen atmosphere. The “thermal wave” is not nearly as pronounced in the simulation as in the experiment. The model used for the electric field is an approximation, which could partly explain the disparity. The imaginary permittivity is dependent on the heating rate, which varies over time. The data used in this work was for a constant heating rate of 15 °C/min. More tabulated data for imaginary permittivity at different heating rates could potentially produce simulation results closer to the experimental results. This would require an iterative process based on the rate of temperature change as well as the temperature. There is no guarantee that such an iteration would converge.

Plots of the radial temperature distribution along the $z = 0$ axis at various times are included for further clarification. For the air case, shown in Figure 5-11, there is a deceleration of the rate of temperature increase as steady state is approached. A temperature gradient is established early, and remains approximately constant thereafter. When ZnO is in a nitrogen atmosphere, as shown in Figure 5-12, there is an acceleration of the rate of temperature increase during the “thermal wave”.

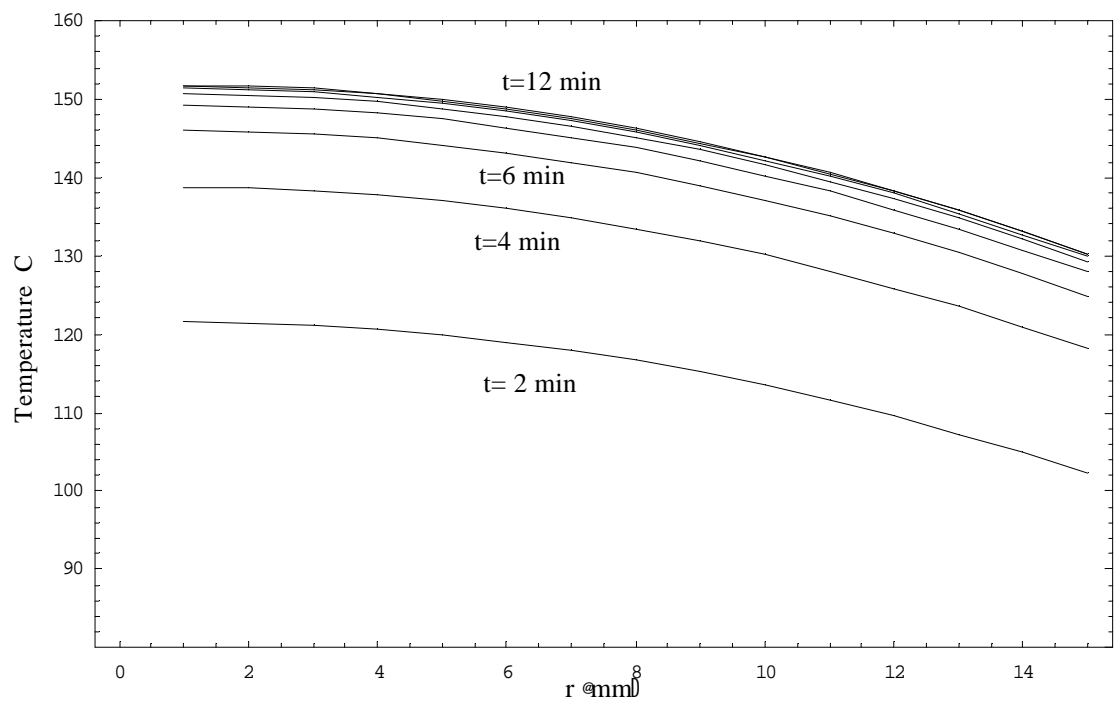


Figure 5-11: ZnO microwave heated in air atmosphere, temperature versus radius at $z=0$ at various times.

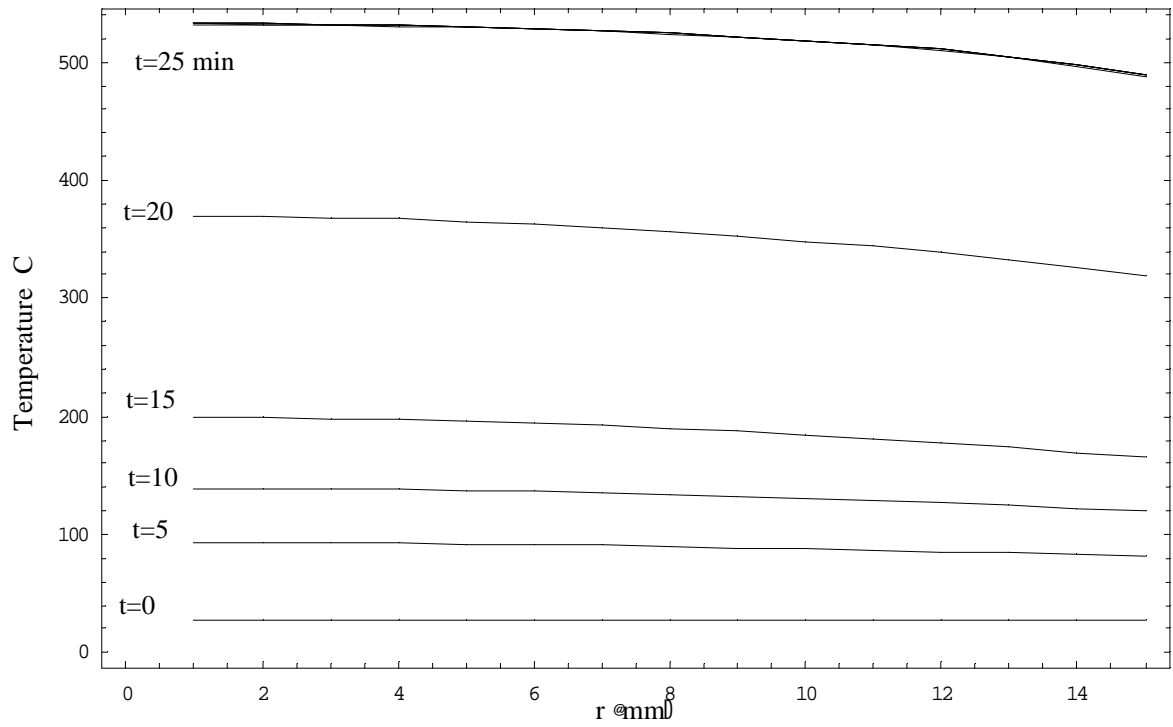


Figure 5-12: ZnO microwave heated in nitrogen atmosphere, temperature versus radius at $z=0$ at various times.

5.4 Effect of the probe on the results

The effect of the thermocouple probe on the temperature of the sample was studied as discussed in section 4.4 of this work. The results are shown in Figures 5-13 and 5-14. First, Figure 5-13 is a comparison between the temperature response found by the general simulation and the temperature response found by the simulation with the probe modeled as if it is not in contact with the sample. The difference is very small, though noticeable on the graph. Figure 5-14 is a comparison between the general case and the case of the probe modeled as in contact with the sample. Two different values for the contact conduction coefficient are shown. The difference is so small that the graphs look identical. Since these two models cover the limiting cases, it can be concluded that the probe has little effect on the temperature of the sample. This work makes no attempt to determine if the thermocouple is measuring the true temperature of the sample.

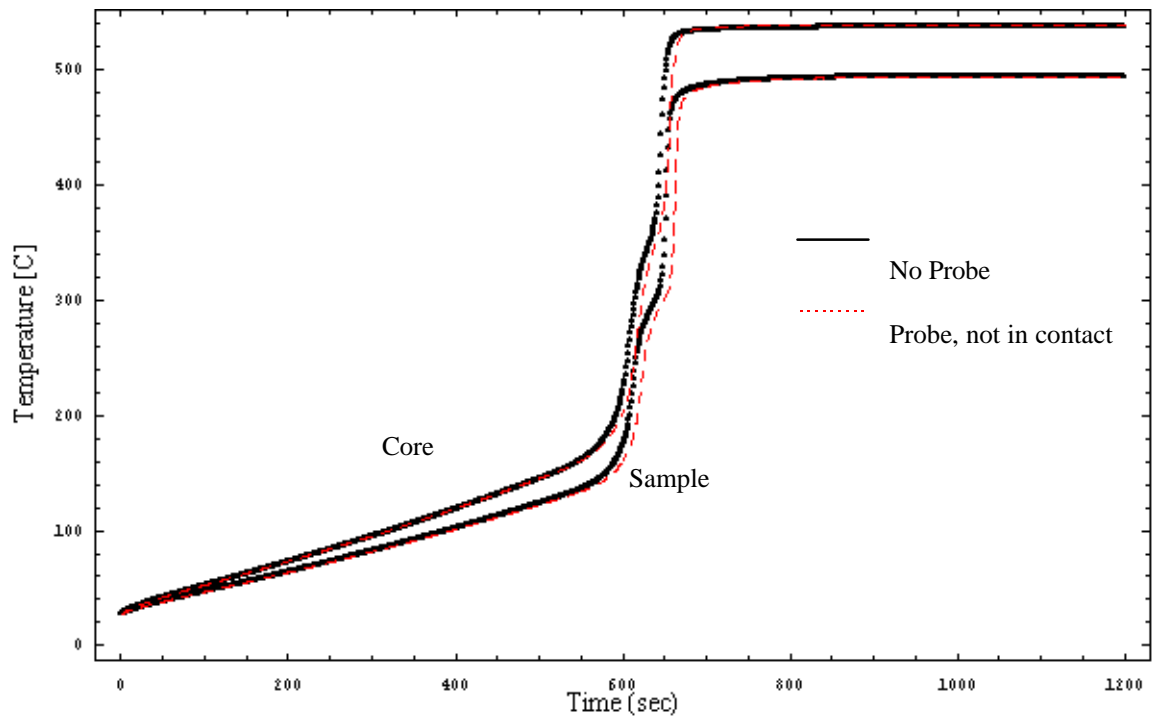


Figure 5-13: Effect of the thermocouple probe on the temperature response, assuming the probe is not in contact with the sample.

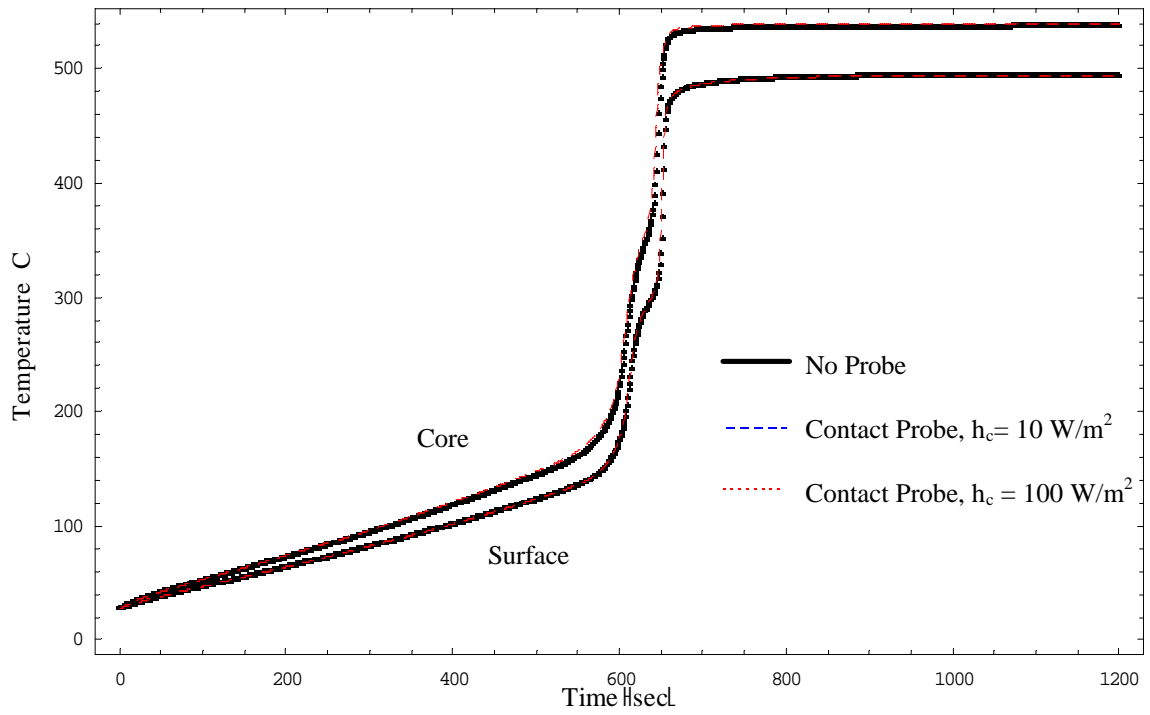


Figure 5-14: Effect of the probe on the results assuming the probe is in contact with the sample.

Chapter 6: Conclusions and Recommendations for Further Work

The simulation predicts a temperature response in qualitative agreement with the measured thermocouple results. The "thermal wave" that occurs in the nitrogen atmosphere is confirmed by the mathematical model. It begins at about 230 °C in both the experiment and the model. The temperature dependence of the imaginary permittivity (dielectric loss) ϵ'' is the primary controlling factor. The sharp peaks in ϵ'' at about 230 °C and 450 °C in a nitrogen atmosphere lead to the thermal wave. The constant electric field assumption predicts faster heating than the experiment. The effect of electric field attenuation is to slow the rate of temperature increase, particularly at large values of ϵ'' . As ϵ'' increases, the attenuation constant increases, causing the local electric field to decrease. This cancels out some of the effect of the sharp increase in ϵ'' , because volumetric heat generation is proportional to both imaginary permittivity and the square of the electric field. The attenuation constant is also highest at the sample center, where the thermal wave starts, further mitigating the effects of the temperature dependence of ϵ'' . However, the attenuation of the electric field is still not enough to prevent the thermal wave from occurring. When attenuation is considered, the simulation is closer to the experimental data. The simulation results indicate that the thermocouple probe has a negligible effect on the temperature of the sample.

The value of this work is that minor modifications to the computer model could be used to predict the results of similar experiments without having to run costly experiments. Also, the computer model provides the ability to predict temperatures throughout the sample, providing much more information than that provided by two thermocouples. This would aid in prediction of the final properties of the sintered sample.

There are several ways in which the simulation could be improved. More data points for imaginary permittivity might improve the accuracy of the simulation. Also, the model in this work did not take into account the effect of densification of the sample. As the temperature increases, the sample's density increases, and the volume decreases. A model that takes into account the effects of densification should be more accurate. The field strength at the surface of the sample is assumed to be constant, although in reality field strength probably varies with time. The electric field attenuation in this work is an estimate, and further work could be done in this area. This would require a full simulation of the electric field in the microwave cavity, necessitating solution of Maxwell's field equations. Combining microwave and conventional sintering may lead to more uniform temperatures during heating, and more uniform final properties of the final sample. Study of this hybrid heating approach would require only minor modifications to this work, and could predict the proper combination of convection and microwave heating to achieve the most uniform heating.

References

1. Gershon, D., D. Dadon, Y. Carmel, K.I. Rybakov, R. Hutcheon, A. Birman, L.P. Martin, J. Calame, B. Levush, M. Rosen. 1996. Observation of an Electromagnetically Driven Temperature Wave in Porous Zinc Oxide During Microwave Heating. Pp. 507-512 in Materials Research Society Symposium Proceedings, Vol. 430, Microwave Processing of Materials V. M.F. Iskander, J.O. Kiggins, Jr., J.C. Bolomey, eds. Pittsburgh, Pennsylvania: Materials Research Society.
2. National Research Council (U.S.). Committee on Microwave Processing of Materials: An Emerging Industrial Technology. 1994. Microwave Processing of Materials. National Academy Press. Washington, D.C.
3. Hutcheon, M., F. Adams, G. Wood, J. McGregor, and B. Smith. 1992. A System for Rapid Measurements of RF and Microwave Properties up to 1400 °C. Pp. 93-99 in Journal of Microwave Power and Electromagnetic Energy, Vol. 27, No. 2. R.V. Decareau, ed. Clifton, VA: International Microwave Power Institute.
4. Zlatev, Z. SIAM Journal of Numerical Analysis, Vol. 17, 1980.
5. Thomas, J.R. 1996. Importance of Dielectric Properties in Modeling of Microwave Sintering of Ceramics.
6. Johnson, D.L. 1994. Microwave Processing of Ceramics at Northwestern University. Pp. 17-28 in Ceramic Transactions, Vol. IV.
7. Brandon, J.R., J. Samuels and W.R. Hodgkins. 1992. Microwave Sintering of Oxide Ceramics. Pp. 237-243 in Materials Research Society Symposium Proceedings, Vol. 269, Microwave Processing of Materials III. R.L. Beatty, W.H. Sutton, and M.F. Iskander, eds. Pittsburgh, Pennsylvania: Materials Research Society.
8. Clark, D.E., I. Ahmad and R.C. Dalton, 1991. Pp. 91-97 in Material Science and Engineering, Vol. A144.
9. Martin, L.P., D. Dadon, M. Rosen, D. Gershon, K.I. Rybakov, A. Birman, J.P. Calame, B. Levush, Y. Carmel, R. Hutcheon. 1997. Effects of Anomalous Permittivity on the Microwave Heating of Zinc Oxide.
10. Iskander, M.F., O. Andrade. 1994. Microwave Processing of Ceramics at the University of Utah -- Description of Activities and Summary of Progress. Pp. 35-48 in Pp. 17-28 in Ceramic Transactions, Vol. IV.
11. Iskander, M.F., R.L. Smith, O. Andrade, H. Kimrey, and L. Walsh. 1993. FDTD Simulation of Microwave Sintering of Ceramics in Multimode Cavities, IEEE Transactions on Microwave Theory and Techniques.
12. Barmatz, M. and H.W. Jackson. 1992. Steady State Temperature Profile in a Sphere Heated by Microwaves. Pp. 97-103 in Materials Research Society Symposium Proceedings, Vol. 269, Microwave Processing of Materials III. R.L.

- Beatty, W.H. Sutton, and M.F. Iskander, eds. Pittsburgh, Pennsylvania: Materials Research Society.
13. Olmstead, W.E., M.E. Brodwin. 1997. A Model for Thermocouple Sensitivity During Microwave Heating, Pp. 1559-1565 in International Journal of Heat and Mass Transfer, Vol. 40, No. 7
 14. Thomas, J.R., J. Katz, and R.D. Blake. 1994. Temperature Distribution in Microwave Sintering of Alumina Cylinders. Pp. 311-316 in Materials Research Society Symposium Proceedings, Vol. 347, Microwave Processing of Materials IV. M.F. Iskander, R.J. Lauf and W.H. Sutton, eds. Pittsburgh, Pennsylvania: Materials Research Society.
 15. Chaussecourte, P.,J.F. Lamaudiere, and B. Maestrali. 1992. Electromagnetic Field Modeling of Loaded Microwave Cavity. Pp. 69-74 in Materials Research Society Symposium Proceedings, Vol. 269, Microwave Processing of Materials III. R.L. Beatty, W.H. Sutton, and M.F. Iskander, eds. Pittsburgh, Pennsylvania: Materials Research Society.
 16. Michener, Michael Douglas. Measurements of Thermal Properties and Blood Perfusion Using the Heat Flux Microsensor, M.S. Thesis, Mechanical Engineering Department, Virginia Polytechnic Institute and State University, Blacksburg, VA (1995).
 17. Balanis, C.A., Advanced Engineering Electromagnetics, Wiley, New York, 1989.
 18. Dadon, D., L.P. Martin, M. Rosen, A. Birman, D. Gershon, J.P. Calame, B. Levush, and Y. Carmel. 1996. Temperature and Porosity Gradients Developed During Nonisothermal Microwave Processing of Zinc Oxide. Pp. 95-103 in Journal of Materials Synthesis and Processing, Vol. 4. No.2.
 19. Gershon, D. Personal communication

APPENDIX A - PROPERTY DATA

Zinc Oxide (ZnO)

Temperature °C	ϵ' in Nitrogen [19]	ϵ'' in Nitrogen [9]	ϵ'' in Air[19]
23	3.84	0.10	0.126
150	3.88	2.0	0.158
200	3.97	4.0	0.255
250	3.93	8.0	0.207
300	3.86	6.0	0.133
350	3.85	5.5	0.101
400	3.88	14.0	0.100
450	3.90	23.0	0.103
500	3.94	8.0	0.105
550	3.97	1.0	0.117
600	4.02	0.10	0.139

Density, $\rho = 3000.0 \text{ kg/m}^3$ [1]

Specific Heat, $c = 500.0 \text{ J/(kg}^\circ\text{C)}$ [1]

Conductivity, $k = 10.0 \text{ J/(m sec }^\circ\text{C)}$ [1]

APPENDIX B - DERIVATION OF FINITE-DIFFERENCE EQUATIONS

General Node

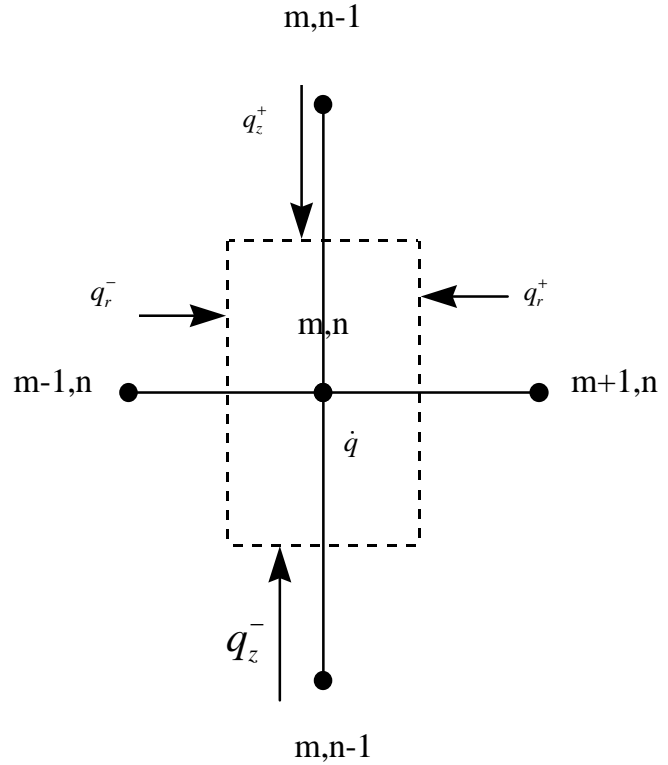
$$A_r^- = 2p \left(r - \frac{\Delta r}{2} \right) \Delta z$$

$$A_r^+ = 2p \left(r + \frac{\Delta r}{2} \right) \Delta z$$

$$A_z^- = A_z^+ = 2p r \Delta r$$

$$V = 2p r \Delta r \Delta z$$

$$\frac{q_r^-}{V} + \frac{q_r^+}{V} + \frac{q_z^-}{V} + \frac{q_z^+}{V} + \dot{q} = r c_p \frac{\dot{T}}{\Delta r}$$



$$\frac{q_r^-}{V} = k_m^- \frac{A_r^-}{V} \frac{(T_{m-1,n} - T_{m,n})}{\Delta r} = k_m^- \left(\frac{r - \frac{\Delta r}{2}}{r \Delta r^2} \right) (T_{m-1,n} - T_{m,n}) = f_m^- (T_{m-1,n} - T_{m,n})$$

$$\frac{q_r^+}{V} = k_m^+ \frac{A_r^+}{V} \frac{(T_{m+1,n} - T_{m,n})}{\Delta r} = k_m^+ \left(\frac{r + \frac{\Delta r}{2}}{r \Delta r^2} \right) (T_{m+1,n} - T_{m,n}) = f_m^+ (T_{m+1,n} - T_{m,n})$$

$$\frac{q_z^-}{V} = k_n^- \frac{A_z^-}{V} \frac{(T_{m,n-1} - T_{m,n})}{\Delta z} = k_n^- \left(\frac{1}{\Delta z^2} \right) (T_{m,n-1} - T_{m,n}) = f_n^- (T_{m,n-1} - T_{m,n})$$

$$\frac{q_z^+}{V} = k_n^+ \frac{A_z^+}{V} \frac{(T_{m,n+1} - T_{m,n})}{\Delta z} = k_n^+ \left(\frac{1}{\Delta z^2} \right) (T_{m,n+1} - T_{m,n}) = f_n^+ (T_{m,n+1} - T_{m,n})$$

$$f_m^-(T_{m-1,n} - T_{m,n}) + f_m^+(T_{m+1,n} - T_{m,n}) + f_n^-(T_{m,n-1} - T_{m,n}) + f_n^+(T_{m,n+1} - T_{m,n}) + \dot{q} = \frac{1}{u}(T_{m,n}^{p+1} - T_{m,n}^p)$$

$$u = \frac{\Delta t}{\tau c_p}$$

Explicit

$$T_{m,n}^{p+1} = T_{m-1,n}^p(f_m^-) + T_{m,n}^p(1 - u(f_m^- + f_m^+ + f_n^- + f_n^+)) + T_{m+1,n}^p(uf_m^+) + T_{m,n-1}^p(uf_n^-) + T_{m,n+1}^p(uf_n^+) + \dot{q}u$$

Implicit

$$T_{m-1,n}^{p+1}(-uf_m^-) + T_{m,n}^{p+1}(1 + u(f_m^- + f_m^+ + f_n^- + f_n^+)) + T_{m+1,n}^{p+1}(-uf_m^+) + T_{m,n-1}^{p+1}(-uf_n^-) + T_{m,n+1}^{p+1}(-uf_n^+) = T_{m,n}^p + \dot{q}u$$

Alternating Direction Implicit, (ADI)

First Time Step (Implicit in r direction, Explicit in z)

$$T_{m-1,n}^{p+1}(-uf_m^-) + T_{m,n}^{p+1}(1 + u(f_m^- + f_m^+)) + T_{m+1,n}^{p+1}(-uf_m^+) = T_{m,n-1}^p(uf_n^-) + T_{m,n}^p(1 - u(f_n^- + f_n^+)) + T_{m,n+1}^p(uf_n^+) + \dot{q}u$$

Second Time Step (Explicit in r direction, Implicit in z)

$$T_{m,n-1}^{p+1}(-uf_n^-) + T_{m,n}^{p+1}(1 + u(f_n^- + f_n^+)) + T_{m,n+1}^{p+1}(-uf_n^+) = T_{m-1,n}^p(uf_m^-) + T_{m,n}^p(1 - u(f_m^- + f_m^+)) + T_{m+1,n}^p(uf_m^+) + \dot{q}u$$

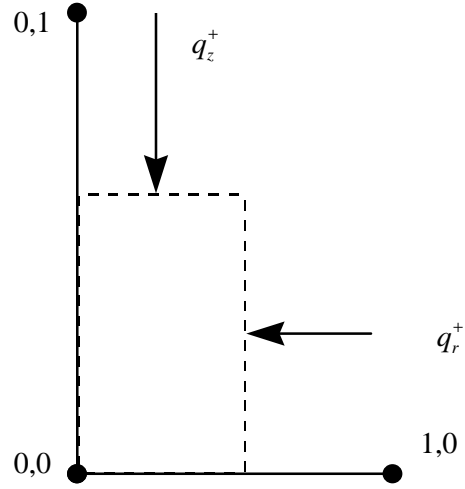
Center Node, $m=0, n=0$

$$A_r = \frac{\rho}{2} \Delta r \Delta z$$

$$A_z = \frac{\rho}{4} \Delta r^2$$

$$V = \frac{\rho}{8} \Delta r^2 \Delta z$$

$$\frac{q_r}{V} + \frac{q_z}{V} + \dot{q} = r c_p \frac{\partial T}{\partial t}$$



$$\frac{q_r}{V} = k_m^+ \frac{A_r}{V} \left(\frac{T_{1,0} - T_{0,0}}{\Delta r} \right) = k_m^+ \left(\frac{4}{\Delta r^2} \right) (T_{1,0} - T_{0,0}) = f_m^+ (T_{1,0} - T_{0,0})$$

$$\frac{q_z}{V} = k_n^+ \frac{A_z}{V} \left(\frac{T_{0,1} - T_{0,0}}{\Delta z} \right) = k_n^+ \left(\frac{2}{\Delta z^2} \right) (T_{0,1} - T_{0,0}) = f_n^+ (T_{0,1} - T_{0,0})$$

$$f_m^+ (T_{1,0} - T_{0,0}) + f_n^+ (T_{0,1} - T_{0,0}) + \dot{q} = \frac{1}{u} (T_{m,n}^{p+1} - T_{m,n}^p),$$

where $u = \frac{\Delta t}{r c_p}$

Explicit

$$T_{0,0}^{p+1} = T_{1,0}^p(uf_m^+) + T_{0,0}^p(1 - u(f_m^+ + f_n^+)) + T_{0,1}^p(uf_n^+) + \dot{q}u$$

Implicit

$$T_{1,0}^{p+1}(-uf_m^+) + T_{0,0}^{p+1}(1 + u(f_m^+ + f_n^+)) + T_{0,1}^{p+1}(-uf_n^+) = T_{0,0}^p + \dot{q}u$$

ADI, First Step

$$T_{0,0}^{p+1}(1 + uf_m^+) + T_{1,0}^{p+1}(-uf_m^+) = T_{0,0}^p(1 - uf_n^+) + T_{0,1}^p(uf_n^+) + \dot{q}u$$

ADI, Second Step

$$T_{0,0}^{p+1}(1 + uf_n^+) + T_{0,1}^{p+1}(-uf_n^+) = T_{0,0}^p(1 - uf_m^+) + T_{1,0}^p(uf_m^+) + \dot{q}u$$

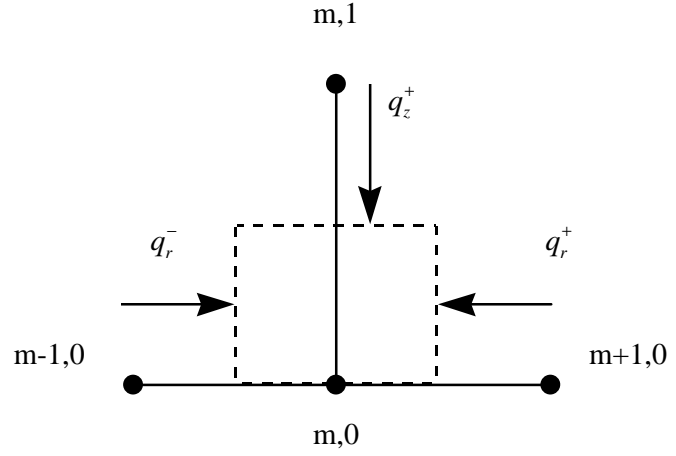
$$0 < m < M, n=0$$

$$A_r^- = \rho \left(r - \frac{\Delta r}{2} \right) \Delta z$$

$$A_r^+ = \rho \left(r + \frac{\Delta r}{2} \right) \Delta z$$

$$A_z^+ = 2\rho r \Delta r$$

$$V = \rho r \Delta r \Delta z$$



$$\frac{\dot{q}_r^-}{V} + \frac{\dot{q}_r^+}{V} + \frac{\dot{q}_z^+}{V} + \dot{q} = r c_p \frac{\dot{T}}{r}$$

$$\frac{\dot{q}_r^-}{V} = k_m^- \frac{A_r^-}{V} \frac{(T_{m-1,0} - T_{m,0})}{\Delta r} = k_m^- \left(\frac{r - \frac{\Delta r}{2}}{r \Delta r^2} \right) (T_{m-1,0} - T_{m,0}) = f_m^- (T_{m-1,0} - T_{m,0})$$

$$\frac{\dot{q}_r^+}{V} = k_m^+ \frac{A_r^+}{V} \frac{(T_{m+1,0} - T_{m,0})}{\Delta r} = k_m^+ \left(\frac{r + \frac{\Delta r}{2}}{r \Delta r^2} \right) (T_{m+1,0} - T_{m,0}) = f_m^+ (T_{m+1,0} - T_{m,0})$$

$$\frac{\dot{q}_z^+}{V} = k_n^+ \frac{A_z^+}{V} \frac{(T_{m,1} - T_{m,0})}{\Delta z} = k_n^+ \left(\frac{2}{\Delta z^2} \right) (T_{m,1} - T_{m,0}) = f_n^+ (T_{m,1} - T_{m,0})$$

$$f_m^- (T_{m-1,0} - T_{m,0}) + f_m^+ (T_{m+1,0} - T_{m,0}) + f_n^+ (T_{m,1} - T_{m,0}) + \dot{q} = \frac{1}{u} (T_{m,0}^{p+1} - T_{m,0}^p)$$

Explicit

$$T_{m,0}^{p+1} = T_{m-1,0}^p(uf_m^-) + T_{m,0}^p(1 - u(f_m^- + f_m^+ + f_n^+)) + T_{m+1,0}^p(uf_m^+) + T_{m,1}^p(uf_n^+) + \dot{q}u$$

Implicit

$$T_{m-1,0}^{p+1}(-uf_m^-) + T_{m,0}^{p+1}(1 + u(f_m^- + f_m^+ + f_n^+)) + T_{m+1,0}^{p+1}(-uf_m^+) + T_{m,1}^{p+1}(-uf_n^+) = T_{m,0}^p + \dot{q}u$$

ADI, First Time Step

$$T_{m-1,0}^{p+1}(-uf_m^-) + T_{m,0}^{p+1}(1 + u(f_m^- + f_m^+)) + T_{m+1,0}^{p+1}(-uf_m^-) = T_{m,0}^p(1 - uf_n^+) + T_{m,1}^p(uf_n^+) + \dot{q}u$$

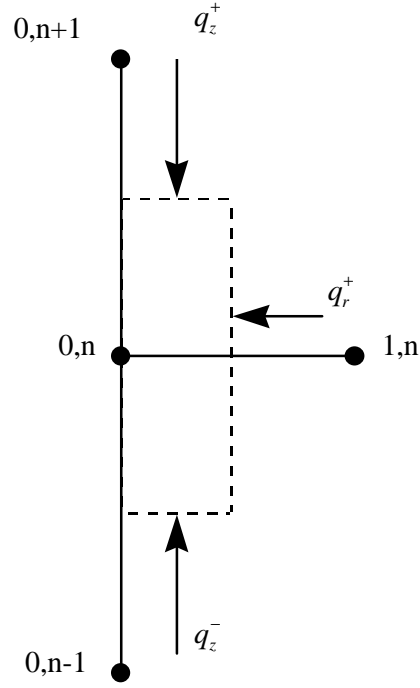
ADI, Second Time Step

$$T_{m,0}^{p+1}(1 + uf_n^+) + T_{m,1}^{p+1}(-uf_n^+) = T_{m-1,0}^p(uf_m^-) + T_{m,0}^p(1 - u(f_m^- + f_m^+)) + T_{m+1,0}^p(uf_m^+) + \dot{q}u$$

$$m = 0, 0 < n < N$$

$$\begin{aligned} A_r^+ &= \rho \Delta r \Delta z \\ A_z^- &= A_z^+ = \frac{\rho}{4} \Delta r^2 \\ V &= \frac{\rho}{4} \Delta r^2 \Delta z \end{aligned}$$

$$\frac{q_r^+}{V} + \frac{q_z^-}{V} + \frac{q_z^+}{V} + \dot{q} = r c_p \frac{\rho T}{4r}$$



$$\frac{q_r^+}{V} = k_m^+ \frac{A_r^+}{V} \left(\frac{T_{1,n} - T_{0,n}}{\Delta r} \right) = k_m^+ \left(\frac{4}{\Delta r^2} \right) (T_{1,n} - T_{0,n}) = f_m^+ (T_{1,n} - T_{0,n})$$

$$\frac{q_z^-}{V} = k_n^- \frac{A_z^-}{V} \left(\frac{T_{0,n-1} - T_{0,n}}{\Delta z} \right) = k_n^- \left(\frac{1}{\Delta z^2} \right) (T_{0,n-1} - T_{0,n}) = f_n^- (T_{0,n-1} - T_{0,n})$$

$$\frac{q_z^+}{V} = k_n^+ \frac{A_z^+}{V} \left(\frac{T_{0,n+1} - T_{0,n}}{\Delta z} \right) = k_n^+ \left(\frac{1}{\Delta z^2} \right) (T_{0,n+1} - T_{0,n}) = f_n^+ (T_{0,n+1} - T_{0,n})$$

$$f_m^+ (T_{1,n} - T_{0,n}) + f_n^- (T_{0,n-1} - T_{0,n}) + f_n^+ (T_{0,n+1} - T_{0,n}) + \dot{q} = \frac{1}{u} (T_{0,n}^{p+1} - T_{0,n}^p)$$

Explicit

$$T_{0,n}^{p+1} = T_{1,n}^p(uf_m^+) + T_{0,n}^p(1 - u(f_m^+ + f_n^- + f_n^+)) + T_{0,n-1}^p(uf_n^-) + T_{0,n+1}^p(uf_n^+) + \dot{q}u$$

Implicit

$$T_{1,n}^{p+1}(-uf_m^+) + T_{0,n}^{p+1}(1 + u(f_m^+ + f_n^- + f_n^+)) + T_{0,n-1}^{p+1}(-uf_n^-) + T_{0,n+1}^{p+1}(-uf_n^+) = T_{0,n}^p + \dot{q}u$$

ADI, First Time Step

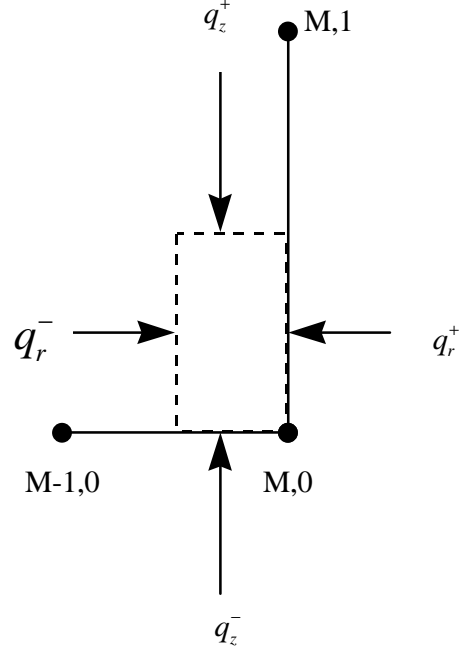
$$T_{0,n}^{p+1}(1 + uf_m^+) + T_{1,n}^{p+1}(-uf_m^+) = T_{0,n-1}^p(uf_n^-) + T_{0,n}^p(1 - u(f_n^- + f_n^+)) + T_{0,n+1}^p(uf_n^+) + \dot{q}u$$

ADI, Second Time Step

$$T_{0,n-1}^{p+1}(-uf_n^-) + T_{0,n}^{p+1}(1 + u(f_n^- + f_n^+)) + T_{0,n+1}^{p+1}(-uf_n^+) = T_{0,n}^p(1 - uf_m^+) + T_{1,n}^p(uf_m^+) + \dot{q}u$$

$$m=M, n=0$$

$$\begin{aligned} A_r^- &= \rho \left(R - \frac{\Delta r}{2} \right) \Delta z \\ A_r^+ &= \rho R \Delta z \\ A_z^- &= A_z^+ = \rho \left(R - \frac{\Delta r}{4} \right) \Delta r \\ V &= \frac{\rho}{2} \left(R - \frac{\Delta r}{4} \right) \Delta r \Delta z \end{aligned}$$



$$\frac{q_r^-}{V} = k_m^- \frac{A_r^-}{V} \left(\frac{T_{M-1,0} - T_{M,0}}{\Delta r} \right) = k_m^- \left(\frac{2 \left(R - \frac{\Delta r}{2} \right)}{\Delta r^2 \left(R - \frac{\Delta r}{4} \right)} \right) (T_{M-1,0} - T_{M,0}) = f_m^- (T_{M-1,0} - T_{M,0})$$

$$\frac{q_r^+}{V} = h \frac{A_r^+}{V} (T_\infty - T_{M,0}) = h \left(\frac{2R}{\Delta r \left(R - \frac{\Delta r}{4} \right)} \right) (T_\infty - T_{M,0}) = f_m^+ (T_\infty - T_{M,0})$$

$$\frac{q_z^+}{V} = k_n^+ \frac{A_z^+}{V} \left(\frac{T_{M,1} - T_{M,0}}{\Delta z} \right) = k_n^+ \left(\frac{2}{\Delta z^2} \right) (T_{M,1} - T_{M,0}) = f_n^+ (T_{M,1} - T_{M,0})$$

$$f_m^- (T_{M-1,0} - T_{M,0}) + f_m^+ (T_\infty - T_{M,0}) + f_n^+ (T_{M,1} - T_{M,0}) + \dot{q} = \frac{1}{u} (T_{M,0}^{p+1} - T_{M,0}^p)$$

Explicit

$$T_{M,0}^{p+1} = T_{M-1,0}^p(uf_m^-) + T_{M,0}^p(1 - u(f_m^- + f_m^+ + f_n^+)) + T_{M,1}^p(uf_n^+) + u(\dot{q} + f_m^+ T_\infty)$$

Implicit

$$T_{M-1,0}^{p+1}(-uf_m^-) + T_{M,0}^{p+1}(1 + u(f_m^- + f_m^+ + f_n^+)) + T_{M,1}^{p+1}(-uf_n^+) = T_{M,0}^p + u(\dot{q} + f_m^+ T_\infty)$$

ADI, First Time Step

$$T_{M-1,0}^{p+1}(-uf_m^-) + T_{M,0}^{p+1}(1 + u(f_m^- + f_m^+)) = T_{M,1}^p(uf_n^+) + T_{M,0}^p(1 - uf_n^+) + u(\dot{q} + f_m^+ T_\infty)$$

ADI, Second Time Step

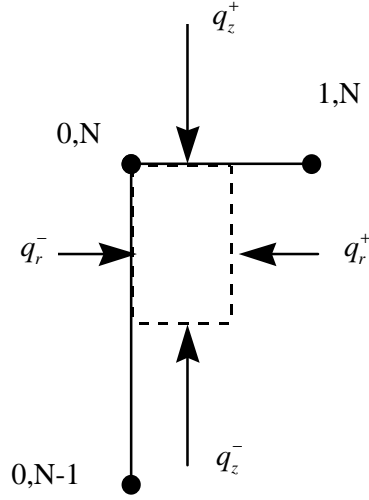
$$T_{M,1}^{p+1}(-uf_n^+) + T_{M,0}^{p+1}(1 + uf_n^+) = T_{M-1,0}^p(uf_m^-) + T_{M,0}^p(1 - u(f_m^- + f_m^+)) + u(\dot{q} + f_m^+ T_\infty)$$

$m=0, n=N$

$$A_r^- = \frac{\rho}{2} \Delta r \Delta z$$

$$A_z^- = A_z^+ = \frac{\rho}{4} \Delta r^2$$

$$V = \frac{\rho}{8} \Delta r^2 \Delta z$$



$$\frac{\dot{q}_r^+}{V} = k_m^+ \frac{A_r^+}{V} \left(\frac{T_{1,N} - T_{0,N}}{\Delta r} \right) = k_m^+ \left(\frac{4}{\Delta r^2} \right) (T_{1,N} - T_{0,N}) = f_m^+ (T_{1,N} - T_{0,N})$$

$$\frac{\dot{q}_r^-}{V} = k_n^- \frac{A_r^-}{V} \left(\frac{T_{0,N-1} - T_{0,N}}{\Delta z} \right) = k_n^- \left(\frac{2}{\Delta z^2} \right) (T_{0,N-1} - T_{0,N}) = f_n^- (T_{0,N-1} - T_{0,N})$$

$$\frac{\dot{q}_z^+}{V} = h \frac{A_z^+}{V} (T_\infty - T_{0,N}) = h \left(\frac{2}{\Delta z} \right) (T_\infty - T_{0,N}) = f_n^+ (T_\infty - T_{0,N})$$

$$f_m^+ (T_{1,N} - T_{0,N}) + f_n^- (T_{0,N-1} - T_{0,N}) + f_n^+ (T_\infty - T_{0,N}) + \dot{q} = \frac{1}{u} (T_{0,N}^{p+1} - T_{0,N}^p)$$

Explicit

$$T_{0,N}^{p+1} = T_{1,N}^p(uf_m^+) + T_{0,N}^p(1 - u(f_m^+ + f_n^- + f_n^+)) + T_{0,N-1}^p(uf_n^-) + u(\dot{q} + f_n^+ T_\infty)$$

Implicit

$$T_{1,N}^{p+1}(-uf_m^+) + T_{0,N}^{p+1}(1 + u(f_m^+ + f_n^- + f_n^+)) + T_{0,N-1}^{p+1}(-uf_n^-) = T_{0,N}^p + u(\dot{q} + f_n^+ T_\infty)$$

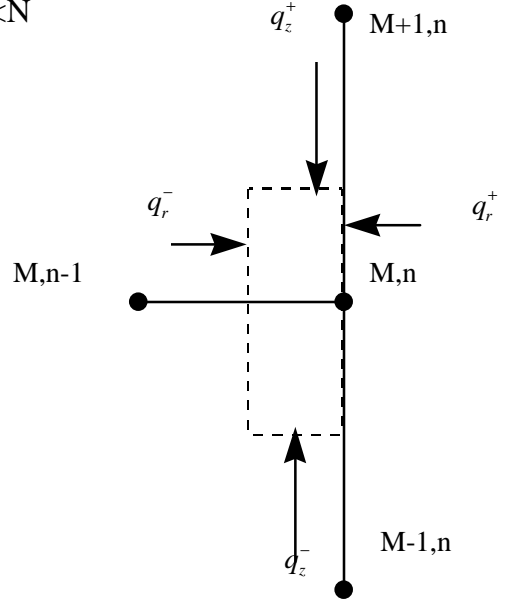
ADI, First Time Step

$$T_{1,N}^{p+1}(-uf_m^+) + T_{0,N}^{p+1}(1 + uf_m^+) = T_{0,N-1}^p(uf_n^-) + T_{0,N}^p(1 - u(f_n^- + f_n^+)) + u(\dot{q} + f_n^+ T_\infty)$$

ADI, Second Time Step

$$T_{0,N-1}^{p+1}(-uf_n^-) + T_{0,N}^{p+1}(1 + u(f_n^- + f_n^+)) = T_{1,N}^p(uf_m^+) + T_{0,N}^p(1 - uf_m^+) + u(\dot{q} + f_n^+ T_\infty)$$

$m=M, 0 < n < N$



$$A_r^- = 2\rho \left(R - \frac{\Delta r}{2} \right) \Delta z$$

$$A_r^+ = 2\rho R \Delta z$$

$$A_z^- = A_z^+ = \rho \left(R - \frac{\Delta r}{2} \right) \Delta r$$

$$V = \rho \left(R - \frac{\Delta r}{2} \right) \Delta r \Delta z$$

$$\frac{q_r^-}{V} = k_m^- \frac{A_r^-}{V} \left(\frac{T_{M-1,n} - T_{M,n}}{\Delta r} \right) = k_m^- \left(\frac{2 \left(R - \frac{\Delta r}{2} \right)}{\Delta r^2 \left(R - \frac{\Delta r}{4} \right)} \right) (T_{M-1,n} - T_{M,n}) = f_1 (T_{M-1,n} - T_{M,n})$$

$$\frac{q_r^+}{V} = h \frac{A_r^+}{V} (T_\infty - T_{M,n}) = h \left(\frac{2R}{\Delta r \left(R - \frac{\Delta r}{4} \right)} \right) (T_\infty - T_{M,n}) = f_2 (T_\infty - T_{M,n})$$

$$\frac{q_z^-}{V} = k_n^- \frac{A_z^-}{V} \left(\frac{T_{M,n-1} - T_{M,n}}{\Delta z} \right) = k_n^- \left(\frac{1}{\Delta z^2} \right) (T_{M,n-1} - T_{M,n}) = f_3 (T_{M,n-1} - T_{M,n})$$

$$\frac{q_z^+}{V} = k_n^+ \frac{A_z^+}{V} \left(\frac{T_{M,n+1} - T_{M,n}}{\Delta z} \right) = k_n^+ \left(\frac{1}{\Delta z^2} \right) (T_{M,n+1} - T_{M,n}) = f_4 (T_{M,n+1} - T_{M,n})$$

$$f_m^- (T_{M-1,n} - T_{M,n}) + f_m^+ (T_\infty - T_{M,n}) + f_n^- (T_{M,n-1} - T_{M,n}) + f_n^+ (T_{M,n+1} - T_{M,n}) + \dot{q} = \frac{1}{u} (T_{M,n}^{p+1} - T_{M,n}^p)$$

Explicit

$$T_{M,n}^{p+1} = T_{M-1,n}^p(uf_m^-) + T_{M,n}^p(1 - u(f_m^- + f_m^+ + f_n^- + f_n^+)) + T_{M,n-1}^p(uf_n^-) + T_{M,n+1}^p(uf_n^+) + u(\dot{q} + f_m^+ T_\infty)$$

Implicit

$$T_{M-1,n}^{p+1}(-uf_m^-) + T_{M,n}^{p+1}(1 + u(f_m^- + f_m^+ + f_n^- + f_n^+)) + T_{M,n-1}^{p+1}(-uf_n^-) + T_{M,n+1}^{p+1}(-uf_n^+) = T_{M,n}^p + u(\dot{q} + f_m^+ T_\infty)$$

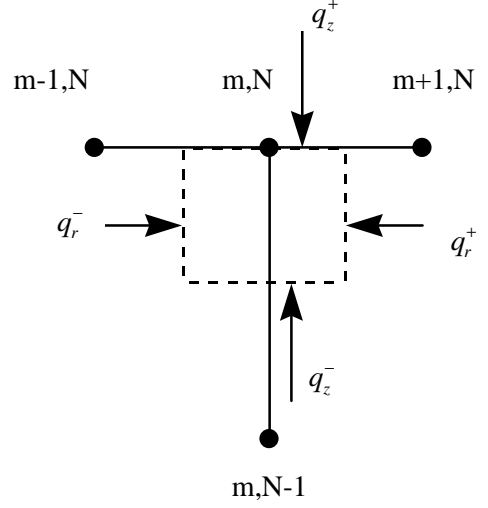
ADI, First Time Step

$$T_{M-1,n}^{p+1}(-uf_m^-) + T_{M,n}^{p+1}(1 + u(f_m^- + f_m^+)) = T_{M,n-1}^p(uf_n^-) + T_{M,n}^p(1 - u(f_n^- + f_n^+)) + T_{M,n+1}^p(uf_n^+) + u(\dot{q} + f_m^+ T_\infty)$$

ADI, Second Time Step

$$T_{M-1,n}^{p+1}(-uf_n^-) + T_{M,n}^{p+1}(1 + u(f_n^- + f_n^+)) + T_{M,n+1}^{p+1}(-uf_n^+) = T_{M-1,n}^p(uf_m^+) + T_{M,n}^p(1 - u(f_m^- + f_m^+)) + u(\dot{q} + f_m^+ T_\infty)$$

$$0 < m < M, n = N$$



$$A_r^- = \rho \left(r - \frac{\Delta r}{2} \right) \Delta z$$

$$A_r^+ = \rho \left(r + \frac{\Delta r}{2} \right) \Delta z$$

$$A_z^- = A_z^+ = 2\rho r \Delta r$$

$$V = \rho r \Delta r \Delta z$$

$$\frac{q_r^-}{V} = k_m^- \frac{A_r^-}{V} \left(\frac{T_{m-1,N} - T_{m,N}}{\Delta r} \right) = k_m^- \left(\frac{r - \frac{\Delta r}{2}}{r \Delta r^2} \right) (T_{m-1,N} - T_{m,N}) = f_1 (T_{m-1,N} - T_{m,N})$$

$$\frac{q_r^+}{V} = k_m^+ \frac{A_r^+}{V} \left(\frac{T_{m+1,N} - T_{m,N}}{\Delta r} \right) = k_m^+ \left(\frac{r + \frac{\Delta r}{2}}{r \Delta r^2} \right) (T_{m+1,N} - T_{m,N}) = f_2 (T_{m+1,N} - T_{m,N})$$

$$\frac{q_z^-}{V} = k_n^- \frac{A_z^-}{V} \left(\frac{T_{m,N-1} - T_{m,N}}{\Delta z} \right) = k_n^- \left(\frac{2}{\Delta z^2} \right) (T_{m,N-1} - T_{m,N}) = f_3 (T_{m,N-1} - T_{m,N})$$

$$\frac{q_z^+}{V} = h \frac{A_z^+}{V} (T_\infty - T_{m,N}) = h \left(\frac{2}{\Delta z} \right) (T_\infty - T_{m,N}) = f_4 (T_\infty - T_{m,N})$$

$$f_m^- (T_{m-1,N} - T_{m,N}) + f_m^+ (T_{m+1,N} - T_{m,N}) + f_n^- (T_{m,N-1} - T_{m,N}) + f_n^+ (T_\infty - T_{m,N}) + \dot{q} = \frac{1}{u} (T_{m,N}^{p+1} - T_{m,N}^p)$$

Explicit

$$T_{m,N}^{p+1} = T_{m-1,N}^p(uf_m^-) + T_{m,N}^p(1 - u(f_m^- + f_m^+ + f_n^- + f_n^+)) + T_{m+1,N}^p(uf_m^+) + T_{m,N-1}^p(uf_n^-) + u(\dot{q} + f_n^+ T_\infty)$$

Implicit

$$T_{m-1,N}^{p+1}(-uf_m^-) + T_{m,N}^{p+1}(1 + u(f_m^- + f_m^+ + f_n^- + f_n^+)) + T_{m+1,N}^{p+1}(-uf_m^+) + T_{m,N-1}^{p+1}(-uf_n^-) = T_{m,N}^p + u(\dot{q} + f_n^+ T_\infty)$$

ADI, First Time Step

$$T_{m-1,N}^{p+1}(-uf_m^-) + T_{m,N}^{p+1}(1 + u(f_m^- + f_m^+)) + T_{m+1,N}^p(uf_m^+) = T_{m,N-1}^p(uf_n^-) + T_{m,N}^p(1 - u(f_n^- + f_n^+)) + u(\dot{q} + f_n^+ T_\infty)$$

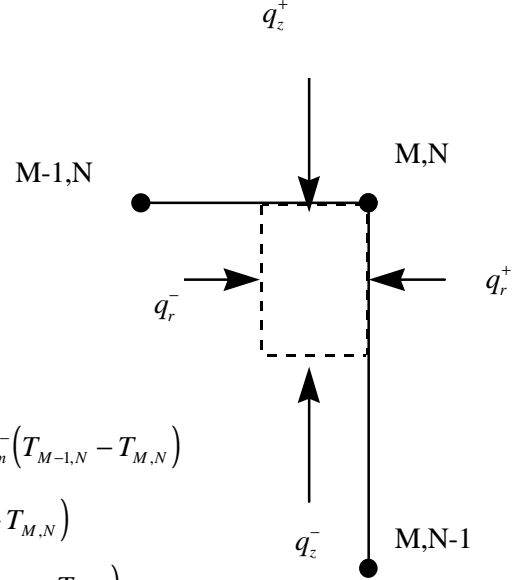
ADI, Second Time Step

$$T_{m,N-1}^{p+1}(-uf_n^-) + T_{m,N}^{p+1}(1 + u(f_n^- + f_n^+)) = T_{m-1,N}^p(uf_m^-) + T_{m,N}^p(1 - u(f_m^- + f_m^+)) + T_{m+1,N}^{p+1}(-uf_m^+) + u(\dot{q} + f_n^+ T_\infty)$$

$$m=M, n=N$$

$$\begin{aligned} A_r^- &= \rho \left(R - \frac{\Delta r}{2} \right) \Delta z \\ A_r^+ &= \rho R \Delta z \\ A_z^- &= A_z^+ = \rho \left(R - \frac{\Delta r}{4} \right) \Delta r \\ V &= \rho \left(R - \frac{\Delta r}{4} \right) \Delta r \Delta z \end{aligned}$$

$$\begin{aligned} \frac{q_r^-}{V} &= k_m^- \frac{A_r^-}{V} \left(\frac{T_{M-1,N} - T_{M,N}}{\Delta r} \right) = k_m^- \left(\frac{2 \left(R - \frac{\Delta r}{2} \right)}{\Delta r^2 \left(R - \frac{\Delta r}{4} \right)} \right) (T_{M-1,N} - T_{M,N}) = f_m^- (T_{M-1,N} - T_{M,N}) \\ \frac{q_r^+}{V} &= h \frac{A_r^+}{V} (T_\infty - T_{M,N}) = h \left(\frac{2R}{\Delta r \left(R - \frac{\Delta r}{4} \right)} \right) (T_\infty - T_{M,N}) = f_m^+ (T_\infty - T_{M,N}) \\ \frac{q_z^-}{V} &= k_n^- \frac{A_z^-}{V} \left(\frac{T_{M,N-1} - T_{M,N}}{\Delta z} \right) = k_n^- \left(\frac{2}{\Delta z^2} \right) (T_{M,N-1} - T_{M,N}) = f_n^- (T_{M,N-1} - T_{M,N}) \\ \frac{q_z^+}{V} &= h \frac{A_z^+}{V} (T_\infty - T_{M,N}) = h \left(\frac{2}{\Delta z} \right) (T_\infty - T_{M,N}) = f_n^+ (T_\infty - T_{M,N}) \end{aligned}$$



$$f_m^- (T_{M-1,N} - T_{M,N}) + f_m^+ (T_\infty - T_{M,N}) + f_n^- (T_{M,N-1} - T_{M,N}) + f_n^+ (T_\infty - T_{M,N}) + \dot{q} = \frac{1}{u} (T_{M,N}^{p+1} - T_{M,N}^p)$$

Explicit

$$T_{M,N}^{p+1} = T_{M-1,N}^p (uf_m^-) + T_{M,N}^p (1 - u(f_m^- + f_m^+ + f_n^- + f_n^+)) + T_{M,N-1}^p (uf_n^-) + u(\dot{q} + (f_m^+ + f_n^+)T_\infty)$$

Implicit

$$T_{M-1,N}^{p+1} (-uf_m^-) + T_{M,N}^{p+1} (1 + u(f_m^- + f_m^+ + f_n^- + f_n^+)) + T_{M,N-1}^{p+1} (-uf_n^-) = T_{M,N}^p + u(\dot{q} + (f_m^+ + f_n^+)T_\infty)$$

ADI, First Time Step

$$T_{M-1,N}^{p+1} (-uf_m^-) + T_{M,N}^{p+1} (1 + u(f_m^- + f_m^+)) = T_{M,N-1}^p (uf_n^-) + T_{M,N}^p (1 - u(f_n^- + f_n^+)) + u(\dot{q} + (f_m^+ + f_n^+)T_\infty)$$

ADI, Second Time Step

$$T_{M,N-1}^{p+1} (-uf_n^-) + T_{M,N}^{p+1} (1 + u(f_n^- + f_n^+)) = T_{M-1,N}^p (uf_m^-) + T_{M,N}^p (1 - u(f_m^- + f_m^+)) + u(\dot{q} + (f_m^+ + f_n^+)T_\infty)$$

Appendix C - Programs

```
c    program awze - ADI Method
c    Program to model small ZnO cylindrical sample
c    in nitrogen atmosphere
c    Variable dielectric properties and electric field
c    For air case, change data in eppa and epa
c    For constant electric field, change ef, so that ef = 1.0
```

```
double precision T(0:50,0:50),Told(0:50,0:50)
double precision q,qo,kmm,kmp,knm,knp,h,rho
double precision dt,dr,dz,RR,Z,r
double precision a(2601),b(2601),c(2601)
double precision g(2601),v(2601)
double precision f1,f2,f3,f4,u,w,er,del,dmax,emax
double precision tmax,Tinf,Ti,avg
double precision em,am,epa,eppa
double precision tem,e1,e2,efi
integer im,jm
integer i,j,k,M,N,p,ind
integer is,js
external epa,eppa
data dt,RR,Z/0.50d0,5.0d0,5.0d0/
data dr,dz/0.10d0,0.10d0/
data h,Tinf,Ti,qo/80000.0d0,300.0d0,300.0d0,5.0d0/
data emax,tmax/0.00010d0,4800.0d0/
data rho/3.0d0/
data/is,js/14,7/
```

```
pmax = int(tmax/dt)
M = int(RR/dr)
N = int(Z/dz)
```

```
c Initialize
```

```
do k = 1,500
    a(k) = 0.0d0
    b(k) = 0.0d0
    c(k) = 0.0d0
    g(k) = 0.0d0
enddo
do j = 0,N
    do i = 0,M
        T(i,j) = Ti
    enddo
enddo
```

c First Time Step

```
do 1 p = 2,pmax,2

do j = 0,N
  do i = 0,M
    Told(i,j) = T(i,j)
  enddo
enddo
ec = 0
10 ind = 0
ec = ec+1
j = 0
i = 0
  ind = ind + 1
  kmp = cal(i+1,j)
  knp = cal(i,j+1)
  q = q0*eppa(T(i,j),i,j)*ef(T(i,j),i,j)
  u = dt/(rho*cap(i,j))
  f1 = 4.0d0*kmp/(dr*dr)
  f2 = 2.0d0*knp/(dz*dz)
  b(ind) = 1.0d0 + u*f1
  c(ind) = -u*f1
g(ind) = q*u+Told(i,j+1)*u*f2+Told(i,j)*(1.0d0-u*f2)

do i = 1,M-1
  ind = ind + 1
  kmp = cal(i+1,j)
  kmm = cal(i,j)
  knp = cal(i,j+1)

r = dble(real(i))*dr
  q = q0*eppa(T(i,j),i,j)*ef(T(i,j),i,j)
  u = dt/(rho*cap(i,j))
  f1 = kmm*(r-dr/2.0d0)/(r*dr*dr)
  f2 = kmp*(r+dr/2.0d0)/(r*dr*dr)
  f3 = 2.0d0*knp/(dz*dz)

  a(ind) = -u*f1
  b(ind) = 1.0d0+u*(f1+f2)
  c(ind) = -u*f2
  g(ind) = q*u+Told(i,j)*(1.0d0-u*f3)+Told(i,j+1)*u*f3
enddo

i = M
  ind = ind + 1
  kmm = cal(i,j)
  knp = cal(i,j+1)
  q = q0*eppa(T(i,j),i,j)*ef(T(i,j),i,j)
  u = dt/(rho*cap(i,j))
  r = dble(real(i))*dr
```

```

f1 = 2.0d0*kmm*(r-dr/2.0d0)/((r-dr/4.0d0)*dr*dr)
f2 = 2.0d0*h*r/((r-dr/4.0d0)*dr)
f3 = 2.0d0*knp/(dz*dz)

c      a(ind) = -u*f1
c      b(ind) = 1.0d0 + u*(f1+f2)
c      g(ind) = (q+f2*Tinf)*u+Told(i,0)*(1.0d0-u*f3)+Told(i,1)*u*f3
b(ind) = 1.0d0
g(ind) = Tinf

do j = 1,N-1
  i = 0
    ind = ind + 1
    kmp = cal(i+1,j)
    knp = cal(i,j+1)
    knm = cal(i,j)
    q = q0*eppa(T(i,j),i,j)*ef(T(i,j),i,j)
    u = dt/(rho*cap(i,j))
    r = dble(real(i))*dr
    f1 = 4.0d0*kmp/(dr*dr)
    f2 = knp/(dz*dz)
    f3 = knm/(dz*dz)

    b(ind) = 1.0d0+u*f1
    c(ind) = -u*f1
    w = 1.0d0-u*(f2+f3)
g(ind) = q*u + Told(i,j-1)*u*f3+Told(i,j)*w+Told(i,j+1)*u*f2

  do i = 1,M-1
    ind = ind + 1
kmp = cal(i+1,j)
    kmm = cal(i,j)
    knp = cal(i,j+1)
    knm = cal(i,j)
    r = dble(real(i))*dr
    q = q0*eppa(T(i,j),i,j)*ef(T(i,j),i,j)
    u = dt/(rho*cap(i,j))
    f1 = kmm*(r-dr/2.0d0)/(r*dr*dr)
    f2 = kmp*(r+dr/2.0d0)/(r*dr*dr)
    f3 = knm/(dz*dz)
    f4 = knp/(dz*dz)
    a(ind) = -u*f1
    b(ind) = 1.0d0 + u*(f1+f2)
    c(ind) = -u*f2
    w = 1.0d0-u*(f3+f4)
g(ind) = q*u+Told(i,j-1)*u*f3+Told(i,j)*w+Told(i,j+1)*u*f4
  enddo

  i = M
    ind = ind + 1
    kmm = cal(i,j)

```

```

knp = cal(i,j+1)
knm = cal(i,j)
r = dble(real(i))*dr
q = q0*eppa(T(i,j),i,j)*ef(T(i,j),i,j)
u = dt/(rho*cap(i,j))
f1 = 2.0d0*kmm*(r-dr/2.0d0)/((r-dr/4.0d0)*dr*dr)
f2 = 2.0d0*h*r/(dr*(r-dr/4.0d0))
f3 = knm/(dz*dz)
f4 = knp/(dz*dz)
c      a(ind) = -u*f1
c      b(ind) = 1.0d0 + u*(f1+f2)
c      w = Told(i,j)*(1.0d0-u*(f3+f4))
c      g(ind) = (q+f2*Tinf)*u+Told(i,j-1)*u*f3+w+Told(i,j+1)*u*f4

b(ind) = 1.0d0
g(ind) = Tinf

enddo

j = N
i = 0
ind = ind + 1
kmp = cal(i+1,j)
knm = cal(i,j)
q = q0*eppa(T(i,j),i,j)*ef(T(i,j),i,j)
u = dt/(rho*cap(i,j))
f1 = 4.0d0*kmp/(dr*dr)
f2 = 2.0d0*knm/(dz*dz)
f3 = 2.0d0*h/dz

c      b(ind) = 1.0d0+u*f1
c      c(ind) = -u*f1
c      w = 1.0d0-u*(f2+f3)
c      g(ind) = (q+f3*Tinf)*u+Told(i,j-1)*u*f2+Told(i,j)*w
b(ind) = 1.0d0
g(ind) = Tinf

do i = 1,M-1
ind = ind + 1
kmm = cal(i,j)
kmp = cal(i+1,j)
knm = cal(i,j)
r = dble(real(i))*dr
q = q0*eppa(T(i,j),i,j)*ef(T(i,j),i,j)
u = dt/(rho*cap(i,j))
f1 = kmm*(r-dr/2.0d0)/(r*dr*dr)
f2 = kmp*(r+dr/2.0d0)/(r*dr*dr)
f3 = 2.0d0*knm/(dz*dz)
f4 = 2.0d0*h/dz

c      a(ind) = -u*f1

```

```

c          b(ind) = 1.0d0 + u*(f1+f2)
c          c(ind) = -u*f2
c          w = 1.0d0-u*(f3+f4)
c          g(ind) = (q+f4*Tinf)*u+Told(i,j-1)*u*f3+Told(i,j)*w
          b(ind) = 1.0d0
          g(ind) = Tinf

          enddo

          i = M
          ind = ind + 1
          kmm = cal(i,j)
          knm = cal(i,j)
          r=RR
          q = q0*eppa(T(i,j),i,j)*ef(T(i,j),i,j)
          u = dt/(rho*cap(i,j))
          f1 = 2.0d0*kmm*(r-dr/2.0d0)/((r-dr/4.0d0)*dr*dr)
          f2 = 2.0d0*h*r/((r-dr/4.0d0)*dr)
          f3 = 2.0d0*knm/(dz*dz)
          f4 = 2.0d0*h/dz

c          a(ind) = -u*f1
c          b(ind) = 1.0d0 + u*(f1+f2)
c          w = 1.0d0-u*(f3+f4)
c          g(ind) = (q+(f2+f4)*Tinf)*u+Told(i,j-1)*u*f3+Told(i,j)*w
          b(ind) = 1.0d0
          g(ind) = Tinf

          is = ind
          if = 1
          l = ind

          call tridag(if,l,is,a,b,c,g,v)

          er = 0.0d0
          ind = 0
          do j = 0,N
            do i = 0,M
              ind=ind + 1
              er = er + ABS(v(ind)-T(i,j))
              T(i,j)=v(ind)
            enddo
          enddo
          if (er .gt. emax) goto 10

c Second Time Step
          do j = 0,N
            do i = 0,M
              Told(i,j) = T(i,j)
            enddo

```

```

enddo

do k = 1,500
  a(k) = 0.0d0
  b(k) = 0.0d0
  c(k) = 0.0d0
  g(k) = 0.0d0
enddo

```

```

20 ind = 0

i = 0
  j = 0
    ind = ind + 1
    kmp = cal(i+1,j)
    knp = cal(i,j+1)
    q = q0*eppa(T(i,j),i,j)*ef(T(i,j),i,j)
    u = dt/(rho*cap(i,j))
    f1 = 4.0d0*kmp/(dr*dr)
    f2 = 2.0d0*knp/(dz*dz)

    b(ind) = 1.0d0+u*f2
    c(ind) = -u*f2
    g(ind) = q*u+Told(i+1,0)*u*f1+Told(i,j)*(1.0d0-u*f1)
  do j = 1,N-1
    ind = ind + 1
    kmp = cal(i+1,j)
    knp = cal(i,j+1)
    knm = cal(i,j)
    q = q0*eppa(T(i,j),i,j)*ef(T(i,j),i,j)
    u = dt/(rho*cap(i,j))
    f1 = 4.0d0*kmp/(dr*dr)
    f2 = knm/(dz*dz)
    f3 = knp/(dz*dz)

    a(ind) = -u*f2
    b(ind) = 1.0d0+u*(f2+f3)
    c(ind) = -u*f3
    g(ind) = q*u+Told(i,j)*(1.0d0-u*f1)+Told(i+1,j)*u*f1
  enddo
  j = N
    ind = ind + 1
    kmp = cal(i+1,j)
    knm = cal(i,j)
    q = q0*eppa(T(i,j),i,j)*ef(T(i,j),i,j)
    u = dt/(rho*cap(i,j))
    f1 = 4.0d0*kmp/(dr*dr)
    f2 = 2.0d0*knm/(dz*dz)
    f3 = 2.0d0*h/dz
    a(ind) = -u*f2

```

c

```

c          b(ind) = 1.0d0+u*(f2+f3)
c          g(ind) = (q+f3*Tinf)*u+Told(i,j)*(1.0d0-u*f1)+Told(i+1,j)*u*f1

b(ind) = 1.0d0
g(ind) = Tinf

do i = 1,M-1
r = dble(real(i))*dr
  j = 0
    ind = ind + 1
    kmp = cal(i+1,j)
    kmm = cal(i,j)
    knp = cal(i,j+1)

    q = q0*eppa(T(i,j),i,j)*ef(T(i,j),i,j)
    u = dt/(rho*cap(i,j))
    f1 = kmm*(r-dr/2.0d0)/(r*dr*dr)
    f2 = kmp*(r+dr/2.0d0)/(r*dr*dr)
    f3 = 2.0d0*knp/(dz*dz)

    a(ind) = 0.0d0
    b(ind) = 1.0d0+u*f3
    c(ind) = -u*f3
    w = 1.0d0-u*(f1+f2)
g(ind) = q*u+Told(i-1,j)*u*f1+Told(i,j)*w+Told(i+1,j)*u*f2
    do j = 1,N-1
      ind = ind + 1
      kmp = cal(i+1,j)
      kmm = cal(i,j)
      knp = cal(i,j+1)
      knm = cal(i,j)
      q = q0*eppa(T(i,j),i,j)*ef(T(i,j),i,j)
      u = dt/(rho*cap(i,j))
      f1 = kmm*(r-dr/2.0d0)/(r*dr*dr)
      f2 = kmp*(r+dr/2.0d0)/(r*dr*dr)
      f3 = knm/(dz*dz)
      f4 = knp/(dz*dz)

      a(ind) = -u*f3
      b(ind) = 1.0d0 + u*(f3+f4)
      c(ind) = -u*f4
      w = 1.0d0-u*(f1+f2)
g(ind) = q*u+Told(i-1,j)*u*f1+Told(i,j)*w+Told(i+1,j)*u*f2
    enddo
  j = N
    ind = ind + 1
    kmm = cal(i,j)
    kmp = cal(i+1,j)
    knm = cal(i,j)
    q = q0*eppa(T(i,j),i,j)*ef(T(i,j),i,j)
    u = dt/(rho*cap(i,j))

```

```

f1 = kmm*(r-dr/2.0d0)/(r*dr*dr)
f2 = kmp*(r+dr/2.0d0)/(r*dr*dr)
f3 = 2.0d0*knm/(dz*dz)
f4 = 2.0d0*h/dz

c      a(ind) = -u*f3
c      b(ind) = 1.0d0 + u*(f3+f4)
c      c(ind) = 0.0d0
c      w = Told(i,j)*(1.0d0-u*(f1+f2))
c      g(ind) = (q+f4*Tinf)*u+Told(i-1,j)*u*f1+w+Told(i+1,j)*u*f2

b(ind) = 1.0d0
g(ind) = Tinf

enddo
i = M
r = RR
j = 0
ind = ind + 1
kmm = cal(i,j)
knp = cal(i,j+1)
q = q0*eppa(T(i,j),i,j)*ef(T(i,j),i,j)
u = dt/(rho*cap(i,j))
f1 = 2.0d0*kmm*(r-dr/2.0d0)/((r-dr/4.0d0)*dr*dr)
f2 = 2.0d0*h*r/((r-dr/4.0d0)*dr)
f3 = 2.0d0*knp/(dz*dz)
c      b(ind) = 1.0d0 + u*f3
c      c(ind) = -u*f3
c      w = 1.0d0-u*(f1+f2)
c      g(ind) = (q+f2*Tinf)*u+Told(i-1,0)*u*f1+Told(i,0)*w

b(ind) = 1.0d0
g(ind) = Tinf

do j = 1,N-1
ind = ind + 1
kmm = cal(i,j)
knp = cal(i,j+1)
knm = cal(i,j)
q = q0*eppa(T(i,j),i,j)*ef(T(i,j),i,j)
u = dt/(rho*cap(i,j))
f1 = 2.0d0*kmm*(r-dr/2.0d0)/((r-dr/4.0d0)*dr*dr)
f2 = 2.0d0*h*r/(dr*(r-dr/4.0d0))
f3 = knm/(dz*dz)
f4 = knp/(dz*dz)
c      a(ind) = -u*f3
c      b(ind) = 1.0d0 + u*(f3+f4)
c      c(ind) = -u*f4
c      w = 1.0d0-u*(f1+f2)
c      g(ind) = (q+f2*Tinf)*u+Told(i-1,j)*u*f1+Told(i,j)*w

```

```

b(ind) = 1.0d0
g(ind) = Tinf

    enddo
    j = N
        ind = ind + 1
        kmm = cal(i,j)
        knm = cal(i,j)
        q = q0*eppa(T(i,j),i,j)*ef(T(i,j),i,j)
        u = dt/(rho*cap(i,j))
        f1 = 2.0d0*kmm*(r-dr/2.0d0)/((r-dr/4.0d0)*dr*dr)
        f2 = 2.0d0*h*r/((r-dr/4.0d0)*dr)
        f3 = 2.0d0*knm/(dz*dz)
        f4 = 2.0d0*h/dz

c          a(ind) = -u*f3
c          b(ind) = 1.0d0 + u*(f3+f4)
          w = 1.0d0-u*(f1+f2)
c          g(ind) = (q+(f2+f4)*Tinf)*u+Told(i-1,j)*u*f1+Told(i,j)*w

b(ind) = 1.0d0
g(ind) = Tinf

is = ind
if = 1
l = ind

call tridag(if,l,is,a,b,c,g,v)
er = 0.0d0
ind = 0
do i = 0,M
    do j = 0,N
        ind=ind + 1
        er = er + ABS(v(ind)-T(i,j))
        T(i,j)=v(ind)
    enddo
enddo
if (er .gt. emax) goto 20

if (MOD(p,100) .eq. 0) then
    write (11,*) T(0,0)
    write (13,*) T(14,0)
endif

1    continue
    end

c-----
subroutine tridag(if,l,is,a,b,c,d,v)
c    implicit double precision(a-h,o-z)
c    dimension a(is),b(is),c(is),d(is),v(is),beta(2000),gamma(2000)
    double precision a(is),b(is),c(is),d(is),v(is)

```

```

    double precision beta(2601),gamma(2601)
c
    beta(if)=b(if)
    gamma(if)=d(if)/beta(if)
    ifp1=if+1
c
    do 1 i=ifp1,l
        beta(i)=b(i)-a(i)*c(i-1)/beta(i-1)
1    gamma(i)=(d(i)-a(i)*gamma(i-1))/beta(i)
c
    v(l)=gamma(l)
    last=l-if
    do 2 k=1,last
        i=l-k
2    v(i)=gamma(i)-c(i)*v(i+1)/beta(i)
c
    return
    end

    function cap(i,j)
c
c    ...heat capacity for Zinc Oxide
c
    double precision ci,cj

    if (i .gt. is) then
        ci = 0.166670d0
    else if (i .lt. is) then
        ci = 0.50d0
    else
        ci = 0.333330d0
    endif
    if (j .gt. js) then
        cj = 0.166670d0
    else if (j .lt. js) then
        cj = 0.50d0
    else
        cj = 0.333330d0
    endif
    cap = 0.50d0*(ci+cj)

    return
    end

    function epa(t)
c
    Calculates real electric permittivity
    double precision epa,t,x(11),e(11),m,a
    integer i,j,k
    data x/23.0d0,150.0d0,200.0d0,250.0d0,300.0d0,350.0d0,400.0d0,

```

```
c450.0d0,500.0d0,550.0d0,600.0d0/
```

```
data e/3.84d0,3.88d0,3.97d0,3.93d0,3.86d0,3.85d0,3.88d0,3.90d0,  
c3.94d0,3.970d0,4.02d0/
```

```
a = t - 273.0d0
```

```
do k = 2,11
```

```
if (a .lt. x(k)) then
```

```
m = (e(k) - e(k-1))/(x(k) - x(k-1))
```

```
epa = e(k-1) + m*(a-x(k-1))
```

```
return
```

```
endif
```

```
enddo
```

```
c extrapolation
```

```
epa = e(11)
```

```
return
```

```
end
```

```
function eppa(t,i,j)
```

```
c Calculates dielectric loss for Zinc Oxide at a given temperature based on the data
```

```
c from University of Maryland at College Park(July 17)
```

```
c Uses Linear Interpolation.
```

```
c This function assumes that the temperature is greater than or equal to 23 C.
```

```
double precision eppa,t,x(11),e(11),m,a
```

```
integer i
```

```
data x/23.0d0,150.0d0,200.0d0,250.0d0,300.0d0,350.0d0,400.0d0,
```

```
c450.0d0,500.0d0,550.0d0,600.0d0/
```

```
data e/0.10d0,2.0d0,4.0d0,8.0d0,6.0d0,5.50d0,14.0d0,23.0d0,
```

```
c8.0d0,1.0d0,0.10d0/
```

```
a = t - 273.0d0
```

```
if (i .gt. 14 .or. j .gt. 7) then
```

```
epa = 0.0d0
```

```
return
```

```
else
```

```
do k = 2,11
```

```
if (a .lt. x(k)) then
```

```
m = (e(k) - e(k-1))/(x(k) - x(k-1))
```

```
eppa = e(k-1) + m*(a-x(k-1))
```

```
return
```

```
endif
```

```
enddo
```

```
c extrapolation
```

```
eppa = e(11)
```

```

c      constant heat generation assumption
c      eppa = 1.0d0
c      return
c      endif
c      end

function cal(i,j)
c
c      ...conductivity for Zinc Oxide
c
      if (i .gt. is .or. j .gt. js) then
          cal=0.0335330d0
      else
          cal=0.10d0
      endif
return
end

function ef(t,i,j)
c      ...normalized local electric field squared (E/Eo)^2
c      double precision ef,t,d
c      double precision a, eppa, epa, s,sr,sz,al
c      integer i,j

c      data a/4.085080d-2/
c      data a/25.654d-2/
c      common/props/dr,dz
c      d = 0.10d0

      if (i .le. is .and. j.le.js) then
          sr = dble(real(is-i))*d
          sz = dble(real(js-j))*d
          if (sr .le. sz) then
              s = sr
          else
              s = sz
          endif
          epp = eppa(t,i,j)
          ep = epa(t)
          z = epp/ep
          y=0.50d0
          w=1.0d0/y

          if (z .lt. y) then
b=0.50d0*z-0.06250d0*z**3+.02730d0*z**5-1.88d-2*z**7

          al = 2.0d0*a*b*sqrt(ep)
          else if (z .lt. w) then

```

```

b=0.50d0*y-0.0625d0*y**3+.02730d0*y**5-1.88d-2*y**7
alb=2.0d0*a*b*sqrt(ep)

x=1.0d0/w
c = 1.0d0-b+0.125d0*x**2-3.91d-2*x**4+2.05d-2*x**6
alc=a*sqrt(2.0d0*ep)*c
slope=(alc-alb)/(w-y)
al=alb+slope*(z-y)
else
x=1.0d0/z
b=0.50d0*x-0.0625d0*x**3+.02730d0*x**5-1.88d-2*x**7
c = 1.0d0-b+0.125d0*x**2-3.91d-2*x**4+2.05d-2*x**6
al = a*sqrt(2.0d0*ep)*c
endif
ef = exp(-2.0d0*al*s)

return
else
ef = 0

endif
return
end

```

```

c    program iw
c    Program to find temperatures for small ZnO sample
c    heated in microwave oven
c    Implicit finite-difference, wit sparse matrix solver
double precision T(0:25,0:25),Told(0:25,0:25)
double precision q,qo,kmm,kmp,knm,knp,h,rho
double precision dt,dr,dz,RR,Z,r
double precision a(9378)
double precision g(676),B(676)
double precision f1,f2,f3,f4,u,w,err,del,dmax,emax
double precision tmax,Tinf,Ti,av
integer row(9378),col(9378)
integer i,j,k,M,N,p,ind,ei
integer ec
c    Variables used as arguments for call y12maf:
double precision piv(676),afl(8)
integer ha(676,11),ifl(10),ifa,eqn,NN,NN1,iha
data dt,RR,Z/0.10d0,5.0d0,5.0d0/
data dr,dz/0.20d0,0.20d0/
data h,Tinf,Ti,qo/80000.0d0,300.0d0,300.0d0,5.0d0/
data emax,tmax/0.00000010d0,600.0d0/
data rho/3.0d0/

pmax = int(tmax/dt)
M = int(RR/dr)
N = int(Z/dz)
eqn = (M+1)*(N+1)

c Initialize
do k = 1,500
a(k) = 0.0d0
b(k) = 0.0d0
a(k) = 0.0d0
g(k) = 0.0d0
enddo
ei = 0
do j = 0,N
do i = 0,M
T(i,j) = Ti
ei = ei + 1
B(ei) = Ti
enddo
enddo

do 1 p = 1,pmax

do j = 0,N
do i = 0,M

```

```

                                Told(i,j) = T(i,j)
                                enddo
                                enddo
                                ec = 0
10                                ind = 0
                                ei = 0
                                ec = ec+1
                                j = 0
                                i = 0
                                ei = ei + 1

                                kmp = cal(i+1,j)
                                knp = cal(i,j+1)
                                q = q0*eppa(T(i,j),i,j)
                                u = dt/(rho*cap(i,j))
                                f1 = 4.0d0*kmp/(dr*dr)
                                f2 = 2.0d0*knp/(dz*dz)
                                ind = ind + 1
                                row(ind) = ei
                                col(ind) = ei
                                a(ind) = 1.0d0 + u*(f1+f2)
                                ind = ind + 1
                                row(ind) = ei
                                col(ind) = ei + 1
                                a(ind) = -u*f1
                                ind = ind + 1
                                row(ind) = ei
                                col(ind) = ei + (M+1)
                                a(ind) = -u*f2
                                g(ei) = q*u+Told(i,j)

                                do i = 1,M-1
                                    ei = ei + 1

                                    kmp = cal(i+1,j)
                                    kmm = cal(i,j)
                                    knp = cal(i,j+1)

                                r = dble(real(i))*dr
                                q = q0*eppa(T(i,j),i,j)
                                u = dt/(rho*cap(i,j))
                                f1 = kmm*(r-dr/2.0d0)/(r*dr*dr)
                                f2 = kmp*(r+dr/2.0d0)/(r*dr*dr)
                                f3 = 2.0d0*knp/(dz*dz)
                                ind = ind + 1
                                row(ind) = ei
                                col(ind) = ei-1
                                a(ind) = -u*f1
                                ind = ind + 1
                                row(ind) = ei
                                col(ind) = ei

```

```

a(ind) = 1.0d0+u*(f1+f2+f3)
ind = ind + 1
row(ind) = ei
col(ind) = ei + 1
a(ind) = -u*f2
ind = ind + 1
row(ind) = ei
col(ind) = ei + (M+1)
a(ind) = -u*f3
g(ei) = q*u+Told(i,j)
enddo

i = M
ei = ei + 1

kmm = cal(i,j)
knp = cal(i,j+1)
q = q0*eppa(T(i,j),i,j)
u = dt/(rho*cap(i,j))
r = dble(real(i))*dr
f1 = 2.0d0*kmm*(r-dr/2.0d0)/((r-dr/4.0d0)*dr*dr)
f2 = 2.0d0*h*r/((r-dr/4.0d0)*dr)
f3 = 2.0d0*knp/(dz*dz)

c      ind = ind + 1
c      row(ind) = ei
c      col(ind) = ei-1
c      a(ind) = -u*f1
c      ind = ind + 1
c      row(ind) = ei
c      col(ind) = ei
c      b(ind) = 1.0d0 + u*(f1+f2+f3)
c      ind = ind + 1
c      row(ind) = ei
c      col(ind) = ei + (M+1)
c      a(ind) = -u*f3
c      g(ei) = (q+f2*Tinf)*u+Told(i,j)
ind = ind + 1
      row(ind) = ei
      col(ind) = ei
a(ind) = 1.0d0
g(ei) = Tinf

do j = 1,N-1
  i = 0
    ei = ei + 1
    kmp = cal(i+1,j)
    knp = cal(i,j+1)
    knm = cal(i,j)
    q = q0*eppa(T(i,j),i,j)
    u = dt/(rho*cap(i,j))

```

```

r = dble(real(i))*dr
f1 = 4.0d0*kmp/(dr*dr)
f2 = knm/(dz*dz)
f3 = knp/(dz*dz)
ind = ind + 1
row(ind) = ei
col(ind) = ei+1
a(ind) = -u*f1
ind = ind + 1
row(ind) = ei
col(ind) = ei
a(ind) = 1.0d0+u*(f1+f2+f3)
ind = ind + 1
row(ind) = ei
col(ind) = ei-(M+1)
a(ind) = -u*f2
ind = ind + 1
row(ind) = ei
col(ind) = ei+(M+1)
a(ind) = -u*f3

g(ei) = q*u + Told(i,j)

```

```
do i = 1,M-1
```

```

ei = ei + 1
kmp = cal(i+1,j)
kmm = cal(i,j)
knp = cal(i,j+1)
knm = cal(i,j)
r = dble(real(i))*dr
q = q0*eppa(T(i,j),i,j)
u = dt/(rho*cap(i,j))
f1 = kmm*(r-dr/2.0d0)/(r*dr*dr)
f2 = knp*(r+dr/2.0d0)/(r*dr*dr)
f3 = knm/(dz*dz)
f4 = knp/(dz*dz)
ind = ind + 1
row(ind) = ei
col(ind) = ei-1
a(ind) = -u*f1
ind = ind + 1
row(ind) = ei
col(ind) = ei
a(ind) = 1.0d0 + u*(f1+f2+f3+f4)
ind = ind + 1
row(ind) = ei
col(ind) = ei+1
a(ind) = -u*f2
ind = ind + 1
row(ind) = ei

```

```

col(ind) = ei-(M+1)
a(ind) = -u*f3
ind = ind + 1
row(ind) = ei
col(ind) = ei+(M+1)
a(ind) = -u*f4

g(ei) = q*u+Told(i,j)

enddo

i = M
ei = ei + 1
kmm = cal(i,j)
knp = cal(i,j+1)
knm = cal(i,j)
r = dble(real(i))*dr
q = q0*eppa(T(i,j),i,j)
u = dt/(rho*cap(i,j))
f1 = 2.0d0*kmm*(r-dr/2.0d0)/((r-dr/4.0d0)*dr*dr)
f2 = 2.0d0*h*r/(dr*(r-dr/4.0d0))
f3 = knm/(dz*dz)
f4 = knp/(dz*dz)
c ind = ind + 1
c row(ind) = ei
c col(ind) = ei - 1
c a(ind) = -u*f1
c ind = ind + 1
c row(ind) = ei
c col(ind) = ei
c a(ind) = 1.0d0 + u*(f1+f2+f3+f4)
c ind = ind + 1
c row(ind) = ei
c col(ind) = ei -(M+1)
c a(ind) = -u*f3
c ind = ind + 1
c row(ind) = ei
c col(ind) = ei+(M+1)
c a(ind) = -u*f4
c
c g(ei) = (q+f2*Tinf)*u+Told(i,j)

ind = ind + 1
row(ind) = ei
col(ind) = ei
a(ind) = 1.0d0

g(ei) = Tinf

enddo

```

```

j = N
  i = 0
    ei = ei + 1
    kmp = cal(i+1,j)
    knm = cal(i,j)
    q = q0*eppa(T(i,j),i,j)
    u = dt/(rho*cap(i,j))
    f1 = 4.0d0*kmp/(dr*dr)
    f2 = 2.0d0*knm/(dz*dz)
    f3 = 2.0d0*h/dz
c    ind = ind + 1
c    row(ind) = ei
c    col(ind) = ei+1
c    a(ind) = -u*f1
c    ind = ind + 1
c    row(ind) = ei
c    col(ind) = ei
c    a(ind) = 1.0d0+u*(f1+f2+f3)
c    ind = ind + 1
c    row(ind) = ei
c    col(ind) = ei-(M+1)
c    a(ind) = -u*f2
c
c    g(ei) = (q+f3*Tinf)*u+Told(i,j)
c    ind = ind + 1
c      row(ind) = ei
c      col(ind) = ei
c    a(ind) = 1.0d0
c
c    g(ei) = Tinf
c
c    do i = 1,M-1
c      ei = ei + 1
c      kmm = cal(i,j)
c      kmp = cal(i+1,j)
c      knm = cal(i,j)
c      r = dble(real(i))*dr
c      q = q0*eppa(T(i,j),i,j)
c      u = dt/(rho*cap(i,j))
c      f1 = kmm*(r-dr/2.0d0)/(r*dr*dr)
c      f2 = kmp*(r+dr/2.0d0)/(r*dr*dr)
c      f3 = 2.0d0*knm/(dz*dz)
c      f4 = 2.0d0*h/dz
c
c      ind = ind + 1
c      row(ind) = ei
c      col(ind) = ei-1
c      a(ind) = -u*f1
c      ind = ind + 1
c      row(ind) = ei
c      col(ind) = ei

```

```

c          a(ind) = 1.0d0 + u*(f1+f2+f3+f4)
c          ind = ind + 1
c          row(ind) = ei
c          col(ind) = ei+1
c          a(ind) = -u*f2
c          ind = ind + 1
c          row(ind) = ei
c          col(ind) = ei-(M+1)
c          a(ind) = -u*f3
c
c          g(ei) = (q+f4*Tinf)*u+Told(i,j)
c          ind = ind + 1
c          row(ind) = ei
c          col(ind) = ei
c          a(ind) = 1.0d0
c
c          g(ei) = Tinf
c
c          enddo
c
c          i = M
c          ei = ei + 1
c          kmm = cal(i,j)
c          knm = cal(i,j)
c          r=RR
c          q = q0*eppa(T(i,j),i,j)
c          u = dt/(rho*cap(i,j))
c          f1 = 2.0d0*kmm*(r-dr/2.0d0)/((r-dr/4.0d0)*dr*dr)
c          f2 = 2.0d0*h*r/((r-dr/4.0d0)*dr)
c          f3 = 2.0d0*knm/(dz*dz)
c          f4 = 2.0d0*h/dz
c
c          ind = ind + 1
c          row(ind) = ei
c          col(ind) = ei-1
c          a(ind) = -u*f1
c          ind = ind + 1
c          row(ind) = ei
c          col(ind) = ei
c          a(ind) = 1.0d0 + u*(f1+f2+f3+f4)
c          ind = ind + 1
c          row(ind) = ei
c          col(ind) = ei-(M+1)
c          a(ind) = -u*f3
c
c          g(ei) = (q+(f2+f4)*Tinf)*u+Told(i,j)
c          ind = ind + 1
c          row(ind) = ei
c          col(ind) = ei
c          a(ind) = 1.0d0

```

```

    g(ei) = Tinf
NN = 3*ind
NN1 = 3*ind
    iha = eqn
    ei = 0
    do j = 0,N
        do i = 0,M
            ei = ei + 1
            B(ei) = g(ei)
        enddo
    enddo

c    ei = 0
c    do j=0,N
c        do i=0,M
c            ei = ei + 1
c            ind = 100+j*(125)
c            if (i .eq. M) print *, i,j,ei,ind,a(ind),B(ei)
c            enddo
c        enddo
c        print *,'before y12 '
c    call y12maf(eqn,ind,a,col,NN,row,NN1,piv,ha,iha,afl,ifl,B,ifa)
c    print *,'after y12'
        if (ifa .ne. 0) then
            print *,'y12 failed, ifail= ',ifa
            stop
        endif

c    ei = 0
c    do j=0,N
c        do i=0,M
c            ei = ei + 1
c            ind = 100+j*(125)
c            if (i .eq. M) print *, i,j,ei,ind,a(ind),B(ei)
c            enddo
c        enddo

err = 0.0d0
ei = 0
do j = 0,N
    do i = 0,M
        ei = ei + 1
c    if (ABS(B(ei)-T(i,j)) .gt. 1.0d0) then
c        print *,ec,i,j,ei,T(i,j),B(ei)

c    endif
        err = err + ABS(B(ei)-T(i,j))
    enddo
enddo

```

```

                T(i,j)=B(ei)
            enddo
        enddo
c      print *,ec,err
        if (err .gt. emax) goto 10

        print *,p,T(0,0),T(7,0),T(8,0),T(M,0)
c      if (MOD(p,10) .eq. 0) then

c          av = 0.0d0
c          do i = 0,14
c              do j = 0,7
c                  av = av + T(i,j)
c              enddo
c          enddo
c          av = av/120.0d0

c          print *,p,T(0,0),av,T(14,0),T(0,7),T(14,7)
c          write (12,*) av
c          print *,p,T(7,3)
c              if (MOD(p,100) .eq. 0) then
c                  write (11,*) T(0,0)
c                  write (13,*) T(14,0)
c              endif
c                  write (14,*) T(5,5)
c                  do i = 0,M
c                      write (12,*) T(i,0)
c                  enddo
c      endif

c      do i = 0,M
c          T(i,N) = 300.0d0
c      enddo
c      do j = 0,N
c          T(M,j) = 300.0d0
c      enddo
1      continue
    end

```

c-----

```

function cap(i,j)
c
c  ...heat capacity for Zinc Oxide
c
c      if (i .gt. 14 .or. j .gt. 7) then
c          cap = 0.166670d0
c      else

```

```

c   cap=0.50d0
c   endif
c   double precision ci,cj
c   if (i .gt. 7) then
c       ci = 0.166670d0
c   else if (i .lt. 7) then
c       ci = 0.50d0
c   else
c       ci = 0.333330d0
c   endif
c   if (j .gt. 3) then
c       cj = 0.166670d0
c   else if (j .lt. 3) then
c       cj = 0.50d0
c   else
c       cj = 0.333330d0
c   endif
c   cap = 0.50d0*(ci+cj)
c   cap = 0.50d0
c   return
c   end

```

function eppa(t,i,j)

```

c   Calculates dielectric loss for Zinc Oxide at a given temperature based on the data
c   from University of Maryland at College Park(July 17)
c   Uses Linear Interpolation.
c   This function assumes that the temperature is greater than or equal to 23 C.

```

```

c   double precision eppa,t,x(11),e(11),m,a
c   integer i
c   data x/23.0d0,150.0d0,200.0d0,250.0d0,300.0d0,350.0d0,400.0d0,
c450.0d0,500.0d0,550.0d0,600.0d0/

```

```

c   data e/0.10d0,2.0d0,4.0d0,8.0d0,6.0d0,5.50d0,14.0d0,23.0d0,
c8.0d0,1.0d0,0.10d0/

```

```

c   a = t - 273.0d0
c   b = 1.0d0
c   if (i .eq. 14) b = b * 0.50d0
c   if (j .eq. 7) b = b * 0.50d0
c
c   if (i .gt. 7 .or. j .gt. 3) then
c       eppa = 0.0d0
c       return
c   else
c   do k = 2,11
c       if (a .lt. x(k)) then
c           m = (e(k) - e(k-1))/(x(k) - x(k-1))
c           eppa = b*(e(k-1) + m*(a-x(k-1)))

```

```

        return
    endif
enddo
c    extrapolation
    eppa = b*e(11)
c    Constant heat generation assumption
c    eppa = 1.0d0
    return
endif
end

```

```

function cal(i,j)
c
c    ...conductivity for Zinc Oxide
c
    if (i .gt. 7 .or. j .gt. 3) then
c        cal = 111.10d0
c        cal = 333.30d0
c        cal=0.050d-3
        cal=0.0335330d0
    else
        cal=0.10d0
    endif
return
end

```

Vita

Patrick Fischer was born on October 26, 1972 in Poughkeepsie, New York. His parents, William and Ellen Fischer, have three other children, Ellen, William, and Frank. Patrick attended in the State University of New York at Stony Brook from August 1990 until May 1994 when he earned a Bachelor of Science in Mechanical Engineering. He attended Virginia Polytechnic and State University from August 1994 until May 1997 when he earned a Master of Science in Mechanical Engineering.